

Master's Thesis

**Chemical kinetics and transport of tropospheric trace compounds  
- implications for environment and air quality**

Author: Stina Ausmeel

Supervisors:

Elna Heimdal Nilsson (Lund University)  
Ole John Nielsen (Copenhagen University)

May 28 2015



**LUND UNIVERSITY**  
Faculty of Science



## Abstract

Fourier transform infrared spectroscopy techniques were used to study the kinetics of gas-phase reactions of three lactones,  $\gamma$ -valerolactone (GVL), 2(5H)-furanone (2(5HF)) and 3-methyl-2(5H)-furanone (3M2(5H)F) with Cl atoms, OH radicals and O<sub>3</sub> respectively. The experiments were performed in a photochemical reactor at a total pressure of 700 Torr at room temperature (298±2 K). Both relative rate and absolute rate methods were used to determine the reaction rate constants (unit cm<sup>3</sup>molecule<sup>-1</sup>s<sup>-1</sup>) yielding  $k_{\text{GVL+Cl}} = (4.56 \pm 0.51) \cdot 10^{-11}$ ,  $k_{\text{GVL+OH}} = (2.94 \pm 0.41) \cdot 10^{-11}$ ,  $k_{2(5\text{H})\text{F+Cl}} = (2.94 \pm 0.41) \cdot 10^{-11}$ ,  $k_{2(5\text{H})\text{F+OH}} = (4.06 \pm 0.073) \cdot 10^{-12}$ ,  $k_{2(5\text{H})\text{F+O}_3} = (6.73 \pm 0.18) \cdot 10^{-20}$ ,  $k_{3\text{M}2(5\text{H})\text{F+Cl}} = (16.1 \pm 1.8) \cdot 10^{-11}$ ,  $k_{3\text{M}2(5\text{H})\text{F+OH}} = (12.6 \pm 0.52) \cdot 10^{-12}$  and  $k_{3\text{M}2(5\text{H})\text{F+O}_3} = (5.42 \pm 1.23) \cdot 10^{-19}$ . Using atmospheric abundances of Cl, OH and O<sub>3</sub> the lifetime of each lactone towards each of the reaction sinks was calculated. The largest sink for all three lactones is through the reaction with OH (lifetimes of tens of days). Removal by Cl atoms can become equally significant when abundant in high concentrations which could be locally important. The lifetime against removal by O<sub>3</sub> (months-years) is relatively long on a tropospheric scale even at high concentrations. No significant reaction products were identified for experiments performed in N<sub>2</sub>. For experiments using an N<sub>2</sub>/O<sub>2</sub> mixture the identified products are formic acid (HCOOH), formyl chloride (CHClO), maleic anhydride (C<sub>2</sub>H<sub>2</sub>(CO)<sub>2</sub>O) and phosgene (CCl<sub>2</sub>O). There are still unidentified reaction products. In addition to the kinetic studies a project was performed where a chemical transport model (GEOS-Chem) was used to study updated reaction rate constants and photolysis rate constants of bromoform (CHBr<sub>3</sub>) and bromine nitrate (BrONO<sub>2</sub>) in the troposphere. The effect on tropospheric inorganic bromine levels, and consequently ozone levels, was insignificant for bromoform and more significant for bromine nitrate.

## Abbreviations and symbols

[A]	Concentration of chemical species A	HNO <sub>3</sub>	nitric acid
2(5H)F	2-(5H)-furanone	HO <sub>x</sub>	HO + HO <sub>2</sub>
3M2(5H)F	3-methyl-2(5H)-furanone	IPCC	Intergovernmental Panel on Climate Change
Br	Bromine, element	IR	infrared
BrONO <sub>2</sub>	bromine nitrate	<i>J</i>	photolysis rate constant
BrO <sub>x</sub>	Br + BrO	JPL	Jet Propulsion Laboratory
Br <sub>y</sub>	inorganic bromine	<i>k</i>	reaction rate constant
C <sub>2</sub> H <sub>2</sub>	acetylene	lactones	GVL + 2(5H)F + 3M2(5H)F
C <sub>2</sub> H <sub>4</sub>	ethylene	$\lambda$	wavelength
C <sub>2</sub> H <sub>6</sub>	ethane	M	third body in chemical reactions
C <sub>3</sub> H <sub>6</sub>	propene	MA	maleic anhydride
CCAR	Copenhagen Center for Atmospheric research	MBL	marine boundary layer
CCl <sub>2</sub> O	phosgene	NO <sub>x</sub>	NO + NO <sub>2</sub>
CH <sub>4</sub>	methane	O <sub>3</sub>	ozone
CHBr <sub>3</sub>	bromoform	OD	deuterated hydroxyl radical
CHClO	formyl chloride	OH	hydroxyl radical
Cl	Atomic chlorine	PBL	planetary boundary layer
Cl <sub>2</sub>	Molecular chlorine	ppb	parts per billion
CO <sub>2</sub>	carbon dioxide	ppm	parts per million
CTM	chemical transport model	ppt	parts per trillion
eV	electron volt	SiC	silicon carbide
FTIR	Fourier Transform Infrared	$\tau$	lifetime
GEOS	Goddard Earth Observing System	THF	tetrahydrofuran
GVL	$\gamma$ -valerolactone	UV	ultraviolet
H <sub>2</sub> O	water	$\nu$	frequency
HCOOH	formic acid	VOCs	volatile organic compounds
Hg	mercury, element		
HIPPO	HIAPER Pole-to-Pole observations		
HIAPER	High-Performance Instrumented Airborne Platform for Environmental Research		

## Table of contents

<b>Abstract</b> .....	<b>i</b>
<b>Abbreviations and symbols</b> .....	<b>ii</b>
<b>PART I – Introduction</b> .....	<b>1</b>
1.1 Atmosphere and climate .....	1
1.1.1 Atmospheric structure .....	1
1.1.2 Climate change and radiative forcing.....	2
1.2 Energy demand and supply .....	3
1.3 Report structure.....	4
<b>PART II – Aims and motivations</b> .....	<b>5</b>
2.1 Important atmospheric removal processes .....	5
2.1.1 Photolysis .....	5
2.1.1 Tropospheric reactants .....	6
2.1.1.1 Hydroxyl radical .....	6
2.1.1.2 Atomic chlorine.....	6
2.1.1.3 Ozone .....	7
2.2 Motivation for PART III and project questions.....	8
2.2 Motivation for PART IV and project questions.....	9
<b>PART III – Atmospheric kinetics of lactones</b> .....	<b>11</b>
3.1 Background .....	11
3.1.1 Biofuels .....	11
3.1.2 Preventive research.....	12
3.1.3 Furans – chemical properties .....	12
3.1.4 Furans – Production and use as fuels and industrial chemicals .....	14
3.1.5 Atmospheric impact of furans .....	15
3.2 Physical concepts .....	16
3.2.1. Molecular physics.....	16
3.2.2 Beer-Lambert Law .....	18
3.2.3 Fourier Transform Infrared Spectroscopy .....	18
3.2.4 Chemical kinetics .....	19
3.2.4.1 First order reactions .....	19
3.2.4.2 Second order and thermonuclear reactions.....	20
3.2.4.3 Pseudo-first-order approximation .....	20
3.2.4.4 Reaction rates and atmospheric lifetime.....	20

3.3 Method .....	21
3.3.1 Introduction .....	21
3.3.2 Experimental setup .....	22
3.3.2.1 Spectrometer properties .....	22
3.3.2.2 Reaction chamber .....	22
3.3.2.3 Manifold.....	23
3.3.2.4 Computers – software and control system.....	24
3.3.3 The relative and absolute rate methods .....	24
3.3.4 Procedure.....	25
3.3.4.1 Sample preparation .....	25
3.3.4.2 Experimental procedure .....	26
3.3.4.3 Control experiments .....	27
3.3.4.4 Chlorine experiments .....	28
3.3.4.5 OH experiments .....	29
3.3.4.6 Ozone experiments.....	30
3.3.5 Data analysis .....	30
3.3.6 Uncertainties in measurements and results .....	31
3.4 Results and discussion .....	32
3.4.1. Reference spectra and control experiments .....	32
3.4.2 Chlorine kinetics.....	33
3.4.2.1 Relative rate studies.....	33
3.4.2.2 Product studies.....	36
3.4.3 OH kinetics.....	38
3.4.3.1 Relative rate studies .....	38
3.4.4 O <sub>3</sub> kinetics .....	41
3.4.4.1 Absolute rate studies .....	41
3.4.4.2 Relative rate studies .....	42
3.7 Conclusions and atmospheric implications.....	43
<b>PART IV - Bromine Chemistry modeling .....</b>	<b>45</b>
4.1 Bromine in the troposphere .....	45
4.1.1 Inorganic bromine (Br <sub>y</sub> ) .....	45
4.1.2 Bromoform (CHBr <sub>3</sub> ).....	45
4.1.2 Bromine nitrate (BrONO <sub>2</sub> ) .....	46

4.1.4 HIPPO-campaign summary.....	46
4.2 Method.....	47
4.2.2 Updated rate constants.....	47
4.2.3 Updated absorption cross section.....	48
4.3 Results and discussion.....	50
4.3.1 CHBr <sub>3</sub> .....	50
4.3.1.1 Benchmark (data obtained for the year 2007).....	50
4.3.1.2 HIPPO-campaign comparisons (2009-2011).....	53
4.3.2 BrONO <sub>2</sub> .....	56
4.4 Conclusions and atmospheric implications.....	57
<b>PART V - Summary and outlook.....</b>	<b>58</b>
<b>References.....</b>	<b>59</b>
<b>Appendix A.....</b>	<b>65</b>

# **PART I - Introduction**

Since the middle of the 18<sup>th</sup> century the amount of greenhouse gases in the atmosphere, such as carbon dioxide (CO<sub>2</sub>), methane (CH<sub>4</sub>) and nitrous oxide (N<sub>2</sub>O), have all increased as a result of human activities arising during the industrialisation [1]. These increased concentrations of greenhouse gases together with other pollutions and influences on the environment have led to apparent changes in the climate which have been measured comprehensively since the 1950's [1]. An important parameter when describing the climate system is the earth surface temperature, which has almost become synonymous with climate change and *global warming* is both a well-known and debated subject in the 21<sup>st</sup> century. From a social point of view climate changes introduce impacts and risks which make knowledge about the climate system and predictions of the future important in order for human societies to make sustainable decisions. Such issues associated to climate changes are drought and rising sea levels, and anthropogenic activities can also have a large impact on local *air quality* affecting human health [2]. A large source of increased greenhouse gases and other air pollutants is *combustion* and the future energy consumption and supply is a growing concern.

This thesis concerns the atmospheric reactivity of both anthropogenic and naturally occurring species. It is necessary to understand these processes in order to do atmospheric predictions and possibly prevent negative effects on the local and global environment. The first section of this introduction will briefly describe the climate system with main focus on the atmosphere. The concept of radiative forcing will be presented and connected to climate changes. The second section will consider the challenges of energy supply over time.

## **1.1 Atmosphere and climate**

### **1.1.1 Atmospheric structure**

The atmosphere is not homogeneous and pressure, temperature as well as the composition changes with height above the ground. The pressure decreases with height due to the gravitational force and the atmospheric temperature profile can be seen in Figure 1.1(a).

The temperature profile in Figure 1.1(a) shows that the atmosphere can be divided into different layers and the lower parts, i.e. the troposphere and the stratosphere, is where the most important chemistry and physics related to anthropogenic emissions take place. The tropopause is located at 10-20 km altitude depending on the temperature in the troposphere and its position is defined by when the change in temperature with height becomes less than 2 K/km. The stratopause is located where a new temperature maximum occurs, at about 50 km altitude.

Vertical mixing within a layer is larger if the temperature decreases with height since hot air will rise and create turbulence. In Figure 1.1(b) it can be seen that the timescale for vertical mixing is fast within the planetary boundary layer (PBL) and in the troposphere in general. On the contrary, it will take several years for a species released at the Earth's surface to reach the stratosphere due to the small exchange of air across the tropopause.



The horizontal transport times, seen in Figure 1.1(c) are fast in the longitudinal direction due to air flows around the globe. Latitudinal air flows are slower and driven by temperature differences between the equator and the poles. The flow across the equator is greatly reduced due to the lack of this thermal forcing [3].

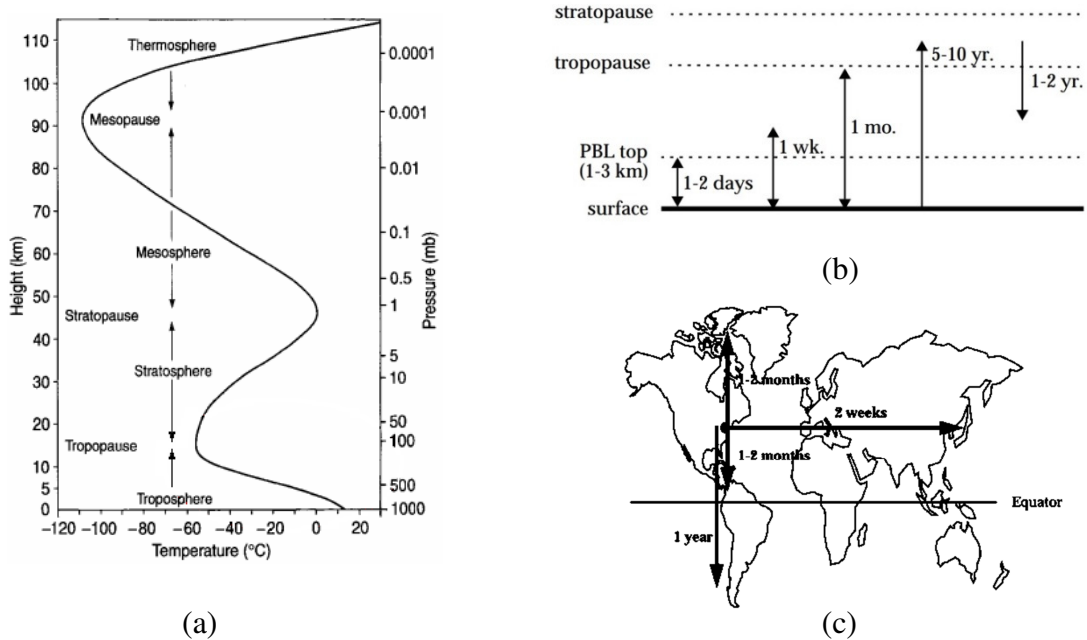


**Figure 1.1.** (a) Vertical temperature profile of the atmosphere with characteristic layers marked. Typical timescales for (b) vertical transportation [3] and (c) tropospheric horizontal transportation [3].

### 1.1.2 Climate change and radiative forcing

Climate is the long-term average of variables such as temperature, precipitation and cloudiness which on a day to day timescale is referred to as weather. The timescale for defining the average climate is usually set to 30 years [4].

The climate system comprises the Earth’s landmasses, biological ecosystems, oceans and freshwater, icecaps, the atmosphere and the energy supply from the sun. The climate system is hence large and complex and changes can be difficult to predict and the effects do not have to be identical in different parts of the world. Winds, ocean currents, topography and different amounts of sunlight produce a variety of local conditions on our planet.

For the atmosphere, natural climate factors are e.g. humidity, particles from oceans and vegetation and natural emissions such as volcanic eruptions. The increase in land use and emissions from human activities introduces other climate factors such as increased amounts of greenhouse gases, particles and compounds depleting the ozone layer etc. [4]. In the first article in the United Nations Framework Convention on Climate Change (the basis for the later Kyoto Protocol) from 1992 [5], *climate change* is defined as being related to human activity while natural changes are referred to as *climate variability*.

When studying and predicting global warming the concept of radiative forcing is of great importance. Radiative forcing is a measurement of change in atmospheric energy flux, usually in the unit  $Wm^{-2}$ , due to a specific driver of climate change [1].

Both natural and anthropogenic factors induce radiative forcing which can be both warming, if the forcing is positive, and cooling, if the forcing is negative. For example greenhouse gases act as warmers since they absorb longwave radiation emitted by the Earth's surface and can reemit the radiation back towards the Earth. This is an enhancement of the natural greenhouse effect. The greenhouse effect without human impact does today cause an increase in surface temperature of about 35 °C compared to an Earth without an atmosphere, making it habitable in the way we know it today. The greenhouse effect has however varied during the history of Earth [4], [6]. Cooling factors are complicated to understand and large uncertainties are related to most of the negative forcing drivers. What is known is that aerosols and clouds as well as ice caps can act as coolers, simply explained by their ability to reflect the sunlight which is hence not absorbed by the climate system.

## 1.2 Energy demand and supply

During the past thousand years the world has experienced a dramatic increase in human population and also in accompanied energy use. Especially after the industrialisation efficient energy sources have been necessary for production and transportation as well as to maintain a new expected living standard in many parts of the world.

The human population increased from 3.7 to 6.9 billion between the years 1970 and 2010 and low to medium estimates predict a population of nine to ten billion by 2100 [7]. These numbers can be compared with the population before the vast increase due to technological development, which was 1.6 billion in the year of 1900 [7]. The accompanying energy demand has been inevitable and Figure 1.2 shows the emissions of CO<sub>2</sub> due to combustion of fossil fuels and cement production from 1750 to 2011 [1]. It is seen in this figure that the growth of CO<sub>2</sub> emissions starts in the mid-1880s and increases with a larger rate further into the 20<sup>th</sup> century. The energy demand is predicted to increase by at least 50% from the year of 2006 until 2025 [8]. The growth is expected to be largest in developing countries and a larger fraction of the population will hence come to live in urban areas. With the urbanization follows higher income correlated with higher energy use [8].

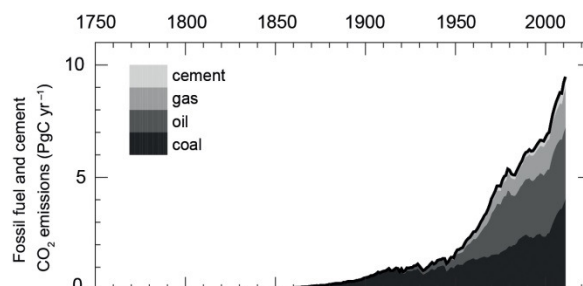


**Figure 1.2.** Anthropogenic CO<sub>2</sub> emissions (in units of 10<sup>15</sup> g Carbon/year) between 1750 and 2011, presented in the 5<sup>th</sup> IPCC Report.

The rapidly increasing energy demand is a motivation to seek new energy sources for at least two reasons. One is that the combustion of fossil fuels (coal, oil and gas) results in a net release of carbon into the climate system (atmosphere, oceans, ice caps etc.). This is due to the fact that the fossil fuels are created in natural processes that are relatively slow compared to the speed of which the fuel is consumed. The slow production processes also explain the second reason for replacing current energy sources.

There is no indication that the trend in human population growth and energy use will change much over the nearest future and the sources we mostly rely on today might eventually be reduced to small available quantities. A shortage in fossil fuels will not make it possible to cover the demand and the fuel prices might become unreasonably high if other sources of energy are not found.

### 1.3 Report structure

The background described in section 1.1 and 1.2 constitutes the basis for searching and understanding new energy alternatives and related compounds which are less harmful to the climate system as well as to the local environment. This project is a part of this search and will contribute with knowledge about biofuel related compounds. The main idea is to investigate the atmospheric implications of emissions of such compounds with focus on reactivity in the troposphere during daytime. This is done by performing experiments at the Copenhagen Centre for Atmospheric Research (CCAR) and analysing data.

An additional project was performed within the field of atmospheric chemistry modeling together with a research group at the School of Engineering and Applied Sciences at Harvard University.

The report is divided into five main chapters, PART I, II, III, IV and V which are shortly presented below.

**PART II – Aim and motivations:** In this chapter a motivation for atmospheric studies in general is given together with motivations specific for the two studies performed in this work. The motivations for the specific studies include the choice of which atmospheric processes that are going to be investigated and the more general climate aspects for each study are described in PART III and IV respectively. Two sets of project questions to be answered by this report are found in in this part.

**PART III – Atmospheric chemistry and kinetics of lactones:** The chapter starts with an introduction about biofuels and related preventive research. The biofuel related compounds investigated are presented as well as a summary of previous studies of interest. A theoretical section presents the physics behind the methods used followed by a description of the experimental method. The results from determining rate constants and reaction products are presented for all compounds and their atmospheric lifetimes are calculated. Discussion regarding the results is given thorough the presentation of the results, answering to the project questions posted in PART II. General conclusions regarding this study are given at the end of the chapter.

**PART IV – Modeling of tropospheric bromides:** The chapter starts with an overview of the atmospheric bromides investigated and information about available measurements. The global chemical transport model used is briefly described followed by the specific updates of the chemical kinetics which are to be investigated. The results from comparing previous and updated model data with observations are presented and possible implications are discussed. The project questions posted in PART II are answered throughout the chapter and general conclusions regarding this study are given at the end.

**PART V – Summary and Outlook:** Here the conclusions from the two studies are presented. Some thoughts on the use of the results as well as suggestions for future work and improvements are given here.

## **PART II - Aims and motivations**

This master's project consists of a main part with focus on biofuels and a secondary part with focus on tropospheric, inorganic bromine. Both parts are relevant for atmospheric research but are of different character and address different types of questions and scientific problems. The first part which concerns biofuels is of practical, preventive diagnostics character while the second part focuses on understanding the natural atmospheric impact due to emission and removal of inorganic bromine in the troposphere.

Motivations for the addressed atmospheric reactions in this project are given below, followed by short descriptions and motivations of the experimental and modeling work performed. The motivation for each subproject is accompanied with a set of project questions which are to be answered throughout the project report.

### **2.1 Important atmospheric removal processes**

Atmospheric reactions can be initiated by several naturally occurring radicals. Some are more abundant or have a higher reactivity towards e.g. organic compounds than others and are hence more important for concluding lifetimes and atmospheric implications. The major tropospheric removal processes of organic compounds are reactions with hydroxyl radicals, chlorine atoms and ozone, respectively, and in some cases photolysis. Each of these removal pathways is presented briefly below to give an idea of how and why these are important for tropospheric chemistry.

Other reactions, for example with nitrogen oxides (NO and NO<sub>2</sub>), could also be of importance, especially during night time when the concentration of e.g. hydroxyl radicals is low due to the lack of sunlight (see reaction (2A)-(2B) below). There will also be a fraction of the organics that are removed from the atmosphere by deposition onto the Earth's surface and via precipitation. These reactions and removal paths are not investigated in the present work.

#### **2.1.1 Photolysis**

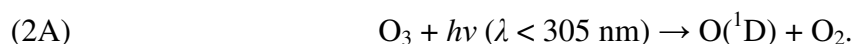
Photolysis, or photo dissociation, is the breakage of a chemical bond due to interaction with an incoming photon (see reaction 3B, on page 21). How likely it is for a molecule to be photolysed in the atmosphere is described by the photolysis rate constant. The photolysis rate constant of a specific molecule depends on the cross section of the molecule (units of cm<sup>2</sup>/molecule), the quantum yield (units of molecules/photon), i.e. the probability that the absorption of a photon will result in photolysis, and the actinic flux (units of photons/cm<sup>2</sup>/s). This gives the rate constant a unit of s<sup>-1</sup>, i.e. a frequency.

The *actinic flux* is the total amount of radiation that is available for photochemical reactions, which includes light reflected and reemitted within the atmosphere, i.e. the irradiation from all directions and the *actinic region* refers to wavelengths larger than 290 nm. The total actinic flux increases with altitude since fewer photons have been absorbed by the atmosphere. Since all the factors contributing to the rate constant are wavelength dependent, the rate constant must be integrated over the entire solar spectrum in order to get the total photolysis rate.

## 2.1.2 Tropospheric reactants

### 2.1.1.1 The hydroxyl radical

The hydroxyl radical (OH) is a central molecule in tropospheric chemistry since it reacts with most volatile organic compounds (VOCs) and several other trace gases such as methane (CH<sub>4</sub>) or nitric acid (HNO<sub>3</sub>). The hydroxyl radical can in principle remove a hydrogen atom from any atmospheric molecule that contains hydrogen to form water [6]. OH can also be added to a double bond and form a hydroxyl group. Although OH can be formed in many ways, the main production route is initiated by the photolysis of ozone (O<sub>3</sub>) followed by reaction with water. O<sub>3</sub> photolysis can result in a single oxygen atom in the first excited state, <sup>1</sup>D, according to the dissociation reaction



The excited oxygen atom can then react with water to form two OH molecules



or it might be de-excited through collisions with surrounding molecules, M, such as N<sub>2</sub> according to



Reaction (2B) and (2C) are competing and the amount of OH formed does hence depend on the concentration of H<sub>2</sub>O and the total pressure [6].

When HO<sub>x</sub> radicals (OH and HO<sub>2</sub>) are present the abundance of OH is sustained via atmospheric reaction cycles, for example through the reaction [6]

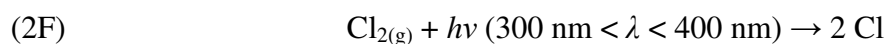
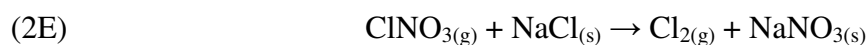


The average global concentration of OH is 10<sup>6</sup> radicals cm<sup>-3</sup> [4, 7]. Using the ideal gas law, this represents a relative concentration of less than one ppt (parts per trillion) at atmospheric pressure. This is a relatively low concentration which is a result of the short lifetime of OH which in its turn is explained by the high reactivity of OH towards many molecules.

### 2.1.1.2 Atomic chlorine

Chlorine atoms (Cl) can react with VOCs in similar ways as OH does, namely through hydrogen abstraction or by adding to a double bond. The rates of chlorine reactions are usually some orders of magnitude larger than the rates of OH reactions [9] towards the same molecule. This makes Cl a possibly significant tropospheric radical even if present in lower concentrations.

In marine areas Cl can be formed through reactions between chlorine nitrate (gas) and sea salt (solid) according to [10]



where  $\text{Cl}_2$  has been photo-dissociated into two Cl atoms. Even if the contribution to atmospheric chlorine from sea salt is still important in the marine boundary layer and in coastal areas, studies show that anthropogenic pollution can form chlorinated molecules which contribute to the importance of chlorine oxidation also in urban areas on the continent [9], [11]. Some molecules that are a result of human activities are  $\text{ClNO}_2$  and  $\text{Cl}_2$  and Cl is a further result of photo dissociation as in (2F) and similarly for  $\text{ClNO}_2$  [11]



From reaction (2F) and (2G) it is evident that light is necessary to produce free chlorine atoms and this is coherent with observations which show that the highest concentration of  $\text{ClNO}_2$  in urban areas are observed in the early morning before sunrise [9]. Consequently the concentration of Cl atoms reaches its maximum some hours after sunrise. Cl concentrations however cannot be measured directly which makes it difficult to estimate the exact contribution of Cl as an atmospheric oxidizer. Cl oxidation of VOCs in the presence of  $\text{NO}_x$  ( $\text{NO}$  and  $\text{NO}_2$ ) can also result in production of OH radicals, so Cl acts both as a primary radical when it reacts directly with the VOC and OH is produced as a secondary radical. On a diurnal average, Cl was shown to make up about 9% of the primary radicals in a large city as Los Angeles and as much as 50% in the mid-morning. Various estimates of Cl concentrations from different areas show an average ranging from  $10^2$  to  $10^5$  radicals  $\text{cm}^{-3}$  [9].

### 2.1.1.3 Ozone

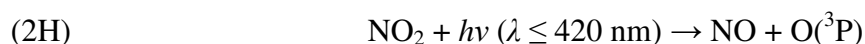
Ozone is an atmospheric oxidant which can react directly with VOCs and also, if exposed to UV light, follow the reactions (2A) and (2B) to generate OH.  $\text{O}_3$  is both produced naturally and as a result of anthropogenic emissions. Most of the  $\text{O}_3$  in the atmosphere is found in the stratosphere, forming the *ozone layer*. This layer shields the surface of the earth from a large fraction of the UV light from the sun by absorbing high energy photons, dissociating (according to reaction (2A)) and reemitting harmless photons of lower energy. The concentration of  $\text{O}_3$  in the stratosphere is about 10 ppm which is several orders of magnitude larger than the tropospheric concentrations which naturally is in the order of tens of ppb, corresponding to  $10^{10}$  molecules  $\text{cm}^{-3}$  [4].

Anthropogenic activities have decreased the amount of stratospheric  $\text{O}_3$  through depletion of the ozone layer by long-lived compounds, mainly containing chlorine and bromine [4]. The opposite effect can be seen on tropospheric concentrations of  $\text{O}_3$  which increase as a consequence of human activities. Tropospheric  $\text{O}_3$  contributes to global warming in the sense that it reduces the  $\text{CO}_2$  uptake by plants [12] and it has negative health effects since it is damaging for the respiratory system [13]. Ozone in the troposphere, together with hydrocarbons, can also compose a part of smog formation in polluted cities.

Tropospheric  $\text{O}_3$  is a secondary pollutant meaning that it is not emitted directly into the atmosphere but is a reaction product originating from other pollutants such as  $\text{NO}_x$ , VOCs, CO and  $\text{CH}_4$  [6].

$\text{NO}_x$  and VOCs are fast in the aspect of  $\text{O}_3$  production and dominant in urban troposphere while CO and  $\text{CH}_4$  are dominant in the remote troposphere, i.e. far away from any anthropogenic pollution sources. These are said to have different “photochemical ozone production potential” which is a measure of the efficiency to produce  $\text{O}_3$ .

An example of an O<sub>3</sub> producing reaction chain is



and this is the most significant source of O<sub>3</sub> in the atmosphere [4]. Once O<sub>3</sub> is formed it will react with NO to re-generate NO<sub>2</sub> or with HO<sub>2</sub> to generate O<sub>3</sub> and the total process is described the photochemical HO<sub>x</sub>- and NO<sub>x</sub> cycles which results in a net production of O<sub>3</sub> molecules. The concentration of O<sub>3</sub> depends on the ratio between NO and NO<sub>2</sub>.

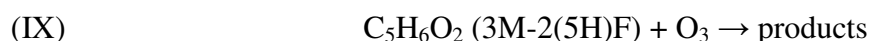
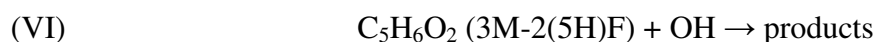
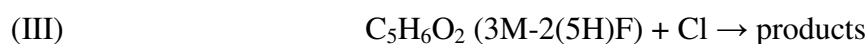
## 2.2 Motivation for PART III and project questions

The major part of this master's project is a study of atmospheric reactivity of cyclic esters, lactones. The study focuses on three species, namely  $\gamma$ -valerolactone (GVL), 2(5H)-furanone (2(5H)F) and 3-methyl-2(5H)-furanone (3M2(5H)F). These are volatile organic compounds (VOCs) which have been suggested as useful, versatile industrial chemicals with biofuels as one application and more detailed information is given in PART III.

VOCs will after being released into the atmosphere eventually be removed through different removal processes which have been described in Section 2.1. To be able to know how anthropogenic emissions will affect the air quality, it is important to know how fast a compound is removed and what products it leaves behind. The aim is hence to use experimental methods to determine reaction rates and product distributions and use the information to interpret atmospheric implications.

The specific questions (Q1-Q4) to be answered by this project are listed below.

**Q1.** What are the rate constants of the following reactions?



- Q2** a. Which products are formed in the reactions (I)-(IX).  
b. What is the difference in product yield when O<sub>2</sub> is present versus absent?  
c. Are any of the products toxic or in other ways a concern for environment or human health?
- Q3.** What are the atmospheric lifetimes of GVL, 2(5H)F and 3M-2(5H)F based on the reactions (I)-(IX)?
- Q4.** Based on the knowledge about atmospheric lifetimes and product distributions, what are the possible atmospheric implications of an increased emission of GVL, 2(5H)F and 3M-2(5H)F?

### 2.3 Motivation for PART IV and project questions

The halogens Cl and Br participate in catalytic ozone destruction cycles in the stratosphere and in polar regions, with bromine being approximately 60 times more reactive towards ozone than chlorine. There is however also a growing interest for the halogens importance in the troposphere and in particular bromine radicals ( $\text{BrO}_x \equiv \text{Br} + \text{BrO}$ ) have been shown to have considerable effect when being implemented in chemical transport models (CTM) [14].

CTM's today are relatively poor at explaining pre-industrial levels of ozone and generally overestimate the concentration, indicating that the natural and anthropogenic climate effects due to radiative forcing of ozone are not fully known [15]. Ozone is as mentioned before oxidized by  $\text{BrO}_x$  and lower ozone levels in the pre-industrial air could have higher Br levels as a consequence. There is a hypothesis that Br also oxidises mercury (Hg) and elevated Br levels would hence yield shorter Hg lifetimes in the atmosphere [14]. Higher ozone emissions could hence further increase the lifetime of Hg when competing in the reactions with  $\text{BrO}_x$ , making it even more of a global pollutant which can be explained by considering the atmospheric transportation seen in Figure 1.1.

Parella et al. [14] included a chemistry scheme with ten bromine containing compounds in a CTM (described in Section 4.1), coupled to the existing chemistry and aerosol physics. The ozone depleting reactions can be found in their paper. By including  $\text{Br}_y$  chemistry in the model Parella et al. showed that simulations of 19<sup>th</sup> century ozone levels improves and a global decrease of present-day  $[\text{O}_3]$  by 6.5% and of  $[\text{OH}]$  by 4% is found.

Recent measurements of photolysis- and reaction rate constants of two compounds included in the model, bromoform ( $\text{CHBr}_3$ ) and bromine nitrate ( $\text{BrONO}_2$ ), suggest different values compared to previous recommendations by Sanders et al. [16]. Since these compounds participate in the  $\text{BrO}_x$  cycling, it is of interest to investigate the effect of the updated rate constants on the global concentration and distribution of bromides.

The aim of this project is to implement the updated rate constants of the kinetic mechanisms of  $\text{CHBr}_3$  and  $\text{BrONO}_2$  respectively and to look at tropospheric effects. The output from model simulations with and without the implementations will be compared. The output from the  $\text{CHBr}_3$  simulations will also be compared with recent aircraft observations [17] to estimate the accuracy of the  $\text{CHBr}_3$  emissions used in the model.



If a difference between observations and model output is found the emission field will be updated to see if a better agreement can be achieved. The implications for tropospheric inorganic bromine ( $\text{Br}_y$ ) and especially  $\text{BrO}_x$  will be analysed and potential effects on ozone interpreted.

The specific questions (Q5-Q8) to be answered by this project are listed below.

- Q5** a. Is the new mechanism with updated  $\text{CHBr}_3$  cross section and  $\text{CHBr}_3 + \text{OH}$  rate constant consistent with HIPPO aircraft campaign observations of  $\text{CHBr}_3$  in the troposphere?
- b. If there are differences between the model output and observations, what is the driving factor for the difference, i.e. can the bias be explained by kinetics or emissions?
- Q6.** How does the updated mechanism affect the  $\text{Br}_y$  and  $\text{BrO}$  distribution in the troposphere, in particular the tropical upper troposphere?
- Q7.** What is the timescale (seconds, hours, days) for Br release due to bromoform photon oxidation and OH oxidation respectively?
- Q8.** How does the new mechanism with updated  $\text{BrONO}_2$  cross section and  $\text{BrO} + \text{NO}_2$  rate constant affect the  $\text{Br}_y$  and  $\text{BrO}$  distribution in the troposphere, in particular the tropical upper troposphere?

# **PART III – Atmospheric kinetics of lactones**

## **3.1 Background**

### **3.1.1 Biofuels**

Suggested alternatives to the petroleum based fuels are biofuels, of which ethanol probably is the most well-known. There is a clear distinction between fossil fuels and biofuels in how the raw material is produced. Fossil materials are formed beneath the Earth's surface from biological material that undergoes anaerobic decomposition for millions of years. Biofuels are produced from biological raw materials that are grown and harvested at much shorter timescales. Biofuels are renewable in the sense that the carbon source is atmospheric carbon in combination with sunlight from the photosynthesis. Hence in a theoretical optimal case the use of biofuels would result in zero net emission of CO<sub>2</sub> into the atmosphere and be so called *carbon-neutral* [18].

A very simple example of a biofuel is wood which can be burnt directly. Other biofuels are produced converting e.g. plant material with long molecules to a smaller molecule such as ethanol. Ethanol is already used in some energy sectors, for example blended with regular gasoline for use in car engines. Ethanol can be produced from fermentation of sugar- or starch-based crops such as sugarcane and corn. Biodiesel is produced from fat molecules, e.g. vegetable oil or animal fat [18].

It is desirable to produce biofuels from cellulosic biomass instead of edible sources such as corn- or sugar-based biomass, otherwise there would be an increased competition between food- and fuel feedstock. Some suggestions which are already under investigation are giant reed [19] and switch grass [20] which has the feature of high production to relatively low inputs in common. The two businesses could even benefit from each other if waste products from agricultural industry, such as stalks and weed, are used in the production of cellulosic biomass [20].

One great challenge in biofuel production and research is to obtain a quality similar to petroleum when it comes to price and energy density. A large energy consuming sector is transportation with heavier vehicles such as trucks, airplanes and ships which need more power than e.g. ethanol can provide [20]. It is difficult to match gasoline in both these aspects but there is ongoing research in developing production techniques that have a high yield to a low price. It is important to consider factors associated to the entire process from biomass to combustion, including e.g. land use, the time and energy it takes to produce and refine the fuel and also the final energy density of different fuel molecules. It has been suggested that it could be favourable with larger alcohols as biofuels [20], with more than five carbon atoms compared to methanol which contains two carbon atoms. The more similar to today's fossil fuels the biofuel molecules could be, the easier it would be to replace the old fuels without the need of drastic changes in the existing infrastructure and materials. Hydrocarbons other than alcohols have also been suggested and some of these will be in focus in this project.

### 3.1.2 Preventive research

In the section 3.1.1 the typical “fuel-properties” of the biofuels were mentioned briefly but it is also important to look at other properties. To avoid undesired environmental effects it is important to investigate the possible effects of a large scale use, such as enhanced global warming and air pollution on both local and global scale. There are historical examples where lack of knowledge has resulted in negative effects on environment and health. Sometimes the effects are not direct and hence discovered at a late phase. One example is the use of Freons (chlorofluorocarbons) as refrigerants, eventually resulting in O<sub>3</sub> depletion in the stratosphere [21].

A biofuel is often rated by how much it reduces CO<sub>2</sub> emissions compared to conventional fuels and hence focus is on reducing the climate change. There can however be other effects of equal importance and one such issue is the local air quality in areas where the fuel might be produced or used. Hence switching to certain biofuels might not be the answer to the overall climate aspect and therefore it is important to look at the air quality in advance as well as the greenhouse gas emissions.

It is relevant to look at the impact not only of the fuel itself but also of precursors in the production process as well as of products from combustion and from atmospheric reactions of the fuel itself. All of these compounds: precursors, biofuels and products, will reach the atmosphere as a result of leaks and there can also be unburnt fuel escaping from engines. There are many properties of these compounds that should be investigated. An example is the vapour pressure which is an important factor for how much of the substance that will be released into the atmosphere just from vaporization. Another property of interest when suggesting substances for biofuels is the water solubility which can become important e.g. in production processes or through dilution by atmospheric humidity [20].

In order to do a prognosis of the atmospheric fate and implications of different compounds there are some specific properties that should be investigated. The reactions between the molecule and OH, Cl and O<sub>3</sub>, respectively, need to be analysed, as motivated in section 2.1. The rates of these reactions will give the lifetime of the compound in the atmosphere and hence how far it can be expected to be transported. The products from these reactions are also interesting since some might be greenhouse gases, toxic or have other implications related to the environment and human health. Different molecules absorb and emit radiation in different wavelengths regions and this can give information on, among other things, their global warming potential [4].

### 3.1.3 Furans – chemical properties

Furans are organic, heterocyclic molecules containing five atoms in a ring structure, of which one is an oxygen atom and four are carbon atoms. The molecule called furan, C<sub>4</sub>H<sub>4</sub>O, is the one with the lowest molecular weight in this group. It has a hydrogen atom connected to each carbon and hence it has two double bonds. The corresponding structure without double bonds, i.e. with four additional hydrogen atoms is called tetrahydrofuran (THF). The structure of furan and THF can be seen in Figure 3.1, where the numbers used for labelling the specific atoms are seen for furan and these are applicable throughout the rest of this work.

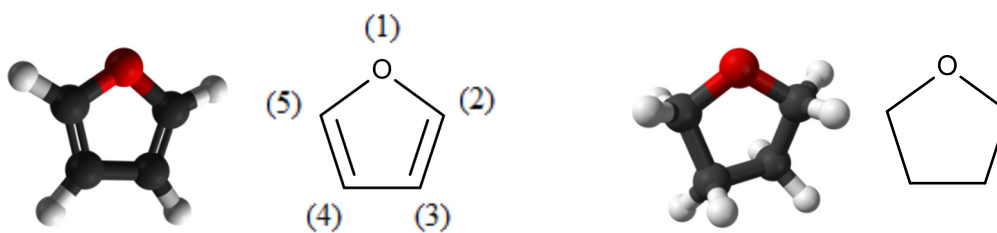


**Figure 3.1.** Chemical structure of furan (left) and tetrahydrofuran (right).

In the present work the focus will be on three different molecules, namely  $\gamma$ -valerolactone (GVL), 2(5H)-furanone (2(5H)F) and 3-methyl-2(5H)-furanone (3M2(5H)F). These all have a five-atom cyclic structure and furthermore they all have a double bonded oxygen atom at the first carbon in common, i.e. these are cyclic esters (lactones). The chemical structures of the molecules are shown in Figure 3.2.

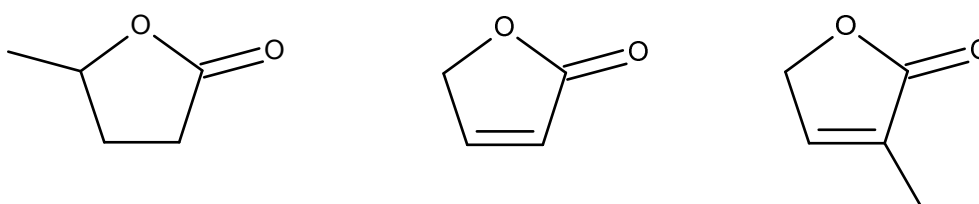


**Figure 3.2.** Chemical structure of  $\gamma$ -valerolactone (left), 2(5H)-furanone (middle) and 3-methyl-2(5H)-furanone (right).

Properties that can be investigated by performing kinetic experiments with these molecules are the possible consequences of a double bond within the ring and the presence of methyl groups in terms of how these affect the reaction rates and product distribution. The physical properties of these substances are not all known but some are listed in Table 3.1 below. The values in Table 3.1 are obtained from Sigma Aldrich Safety Sheets [32] if nothing else is stated.

**Table 3.1.** Physical properties of three lactones and ethanol.

	GVL	2(5H)F	3M2(5H)F	Ethanol
Boiling point (°C) at atm. pressure	207-208	212-214 [23]	222 [24]	78-80
Ignition point (°C)	96	101	93	14
Vapour pressure (kPa) at 298 K	0.65 [25]	No data	No data	5.95
Solubility (%)	100 [26]	No data	No data	100
MW/g mol <sup>-1</sup>	100.12 [25]			46.07 [25]

In Table 3.1 it can be seen that, at least for GVL, the vapour pressure is about one order of magnitude lower than for ethanol. A low vapour pressure is desirable in order to reduce the emissions into the atmosphere due to vaporization.

### 3.1.4 Furans - Production and use as fuels and industrial chemicals

Even if many properties of GVL, 2(5H)F and 3M2(5H)F have not been investigated, including the atmospheric impact, there is more literature in the field of production. The furan derivatives belong to the so called *second generation* biofuels since they are produced from lignocellulose, compared to the *first generation* biofuels which are produced from sugars, starch and vegetable oil. The most investigated of the three lactones is GVL and some examples of studies performed and results are presented below.

Transforming lignocellulose to useful molecules usually requires an advanced process but it has been shown that there is a comparatively simple and also cheaper way to produce valuable compounds such as *levulinic acid* without breaking down the cellulose to simple sugars first. Levulinic acid and its derivatives, including GVL, constitutes a platform of molecules referred to as *valeric biofuels* by Lange et al. and others thereafter. [27] In the paper by Lange et al. the manufacturing process of valeric biofuels is described together with a study which showed that the valeric biofuels are compatible with gasoline in the aspects most important for replacing current fuels or use mixtures of valeric and current fuels. Another example of compatibility can be found in Bereczky et al. [28] who have shown that mixtures of GVL and diesel used in engines result in little effect on performance and NO<sub>x</sub> emissions but reduced CO emissions as well as black carbon and unburnt fuel escaping the engine.

A more detailed description of processes for converting lignocellulosic biomass to valeric biofuels can be found in e.g. the paper by Wettstein et al. [29] and specifically the conversion from fructose to dimethylfuran through dehydration and hydrogenolysis in the paper by Román-Leshkov et al. [30]. Valeric biofuels are thus not produced through fermentation in contrast to ethanol.

As mentioned before, the quality of the fuel, the cost and the possibility for large scale, commercial production are in focus. Reducing the number of steps in the production process is a good way of keeping the cost down. In a study by Galletti et.al. [19] a process is described where GVL is formed in a combined process directly from the biomass raw material. Some other examples of converting biomass sources to useful chemicals and fuels which have been tested are furfural (C<sub>4</sub>H<sub>3</sub>OCHO) as a biofuel produced from e.g. corncobs using GVL as a solvent [31], dimethylfuran as a biofuel from biomass-derived fructose [30].

Furan derivatives have not only been suggested as biofuels but the properties of valeric platform molecules makes them precursors of many other valuable chemicals, for example “green solvents”, implying solvents with reduced health and environmental hazardousness. [32] If GVL e.g. can be used as a solvent in further biofuel production since it solubilize lignocellulose it might not even be necessary to remove it from the end product since GVL is also functional as a fuel. GVL can also be processed further to hydrocarbons like butene, which can be used as gasoline or be combined into longer molecules for us as jet fuel.

GVL has also been observed as a product from the reaction 2-methyl-tetrahydrofuran + Cl in a previous study of tetrahydrofurans by C. Andersen at Copenhagen University [22] and 2(5H)F is formed by atmospheric oxidation of toluene (C<sub>7</sub>H<sub>8</sub>) [33].

### 3.1.5 Atmospheric impact of furans

Atmospheric studies on GVL, 2(5H)F and 3M-2(5H)F are almost non-existing. The only studies available are of the rate constant for the reaction between GVL and OH by Barnes et al. from 2014 [34] and the rate constant for the reaction between 2(5H)F and O<sub>3</sub> by Grosjean and Grosjean from 1998 [35]. These are otherwise common types of experiments within atmospheric chemistry and physics and there are some studies on compounds that are similar to these. Such previous studies could give indications on approximate expected reaction rates and perhaps also some hints on favourable reaction pathways.

In Table 3.2 a summary over several cyclic compounds and their reaction rate constants with Cl, OH and O<sub>3</sub> are presented.

**Table 3.2** Summary of literature rate constants of the atmospheric reactions for several furan derivatives with Cl, OH, and O<sub>3</sub>.

Name	Structure	$k_{Cl} \cdot 10^{-10}$ /cm <sup>3</sup> molecule <sup>-1</sup> s <sup>-1</sup>	$k_{O_3} \cdot 10^{-18}$ /cm <sup>3</sup> molecule <sup>-1</sup> s <sup>-1</sup>	$k_{OH} \cdot 10^{-11}$ /cm <sup>3</sup> molecule <sup>-1</sup> s <sup>-1</sup>
2(5H)-furanone		-	0.22 ± 0.05 [35]	-
Maleic anhydride		-	-	0.145 ± 0.01 [36]
γ-valerolactone		-	-	0.281 ± 0.034 [34]
Tetrahydrofuran		2.50 ± 0.39 [37] 2.71 ± 0.34 [38]	-	0.88 ± 0.18 [39] 1.80 ± 0.07 [40] 1.78 ± 0.16 <sup>a</sup> [41] 1.59 ± 0.39 <sup>b</sup> [42]
2-methyl-tetrahydrofuran		-	-	2.2 [43]
Furan		2.0 ± 0.2 [44]	2.42 ± 0.28 [45]	4.19 ± 0.21 [46] 4.01 ± 0.30 [45]
2(3H)-furanone		-	-	4.45 ± 0.26 [36]
2,5-dihydrofuran		4.48 ± 0.59 [37]	16.55 ± 3.1 [47]	6.45 ± 1.69 [47]
5-methyl-2(3H)-furanone		-	-	6.90 ± 0.46 [36]
2-methylfuran		4.1 ± 0.2 [44]	-	7.31 ± 0.35 [48] 6.19 ± 0.30 [46]
3-methylfuran		4.2 ± 0.3 [44]	-	9.1 ± 0.3 <sup>1</sup> [49] 11.3 ± 2.2 [50] 8.73 ± 0.18 [48]
2-ethylfuran		4.6 ± 0.3 [44]	-	10.77 ± 2.11 [46]
2,3-dihydrofuran		4.52 ± 0.99 [37]	4432.0 ± 790 [47]	11.95 ± 2.79 [47]
2,3-dimethylfuran		-	-	12.6 ± 0.4 [48]
2,5-dimethylfuran		5.7 ± 0.3 [44]	420 ± 90 [51]	12.5 ± 0.4 [48] 13.21 ± 0.92 [46]

<sup>1</sup> At low pressure, < 10 Torr.

There is most data is available for reactions with OH, and in the table the molecules are ordered by increasing rate constant towards OH. If nothing else is stated, all rate coefficients are for the conditions of roughly room temperature and atmospheric pressure, or are an average from measurements over a range of temperatures and pressures in these regions. Where no data is presented, there are no available results to the best of my knowledge.

Some trends that can be observed by comparing the kinetic data in Table 3.2 are that carbonyl (double bonded oxygen) groups seem to decrease the reactivity of furan derivatives towards OH while addition of substituents (methyl- and ethyl groups) seem to increase the reactivity. The effect on reactivity due to number and position of double bonds is not straightforward from the available data. The reaction rates for Cl and O<sub>3</sub> reactions follow a similar trend with some exceptions.

## 3.2 Physical concepts

In this section some principles and approximations are described which are necessary for understanding, performing and interpreting the experimental work described in Section 3.3.

### 3.2.1. Molecular physics

In order to do atmospheric investigations there must be a way to identify and quantify gaseous compounds in a mixture. In this project the physical properties of different bonds between atoms is utilized for such diagnostic measurements. From atomic and molecular physics it is known that atoms and molecules have several energy states and this energy can be measured by observing either emitted or absorbed light from a sample. In this project no atomic compounds are measured and hence the focus will be on molecular physics.

The total energy of a molecule is built up of its electronic, vibrational and rotational energy, which are in the order of 1 eV, 0.1 eV and 0.001 eV respectively. A molecule can transfer from a lower energy state,  $E_1$ , to a higher,  $E_2$ , by absorbing a photon of the energy  $E_2 - E_1$ , see Figure 3.3a. The molecule will eventually go from this excited state to the ground state or another lower energy level if no further energy is supplied to the system and it will then emit a photon with an energy corresponding to the transition, also seen in Figure 3.3a.

When a molecule absorbs and emits electromagnetic radiation in the infrared (IR) region it is called *IR active*. The IR radiation is of relatively low energy which corresponds to the typical energies of molecular vibrations. Molecules that vibrate can have an oscillating dipole moment which can interact with the oscillations of the electromagnetic radiation. Hence an IR photon can be absorbed by a molecule and leave it in a higher vibrational state. Molecules that are not IR active are those where the vibrations are symmetrical around the center and hence no oscillating dipole is produced, for example symmetrical homonuclear, diatomic molecules like O<sub>2</sub> and N<sub>2</sub>. The vibrational frequencies are unique for each molecule but there are also characteristic frequencies found in well-defined regions for specific functional groups. Since the background gases O<sub>2</sub> and N<sub>2</sub> are “invisible” to IR light while other molecules such as VOCs and some radicals are not, IR spectroscopy is a good method for performing atmospheric investigations.

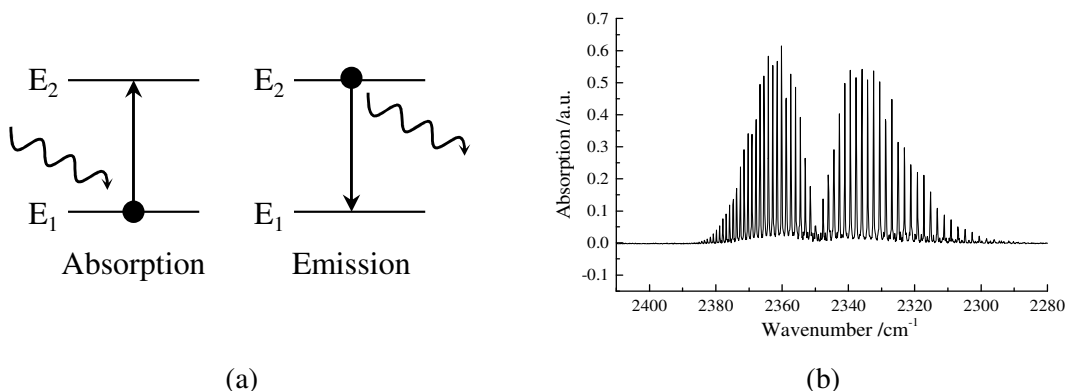


**Figure 3.3.** (a) Illustration of energy transition due to photon absorption and emission. (b) Rotational vibrational spectrum of  $\text{CO}_2$ .

For smaller molecules it can be possible to see features of the rotational transitions (order of 0.001 eV) as well as vibrational (0.1 eV) in so called rotational-vibrational spectra, of which an example is shown in Figure 3.3b which shows the absorption spectrum of  $\text{CO}_2$  in a limited wavenumber region.

Due to the unique characteristics of the vibrations of individual bonds or functional groups in different molecular constructions, these are associated with so called characteristic group frequencies of which some are listed in Table 3.3. Different vibrational modes will also result in different absorption frequencies even if present in identical functional groups. The possible vibrations between three atoms are shown in Figure 3.4.

The characteristic group frequencies are mainly found in a region above  $1500\text{ cm}^{-1}$ , which can be seen from Table 3.3. Features below this frequency generally belong to the entire molecule, i.e. a combination of the vibrations and is hence unique for every molecule. For this reason, the frequency region below  $1500\text{ cm}^{-1}$  is typically called the finger-print region [52].

**Table 3.3.** Some functional groups and important corresponding characteristic group frequencies. When a general relative intensity is known this is shown as well. [52].

Structure	Frequency region / $\text{cm}^{-1}$	Intensity
Saturated C-H stretch	2960-2850	strong
C-H deformations	1470-1430	variable
$-\text{CH}_3$ symmetrical deformation	1390-1370	medium
O-H bending (alcohol)	1410-1260	strong
C-O stretch, saturated ethers	1150-1040	strong
C=O, (carbonyl) stretch	1850-1700	strong
$-\text{COCl}$ , acid chlorides	1815-1790 (saturated) 1790-1750 (unsaturated)	
$-\text{CHO}$ , aldehydes	1725-1700	
$-\text{CO}_2\text{H}$ , saturated carboxylic acid	1725-1700 3000-2500	
$-\text{CO-O-CO-}$ , acid anhydrides	1800-1850 (more intense if acyclic) 1790-1740 (more intense if cyclic)	



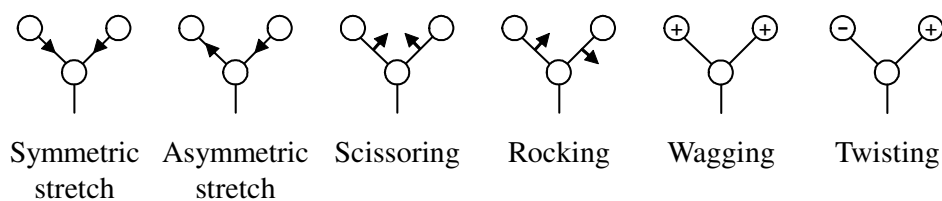


**Figure 3.4.** Vibrational modes for a tri-atomic group.

### 3.2.2 Beer-Lambert law

The Beer-Lambert law describes the relation between the intensity of electromagnetic radiation before and after absorption by a sample. By looking at light which has passed through a medium and comparing it to unaffected light it is possible to determine the content of the medium. In Figure 3.5 the intensity is shown as a function of distance, where  $l$  is the length of the sample and  $n$  is the refractive index of the sample [49], [8].

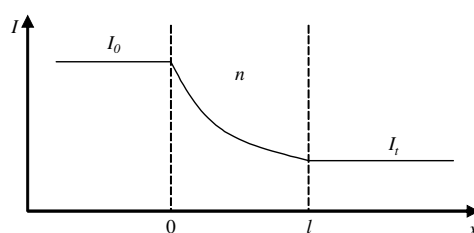


**Figure 3.5.** Illustration of absorption and the Beer-Lambert law.

The absorbance can be related to the initial intensity  $I_0$  and the transmitted intensity  $I_t$  as

$$A = \ln \frac{I_0}{I_t} = \ln T^{-1} \quad (3.3)$$

where  $A$  is absorbance,  $T$  is transmittance and  $T$  ranges from zero to one. The absorbance depends on the absorption cross section ( $\sigma$ ) and the number density of the molecules in the sample ( $c$ ) as well as on the optical path length ( $l$ ) and the Beer-Lambert law can alternatively be expressed as

$$A = \sigma cl. \quad (3.4)$$

This relation is useful when converting the concentration between spectra obtained with different path lengths. When using IR spectroscopy the absorbance and transmittance are treated as functions of photon wavelength, since molecules can be highly absorbing in some wavelength ranges while transparent in others.

### 3.2.3 Fourier Transform Infrared Spectroscopy

When studying the absorption or emission of a sample, the choice of light source, spectroscopic method and detector depends on what is of interest to observe. When looking at how a mixture of gases changes with time in atmospheric conditions it is desirable to resolve a spectrum of different wavelengths simultaneously with good resolution. This can be obtained with a Fourier transform spectrometer, specifically in the present study a Michelson interferometer is used.

The principle behind a Michelson interferometer, and other dual-beam interferometric spectrometers, is to use a single broadband light source, split the light into two different paths and in a controlled way successively introduce a difference in path length before recombining the light again. An illustration of a Michelson interferometer can be seen in Figure 3.6.

In Figure 3.6 the optical components of the interferometer are shown where the light is introduced via some inlet aperture. The beam splitter is partially reflective and transmits fifty percent of the incident light, splitting the light into two perpendicular paths which are in turn reflected back by the planar mirrors M1 and M2 and are recombined at the beam splitter, travelling as one wave towards the detector. The mirror denoted M1 is fixed while the mirror M2 is movable. When the distance  $L1$  is equal to the distance  $L2$  the path difference is zero and the light will interfere constructively when recombined. If the mirror instead is moved a distance  $d/2$  from this position, a path difference of  $d$  is introduced. When  $d$  is equal to an integer number of the wavelength of the incoming light there will still be constructive interference and similarly a half integer value of the wavelength gives destructive interference. When scanning the mirror M2 over a longer distance a periodic fringe pattern can be measured at a detector. This signal, as a function of path difference,  $d$ , is called an interferogram and is the Fourier transform of the spectrum of the light that reaches the detector. The idea of Fourier transform spectroscopy is consequently to measure an interferogram, and calculate its Fourier transform to obtain a spectrum with intensity as function of frequency instead of length [53], [54].

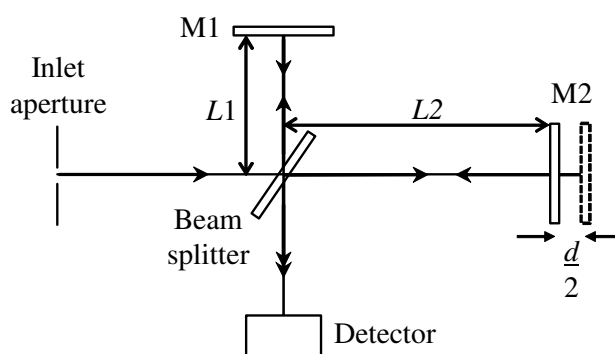


Figure 3.6. Schematic illustration of a Michelson interferometer.

### 3.2.4 Chemical kinetics

#### 3.2.4.1 First order reactions

In chemical kinetics a reaction can be characterized by the number of reactants involved, of which the simplest is a unimolecular reaction known as a first-order reaction. Such a reaction can be written as



which could for example be illustrate by photo dissociation, or photolysis, which is written as



The rate of change in concentration of compound A can be expressed as

$$\frac{d[A]}{dt} = -k_1[A] \quad (3.8)$$

where  $k_1$  is the first-order rate coefficient and has the unit  $s^{-1}$ [4]. It is standard to use the notation  $J$  instead of  $k$  specifically for rate constants referring to photolysis [4].

The solution to this differential equation is a concentration which decays exponentially with time from an initial concentration  $[A]_0$ ,

$$[A]_t = [A]_0 e^{-k_1 t}. \quad (3.9)$$

#### 3.2.4.2 Second order and thermonuclear reactions

A second-order reaction, or bimolecular reaction, can be written as



or as



where M is another molecule which does not react but removes excess energy if the molecules A and B produce an excited intermediate product. Reaction (3D) is called a thermonuclear, or third-order, reaction and in the atmosphere M is generally either O<sub>2</sub> or N<sub>2</sub>.

The rate of change of the concentration of compound A in a second-order reaction is

$$\frac{d[A]}{dt} = -k_2[A][B] \quad (3.10)$$

where  $k_2$  is the second-order rate coefficient and has the unit cm<sup>3</sup>molecule<sup>-1</sup>s<sup>-1</sup>[4].

#### 3.2.4.3 Pseudo-first-order approximation

The rate law for a second order reaction is given in equation (3.10) above. If compound B exists in large excess its concentration can be approximated to be unchanged with time, i.e. [B] can be replaced with a constant value [B]<sub>0</sub>. The second-order rate law can then be expressed as a first-order rate law instead, which is called the pseudo-first-order approximation, and equation (3.10) can instead be written as

$$\frac{d[A]}{dt} = -k'[A] \quad (3.11)$$

where

$$k' = k_2[B]_0. \quad (3.12)$$

The solution to (3.11) is an exponential function as in (3.9).

#### 3.2.4.4 Reaction rates and atmospheric lifetime

The atmospheric lifetime of a compound is a representation of the average duration of all the fates a compound can undergo from emission to removal. The lifetime,  $\tau$ , of a compound is defined as the time it takes for the concentration to reach  $1/e$  of its original value. From the equation  $[A]_t = [A]_0 e^{-k_1 t}$ , the lifetime of compound A for removal by chemical processes is equal to the inverse of the rate, according to

$$\tau_A = \frac{1}{k[\text{radical}]} \quad (3.13)$$

If several radicals, say B and C, react with compound A the reciprocals of the individual lifetimes add up to give the total lifetime of A which can be written as

$$\frac{1}{\tau_A} = \frac{1}{\tau_{AB}} + \frac{1}{\tau_{AC}} = k_{AB}[B] + k_{AC}[C] \quad (3.14)$$

and the effectiveness of a removal process does hence depend both on the rate constant and the abundance of the radical. A compound will however not only be removed via chemical reactions so a more accurate description of the total lifetime includes the removal through dry deposition, wet deposition as well as transport to the stratosphere. This can be written as

$$\tau_A = \frac{1}{k_A^D + k_A^W + k_A^T + k_A^C} \quad (3.15)$$

where A denotes the species removed and  $k^D$  is the loss rate constant for dry deposition,  $k^W$  for wet deposition,  $k^T$  for transport and  $k^C$  for all the chemical reactions.

## 3.3 Method

### 3.3.1 Introduction

In this project in situ Fourier Transform Infrared (FTIR) Spectroscopy was used to investigate atmospheric fates of the molecules described in Section 3.1.3. Some advantages of this method, in addition to the general advantages of IR spectroscopy mentioned in section 3.2.3, is that the measurements are fast making temporal measurements of reactions performable and the FTIR system directly gives spectra with intensity (absorption or transmission) as a function of wavenumber.

The aim of a typical experiment in this project is to identify molecules in an enclosed volume and follow their concentrations to get an idea of reaction rates and mechanisms. There is as previously described a method which can give the composition of a gas mixture in a manageable way. The FTIR spectrometer must also be combined in a setup with a container, where gases can be let in and out in a controlled way, as well as a detector. The detailed features of such the setup used are described in the following section.

### 3.3.2 Experimental setup

In this project, laboratory experiments were carried out in a *photochemical reactor* [55] also known as a smog chamber. This photochemical reactor is situated at the Copenhagen Centre for Atmospheric research (CCAR) at the Department of Chemistry, University of Copenhagen. The equipment consists of a few main parts; the manifold, the reaction chamber and a spectrometer setup. There are also control systems for temperature and lamps for irradiation of the sample, some optic equipment and pumps to evacuate the different parts. The setup has been used for a number of similar studies, of which some can be found in the paper by Andersen et al [56] and by Sulbaek Andersen et al. [57]. A sketch of the photochemical reactor setup used is shown in Figure 3.7. The different parts are described in more detail below.

#### 3.3.2.1 Spectrometer properties

The spectrometer used is of the type Bruker IFS 66v/S which covers a wide spectral range in the IR and visible regions. It is possible to switch between different light sources, beam splitters and detectors for different purposes and spectral regions.

The standard light source which was used is a SiC globar which is heated to emit mid-infrared (MIR) light, corresponding to a spectral range of  $7500\text{-}30\text{ cm}^{-1}$ . The interferometer is a high throughput Michelson interferometer (described in section 3.2.3) and the position of the moving mirror is controlled using a HeNe laser at  $633\text{ nm}$  with  $1\text{ mW}$  output. The standard beam splitter consists of a multilayer coating on KBr and a semiconductor detector of type MCT (mercury cadmium telluride) was used. The detector operates at low temperatures and is cooled with liquid nitrogen. The resolution used in the data collection was  $0.25\text{ cm}^{-1}$ .

#### 3.3.2.2 Reaction chamber

The reaction chamber is made of quartz glass, has the shape of a cylinder with a length of two meters and a volume of 101.4 liters. This chamber is situated in an insulated box which also contains 8 UV-A lamps with a wavelength range of  $325\text{-}380\text{ nm}$ , 16 UV-C lamps with the wavelength  $254\text{ nm}$  and 12 “sunlight lamps” with a broad wavelength range from about  $300\text{ nm}$  up to infrared light. There is a flow of air around the chamber cylinder and it is possible to vary the temperature with a built in ventilation system. The temperature is in this study set to  $298 \pm 3\text{ K}$ . The sample is heated when irradiated with UV lights and the ventilation is adjusted accordingly, but there is still a variation of a few degrees in temperature.

There is a pump system to evacuate the chamber and the chamber is also connected to the manifold which is used as an inlet system of desired gases. When the gases enter the chamber, the flow is distributed over many holes along the inlet tube to get a well-mixed sample. At the ends of the quartz glass cylinder there are gold-coated mirrors which can reflect IR radiation.

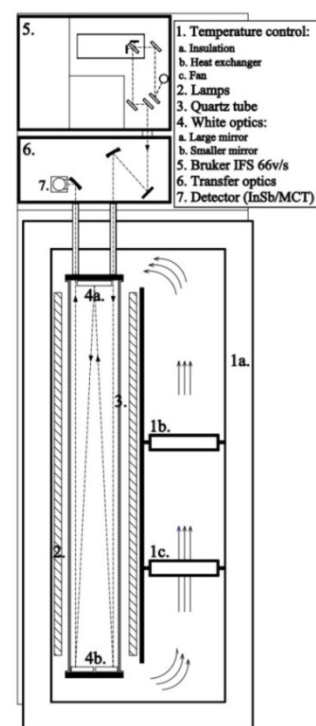


**Figure 3.7.** Schematic view of the photochemical reactor setup at CCAR, including (from the top) spectrometer, optics and reaction chamber with lamps and temperature control. [55]

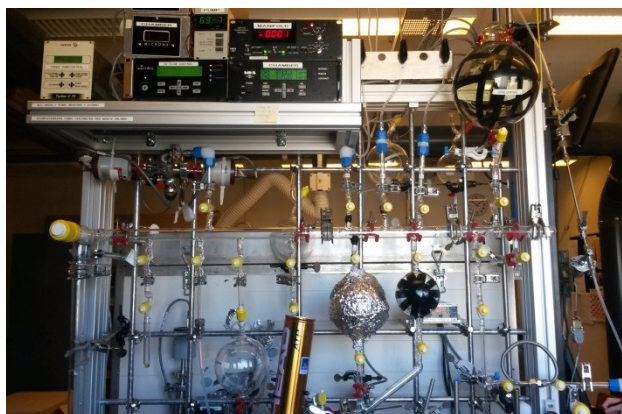
These mirrors, two spherical in one end and one flat in the other end, can be adjusted so that the light from the IR source will be focused and travel through the chamber more than once in order to create a longer path length than the 2 meters of the tube itself. In this study an optical path length of 64 m, 50.75 m or 42.86 m was used. The path length was changed after realignment which was done a couple of times due to reparation of the setup.

### 3.3.2.3 Manifold

The purpose of the manifold system is to make it possible to introduce a certain amount of a specific gas into the reaction chamber in a controlled way. The manifold is situated at one of the short sides of the reaction chamber container.

There is a main glass tube (horizontal) on which several subparts can be connected (vertical). The bath gases  $N_2$ ,  $O_2$  and Air (synthetic) are always connected through pipes to larger tubes. There is also a chlorine gas container and an  $O_3$  container connected, which can be seen in Figure 3.8. The rest of the connections are easily replaceable and it is possible to connect e.g. gas bottles through Teflon hoses or finger tubes with liquids. There are a couple of containers with known volumes that can be sealed off and used to measure the amount of gas which is finally inserted into the chamber, since the volume fractions between these small containers and the chamber are known.

These reference volumes are located in between the horizontal glass tube and the inlet to the chamber which can be seen in Figure 3.9. A pump with a trap cooled with liquid nitrogen is situated at the far left end of the manifold. There is a pressure gauge connected to the manifold which measures the pressure over the entire manifold system, or to be exact, over those parts that are open and connected for the moment.



(a)



(b)

**Figure 3.8.** (a) Manifold gas inlet system for the photochemical reactor. (b) Close-up view of the  $O_3$  trap after approximately 70 min of  $O_3$ -generation .

### 3.3.2.4 Computers – software and control system

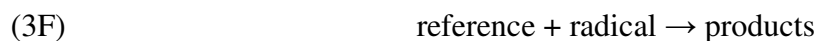
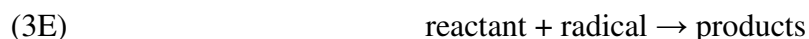
For controlling the spectrometer and managing data a software called OPUS is used. It is provided by the Bruker Corporation, which is the manufacturer of the spectrometer used (see Section 3.3.2.1). This software is used for everything from setting optics parameters and acquiring data in different ways to view, manipulate and edit data files. More information on how OPUS is used in this project is described in Section 3.3.3.5 and 3.3.4.

In a few parts of this project software is used to do spectrum fitting for quantitative measurement of species. The program *MALT* (Multiple Atmospheric Layer Transition) uses molecular frequencies from a database and calculates spectra from known parameters and uses these to fit spectra to measurements [58]. When using *MALT* parameters from the measurement such as temperature, pressure and path length are included and several species can be quantified simultaneously. Through iteration the best fit is obtained and the concentration is given in the output.

A computer is also used to control the pressure in the O<sub>3</sub> generator, which can be set to a minimum and a maximum threshold value. Temperatures in different parts of the setup are measured with thermocouples and displayed momentarily. The temperature is logged and saved for entire experiments. The lamps are also controlled by a computer program, LabView, and a pedagogical view over all the lamps in the chamber container is shown. The desired lamps and photolysis time can be chosen. When the timer is started the lit lamps are indicated on the screen and there is also a web camera inside the chamber container which shows live images of the chamber and lamps.

### 3.3.3 The relative and absolute rate methods

Reaction rate constants can be determined using the relative rate method [59]. With this method two reactions are compared of which one has a known rate constant. When two compounds, from now on called reactant and reference respectively, react in parallel with the same radical it is possible to find the unknown rate constant by following and comparing the change in concentration over time for both compounds. Suppose that the only reactions taking place are the following:



where the rate constant is  $k_{react}$  for (3E) and  $k_{ref}$  for (3F). The change of concentration with time can then be expressed as for second-order reactions, described in section 3.2.4,

$$\frac{d[\text{reactant}]}{dt} = -k_{react}[\text{reactant}][\text{radical}] \quad (3.16)$$

and

$$\frac{d[\text{reference}]}{dt} = -k_{ref}[\text{reference}][\text{radical}]. \quad (3.17)$$

The two reaction rate constants can then be related through

$$\ln\left(\frac{[\text{reactant}]_0}{[\text{reactant}]_t}\right) = \frac{k_{\text{react}}}{k_{\text{ref}}} \ln\left(\frac{[\text{reference}]_0}{[\text{reference}]_t}\right). \quad (3.18)$$

where  $[\text{reactant}]_0$  and  $[\text{reference}]_0$  are the initial concentrations and  $[\text{reactant}]_t$  and  $[\text{reference}]_t$  are the concentrations at time  $t$ . There is hence a linear relation between the natural logarithm of the change in concentration of the reactant and the reference respectively. A plot of  $\ln([\text{reactant}]_0/[\text{reactant}]_t)$  versus  $\ln([\text{reference}]_0/[\text{reference}]_t)$  will yield a straight line with a slope  $k_{\text{slope}}$ , which from equation (3.18) is equal to  $k_{\text{react}}/k_{\text{ref}}$ . With  $k_{\text{slope}}$  and  $k_{\text{ref}}$  known, the rate coefficient for the reaction between the reactant and the radical is

$$k_{\text{react}} = k_{\text{slope}} \cdot k_{\text{ref}}. \quad (3.19)$$

The rate constant of the reference reaction should preferably be in roughly the same order of magnitude as the expected  $k_{\text{reactant}}$ . At least two different references should be used when determining reaction rates with the relative rate method.

For absolute measurements of rate constants a plot of  $\ln([A]_t/[A]_0)$  versus time  $t$ , where  $[A]_t$  and  $[A]_0$  are the concentrations of compound A at time zero and  $t$  respectively, will yield points on a straight line with the slope  $k'$ . The value of  $[B]_0$ , can be varied slightly between measurements in order to get slightly varying  $k'$ . The values obtained for  $k'$  can then be plotted as a function of  $[B]_0$ , yielding a straight line with a slope which is the rate constant for the “absolute pseudo-first-order measurement”, i.e.  $k_2$  in the equation (3.12) [60], [61].

In Table 3.4. the reaction rate constants of the references used in this work are presented. Most values are from a recent evaluation by Sander et al. [16] For the reactions  $\text{C}_2\text{H}_2 + \text{Cl}$  and  $\text{C}_3\text{H}_6 + \text{Cl}$  there were large differences between the different data compilations as a result of rather scarce and scattered data in the literature. Hence for these reactions, marked with “\*” in Table 3.4, the most values from the recent publication by Iwasaki et al. [3] are used as references for the present study.

**Table 3.4.** List of compounds used as references/scavenger and their rate constants.

Reference/scavenger	$k_{\text{Cl}} \cdot 10^{-11}$ /cm <sup>3</sup> molecule <sup>-1</sup> s <sup>-1</sup>	$k_{\text{O}_3} \cdot 10^{-18}$ /cm <sup>3</sup> molecule <sup>-1</sup> s <sup>-1</sup>	$k_{\text{OH}} \cdot 10^{-12}$ /cm <sup>3</sup> molecule <sup>-1</sup> s <sup>-1</sup>
$\text{C}_2\text{H}_2$	5.1*	0.01 ± 0.02	8.19 ± 0.82
$\text{C}_2\text{H}_4$	Not used	1.7 ± 0.4	75.4 ± 15.1
$\text{C}_2\text{H}_6$	5.7 ± 0.4	Not used	2.50 ± 0.18
$\text{C}_3\text{H}_6$	26*	Not used	Not used

### 3.3.4 Procedure

#### 3.3.4.1 Sample preparation

Most of the samples prepared in this project are liquid at room temperature. Before using a liquid sample in measurements it is important to make sure it is clean. Gases can have dissolved in the liquid for example when pouring it into a sample container, which in this case is a finger tube which is like a sealable sampling tube, see Figure 3.8(b).



By cooling a sample with liquid nitrogen, the liquid will freeze. The manifold (mentioned in section 3.3.2.3 and described in more detail in section 3.3.3.2) to which the finger tubes are connected can be evacuated with a high performance pump. When opening the finger tube with the frozen sample to the evacuated manifold, the gases dissolved in the sample will evaporate before the sample itself does so due to the difference in vapor pressure. By observing the pressure in the tube (manifold) it is possible to see if there was any contamination. The sample is then sealed from the manifold which is emptied, and the sample is heated with a water bath until liquid. This purification procedure is called *freeze-pump-thaw cycling* and is repeated three times for each new sample or until there is no sign of gas contamination.

Gaseous samples are available at the laboratory and the preparation includes attaching the gas bottle to the manifold and making sure there are no leaks. The hose and connection devices must be evacuated to remove air before using the gaseous sample.

In experiments with O<sub>3</sub>, the O<sub>3</sub> must be created, contained and handled with care since it is explosive. An O<sub>3</sub> generator, or ozoniser, is used which converts gaseous O<sub>2</sub> to O<sub>3</sub> using electrical discharges. A flow of oxygen is kept through the ozoniser at a pressure of 300-600 Torr. At higher flow rates, there will be a significant amount of O<sub>2</sub> which is not converted to O<sub>3</sub> and lower pressure can damage the hose. Sudden changes in pressure should be avoided e.g. when connecting the ozoniser to the O<sub>3</sub> trap under vacuum. The O<sub>3</sub> trap is a quartz-glass construction filled with silica gel with a large surface to bind the O<sub>3</sub>. The trap is cooled to about -80°C using isopropanol and dry ice and is under vacuum before starting the ozoniser. O<sub>3</sub> is generated for about 60 minutes to fill the trap.

#### 3.3.4.2 Experimental procedure

A description of a general procedure using the manifold system is given in this section and all quantities and numbers refer to Figure 3.9.

1. All valves, yellow in Figure 3.9, are closed except for number **1** and **4** (or equivalent for other the reference volume) to empty the manifold and the intermediate reference volume,  $V_{ref1}$  or  $V_{ref2}$  before any experiment. The chamber is also under vacuum.
2. The desired samples are connected to the manifold. It can be seen that each connection to removable parts has two valves and an intermediate volume between. The reason for this is to be able to keep the sample and manifold under vacuum when connecting and removing samples. When connecting a sample, valve **2** and **3** are both closed. **2** is opened and the intermediate volume is emptied from air by opening **1**, if not already open. If the sample needs to be freeze-pumped, as described in section 3.3.3.1, this is done by using valve **1**, **2** and **3** (or equivalent for other tubes).
3. When all compounds necessary for the experiment are connected, **1** is closed and it is possible to see if everything is closed tightly if the pressure in the manifold,  $p_{manifold}$ , is stable. Open the valves to the desired chemical and watch the pressure in the manifold rise and seal when correct amount is reached. Close **4** to the reference volume and evacuate the rest of the manifold. It is possible to fill another compound on top of the first one if they are not reactive towards each other, e.g. Cl<sub>2</sub> which does not react until photolysed. In that case there must be a larger amount of the second compound than of the first since the gases are driven towards the lower pressure, i.e.  $p_1 > p_2$  before

opening **4**. As soon as  $p_{\text{manifold}}$  stabilizes after opening **4**, close **4** to avoid leakage back into the manifold of the first gas. Evacuate manifold again, using **1**.

- Open **6** (or equivalent) to fill manifold with  $\text{N}_2$ ,  $\text{O}_2$  or air until the pressure is higher than in the reference volume,  $p_1 > p_2$ , open **4**, and when the total pressure is then higher than in the chamber, i.e.  $p_{\text{manifold}} > p_{\text{chamber}}$ , open **5**. The compounds are then pushed into the chamber and **6** and **5** are closed after flushing with nitrogen to the desired total chamber pressure. This can be done in several steps and it is not necessary to start with an empty chamber. For example if two reactants start to react immediately it is best to pump one compound in, then almost fill the chamber, and finally pump in the last compound and fill the chamber. An IR spectrum can then be measured rather fast before too much of the compounds have reacted.

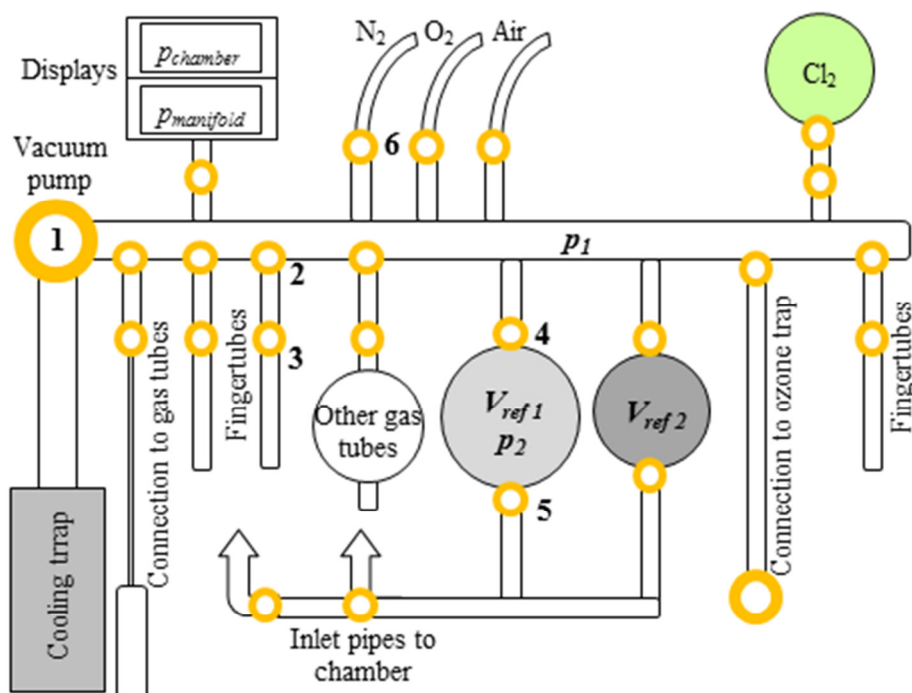


**Figure 3.9.** Schematic picture of the manifold system.

### 3.3.4.3 Control experiments

A number of standard procedures and control experiments are to be performed in association with the experimental work in order to ensure the validity of the results and highlight possible issues.

For each of the molecules GVL, 2(5H)F and 3M2(5H)F, a *reference spectrum* must be measured and calibrated for use in later identification and quantification. A reference spectrum is a spectrum with a known concentration of the compound in a background of  $\text{N}_2$  gas and a known path length. The concentration is relatively well known from measuring the pressure in the reference volume, see experimental procedure in Section 3.3.4.2, but to determine the concentration in the chamber more exactly a calibration is performed. Calibrating the spectrum is done by evacuating the chamber with the compound and  $\text{N}_2$  to about half the pressure, filling up with nitrogen to dilute the known volume of the compound

and measure a new spectrum. This is performed 5 times and for each full and half-full chamber, the total pressure is measured accurately. By scaling the partial pressure, i.e. the concentration, of the compound with the loss from evacuating, a list of decreasing concentration is obtained. The spectra are then compared relative to each other to get the corresponding decrease in absorption. Plotting concentration versus absorption and performing a linear regression through the origin yields a line with the slope equal to the concentration for the reference spectrum. Such spectra are also collected for molecules which are suspected or identified products, if not available in any databases.

When measuring chemical rate constants it is important to ensure that the compounds do not adsorb to the walls of the chamber, are photolysed or react with precursors, reference compounds or scavengers. A scavenger is a molecule which is introduced to remove unwanted species. For example if OH and O<sub>3</sub> is present simultaneously but it is only the reaction with O<sub>3</sub> that is of interest, a molecule which reacts fast with OH but slow with O<sub>3</sub> is added as a scavenger to remove excess OH. The stability towards wall losses in the experimental chamber was investigated by letting the compound be present in the chamber at room temperature and atmospheric pressure without any further impact for 20-30 minutes. Comparing a spectrum from before and after gives information on the dark loss rate. Comparing spectra from before and after 5 minutes of photolysis with UVA and UVC lamps respectively gives information on the photolysis rates of the compounds. To test for unwanted reactions, a gas mixture later used for an experiment is left in the dark for approximately 25 minutes and the spectrum taken before and after are compared.

When possible, two reference molecules can be used simultaneously in the relative rate experiments. If there is no important spectral overlap and the references are not reactive towards each other this is advantageous since the rate constants of references also can be compared with each other. This gives additional information about the accuracy of the experiment and it is also time-saving.

#### 3.3.4.4 Chlorine experiments

The experiments including chlorine are of the following type: relative rate and product studies.

In the relative rate experiments with chlorine, the compound of interest is inserted together with Cl<sub>2</sub> gas and a reference compound (e.g. C<sub>2</sub>H<sub>2</sub> or C<sub>2</sub>H<sub>6</sub>) and the chamber is then filled with nitrogen gas. Since the VOCs react with chlorine atoms, nothing will happen until the sample is photolysed, according to reaction (2F). In general one to two UVA lamps were used to stepwise photolyse a fraction of the chlorine molecules. There is as mentioned in section 3.3.2.4 a computer program where the photolysis time can be set, but this time is not very exact. Generally it takes a second or two for the lamps to light, sometimes the connection is unreliable and the lamps might flicker or not shut off correctly. However in general, a photolysis time of 2-10 seconds is good and can quite easily be achieved by being careful. Since the reaction rate is unknown from the beginning it is good to start with a shorter photolysis time and then increase it if it turns out that the reaction is slower than expected.

The procedure starts by an initial spectrum being measured before any photolysis. Then the sample is photolysed and afterwards left to rest for about 30-60 seconds to let the reactions be completed. A single spectrum is then taken and the sample can be photolysed again with a proper light time with respect to the decrease of the molecule of interest and the reference

compound, respectively. This is repeated until there is too little of the reactants left to give reasonable results, usually around ten percent, or when sufficiently many data points are collected for the relative rate plot. In this study about ten photolysis steps were performable and sufficient for analysis.

In product studies with chlorine the procedure is similar to the one described above, there is however no reference compound present. These reactions are performed in both nitrogen gas and in technical air in order to compare the difference between presence and absence of oxygen. The photolysis and collection of spectra is as described before but it is important to let all of the compound react.

It is of interest to get good reaction steps, i.e. not only to look at the initial and final spectra in order to tell whether specific products are formed early or late and if they follow a linear increase or not. This can give information about which reaction pathways are favorable.

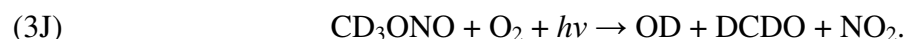
#### 3.3.4.5 OH experiments

According to an experimental protocol presented by Atkinson et al. in 1981 the use of methyl nitrite ( $\text{CH}_3\text{ONO}$ ) as an OH-precursor is a suitable method for determining relative rate constants for organic compounds [62]. OH is obtained from photolysis of  $\text{CH}_3\text{ONO}$  in the presence of  $\text{O}_2$ , according to the following reaction scheme



$\text{O}_3$  can be formed in competing reactions but the advantage of this method is that the yield of OH is high and hence the influence of  $\text{O}_3$  reactions is suppressed. With the limitation due to  $\text{O}_3$  reactions, this technique still allows rate constants larger  $3 \cdot 10^{-13} \text{ cm}^3 \text{ molecule}^{-1} \text{ s}^{-1}$  to be determined [62].

In the present study OD was used as reactant instead of OH, where deuterium (D or  $^2\text{H}$ ) is a hydrogen isotope. Due to overlapping spectra making the analysis difficult and also due to availability,  $\text{CD}_3\text{ONO}$  was used to obtain the radicals instead of  $\text{CH}_3\text{ONO}$ , or  $\text{C}_3\text{H}_7\text{ONO}$  which could be used equivalently [63]. Hence the reactions with OD were studied to get an estimate of the rate constant of the corresponding OH-reactions. With the deuterated precursor, the corresponding net reaction for the radical production is hence



The rates of reactions are not expected to be significantly different as a result of deuterium substitution, since the hydrogen or deuterium does not take active part in the chemical reactions. Greiner [64] compared reactions of  $\text{C}_2\text{H}_6$  with OH and OD, and concluded that the values for the reactions were within experimental error bars.

#### 3.3.4.6 Ozone experiments

The experiments including O<sub>3</sub> are of the following type: absolute rate and relative rate.

The experiments with O<sub>3</sub> differ from the chlorine experiments in the respect that the radical is inserted directly into the reaction chamber and no photolysis is required. The O<sub>3</sub> is always let directly into the chamber without using the metal inlet tubes from the manifold, only the Teflon tubes, since the O<sub>3</sub> can damage metallic parts. An excess amount of O<sub>3</sub> is used and it is important to insert the compound of interest as late as possible so that the first spectrum does not include too much of the reaction products.

The procedures for the absolute and relative rate experiments are identical and the difference is just the absence or presence of a reference compound. For the absolute measurements of the rate coefficient, the timing of when the spectra are collected is of greater importance since the time steps are used in the plots and the calculations of the rate coefficient. A feature in OPUS called “repeated measurements” is used here and spectra are taken automatically, for example every two minutes for approximately 30 minutes. When the absolute rate constant is determined several measurements are required with a slightly varying O<sub>3</sub> concentration to get the concentration dependence for a pseudo-first-order reaction described in section 3.2.6.

It is important to use a scavenger compound in the O<sub>3</sub> experiments in order to remove OH-radicals which will form and otherwise start to react with the molecule of interest. This will give a rate constant which is due to both O<sub>3</sub> and OH and hence the value will give no meaning without further or different experiments. The requirements of the scavenger are that it has to react much faster with OH than the other molecules do and at the same time react much slower with O<sub>3</sub>. This goes for both the compound of interest and the reference compound in the case of relative rate studies. The OH-scavenger used throughout this work was cyclohexane (C<sub>6</sub>H<sub>12</sub>).

#### 3.3.5 Data analysis

The results are, as mentioned earlier, obtained as spectra with absorbance, as a function of wavenumber for a gaseous compound or a mixture of gases and OPUS does automatically subtract the background spectrum.

In most experiments in the present work it is the relative concentrations that are of importance, i.e. it is not necessary to determine the exact concentrations but rather to get the ratio between two subsequent spectra. This can be done with a function called “spectrum subtraction” in OPUS where two spectra can be compared and scaled relative to each other. A good fit means that the residual between the spectra shows no features of the molecule of interest and should rather look like noise, and if no product peaks are in the specific area the baseline should be straight. The spectral features of the molecules used in this work are in general rather distinct from each other. Hence there is no need for a computer to evaluate the spectra but rather it is done manually in OPUS. The only time a computational determination of concentrations is done is when determining O<sub>3</sub> concentrations for absolute measurements of rate constants. In this case the O<sub>3</sub> concentrations are used to plot and determine the rate constants and hence the program MALT is used.

In the product studies, the analysis is in short to identify the products. As mentioned in section 3.2.1 the spectral features can give some information on the molecular structure. For example presence of features in characteristic regions can tell which types of molecules and bonds that

should be present. Distinguishable details can also tell something about the size of the molecule since for example the fine rotational-vibrational structure is mainly seen for smaller molecules while a smeared spectrum indicates a larger molecule. The product spectrum is then compared with reference spectra which are either collected through measurements using the setup described above, found in literature or computed. When all, or the major, products are identified it will also be important to quantify them, which requires known concentrations in the reference spectra. It is then possible to determine product yields both for linear product formation and if secondary chemistry is present yielding nonlinear decrease of the lactone or increase of a product. Reaction pathways can be suggested with the knowledge of products and product yields.

### 3.3.6 Uncertainties in measurements and results

The uncertainties related to the experimental results arise from the physical limitations of the setup, the uncertainty in reference reaction rate constants and errors from fitting to data. For each spectrum 32 interferogram are co-added yielding a good signal to noise ratio and good quality spectra. The path length used is larger than 30 meters which gives a good accuracy of the average concentrations without losing too much of the intensity which could decrease the signal to noise ratio.

For each linear regression performed using the software Sigma Plot, a standard error,  $\sigma$ , is obtained. The total error,  $\varepsilon$ , for a measured rate constant is in this kind of work [66] usually calculated using two standard deviations as well as an uncertainty associated to the analysis of the spectra, which is approximated to be less than 5 %, i.e.

$$\varepsilon = \sqrt{(2\sigma)^2 + 0.05^2}. \quad (3.25)$$

The error in the analysis is set to 5 % since this was the worst accuracy with which the concentrations could be determined using the spectrum subtraction method. Several measurements are performed for each rate constant and the final constant value is an average of these measurements and the final error,  $E$ , for this average is obtained by taking the root mean square of the total errors, i.e.

$$E = \sqrt{\varepsilon_1^2 + \varepsilon_2^2 + \dots + \varepsilon_n^2}. \quad (3.26)$$

In Section 3.4.2.1 a more detailed discussion on the uncertainties associated with the rate constant measurements is given. No error bars are included in the figure in the results since the exact error for each data point is not known well enough.

## 3.4 Results and discussion

### 3.4.1 Reference spectra and control experiments

A number of standard procedures and control experiments were performed in this work. A calibrated reference spectrum was collected for GVL, 2(5H)F and 3M-2(5H)F, respectively. The calibrated spectrum of GVL is shown in Figure 3.10. The concentration corresponds to the slope of the linear plot in the figure. The reference spectra of 2(5H)F and 3M2(5H)F are found in Appendix A. A number of reference spectra were also measured for suspected products formed from the studied reactions. The reference spectra were measured at a path length of 50.75 m and the concentrations were 3.69 ppm, 3.01 ppm and 3.24 ppm for GVL, 2(5H)F and 3M-2(5H)F respectively.

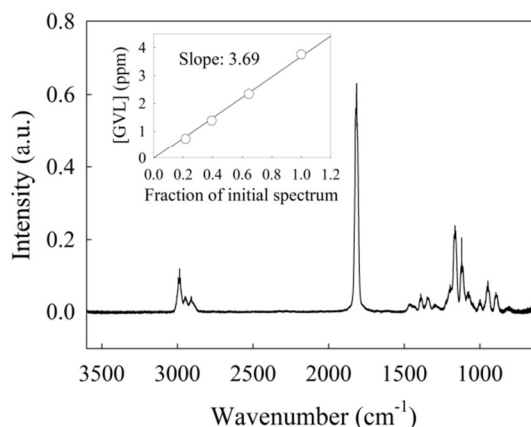


**Figure 3.10.** Calibrated spectrum of GVL. Embedded plot show calibration data and spectrum is of GVL in N<sub>2</sub>.

The stability of the compounds towards wall losses and photolysis in the experimental chamber was investigated as described in Section 3.3.4.3. It was seen that the only compound undergoing wall losses was 2(5H)F and all compounds were to a small extent photolysed by UVA radiation while 2(5H)F and 3M-2(5H)F were more greatly photolysed by UVC radiation than GVL. The result is summarized in Table 3.5. In general the effects of wall losses and UVA photolysis are small compared to the timescales used in the experiments and can hence be considered as negligible within the uncertainty limits. The photolysis of 2(5H)F and 3M2(5H)F by UVC radiation might be important and can affect the linearity of the relative rate method. This was considered when analysing the results.

An effort was made to shorten the duration of the experiments as much as possible in order to reduce the effects of unwanted loss mechanisms. Due to a breakdown in the lab, UVA lamps were not available for all experiments but some were performed with the less preferable UVC lamps. For these experiments the deviation from linearity of the data occurs earlier and hence it is possible that this can be explained by adsorption and photolysis.

**Table 3.5.** Results from control experiments of wall losses and photolysis. All lamps were lit, i.e. 8 UVA and 16 UVC.

Compound	Loss mechanism		
	Wall adsorption	UVA photolysis	UVC photolysis
GVL	0% / 25 min	2% / 5 min	3% / 5 min
2(5H)F	5% / 25 min	2% / 5 min	25% / 5 min
3M-2(5H)F	0% / 25 min	1% / 5 min	30% / 5 min

For all experiments where reference molecules or scavengers were used, it was tested if these were reactive towards the lactones. None of the references (C<sub>2</sub>H<sub>2</sub>, C<sub>2</sub>H<sub>4</sub>, C<sub>2</sub>H<sub>6</sub>, C<sub>3</sub>H<sub>6</sub>), the scavenger (C<sub>6</sub>H<sub>12</sub>) or the precursors (Cl<sub>2</sub> or CD<sub>3</sub>ONO) were reactive towards GVL, 2(5H)F or 3M-2(5H)F, neither were the references and the precursors reactive towards each other.

### 3.4.2 Chlorine kinetics

All the experiments in this section were carried out at room temperature at a total pressure of 700 Torr in N<sub>2</sub> diluent if nothing else is stated.

Two separate experiments were performed with each reference compound for each lactone respectively as described in section 3.3.4.4 “Chlorine experiments” and the result was plotted according to Equation (3.18). The references were acetylene (C<sub>2</sub>H<sub>2</sub>), ethane (C<sub>2</sub>H<sub>6</sub>) for all lactones. Propene (C<sub>3</sub>H<sub>6</sub>) was tried as a reference but was unsuitable due to its reaction rate constant. The reaction rate constants of the references can be found in Table 3.4.

When the plotted data from relative rate measurements do not follow a linear trend some data point towards the end of an experiment are excluded. This is only done when it is clear that the linearity of the relative rate method is not fulfilled and the data does not contribute with any valid information.

#### 3.4.2.1 Relative rate studies

The details of the relative rate experiments with chlorine are shown in Table 3.6. The slopes of linear regressions as well as the calculated rate constants are given in the table and not in each figure. The “Experiment Number” is used as a reference and is correlated with the numbers referred to in figure legends.

**Table 3.6.** Details of chlorine kinetics experiments. Each row contains a labelling of the experiment, the participating compounds and their concentration, the total photolysis and the slope obtained from linear regression in SigmaPlot. The lactone rate constant obtained for each experiment is given together with the average value (**bold**). Rate constants within parenthesis are not included in the average value.

Exp. No.	Compound (ppm)	Radical precursor (ppm)	Reference (ppm)	Photolysis lamp and time	Slope	$k_{\text{compound}}/10^{-11}$ (cm <sup>3</sup> molec <sup>-1</sup> s <sup>-1</sup> )
1	GVL (3.40)	Cl <sub>2</sub> (53.0)	C <sub>3</sub> H <sub>6</sub> (14.2)	1 UVA 15s	0.233	(6.05)
2	GVL (3.59)	Cl <sub>2</sub> (50.9)	C <sub>3</sub> H <sub>6</sub> (8.26)	1 UVA 10s	0.182	(4.74)
3	GVL (3.50)	Cl <sub>2</sub> (47.3)	C <sub>2</sub> H <sub>2</sub> (8.97)	1 UVA 75s	0.946	4.82
4a	GVL (3.81)	Cl <sub>2</sub> (76.7)	C <sub>2</sub> H <sub>2</sub> (9.76)	2 UVA 120s	0.914	4.66
4b	GVL (3.81)	Cl <sub>2</sub> (76.7)	C <sub>2</sub> H <sub>6</sub> (10.1)	2 UVA 120s	0.752	4.29
5	GVL (3.74)	Cl <sub>2</sub> (53.4)	C <sub>2</sub> H <sub>6</sub> (10.1)	1 UVA 15s	0.786	4.48
GVL						<b>4.56</b>
6	2(5H)F (1.81)	Cl <sub>2</sub> (52.1)	C <sub>2</sub> H <sub>2</sub> (9.69)	1 UVA 75s	0.616	3.14
7	2(5H)F (2.09)	Cl <sub>2</sub> (59.6)	C <sub>2</sub> H <sub>6</sub> (10.6)	1 UVA 40s	0.529	3.02
8	2(5H)F (2.50)	Cl <sub>2</sub> (77.3)	C <sub>2</sub> H <sub>2</sub> (11.4)	4 UVC 150s	0.563	2.87
9	2(5H)F (2.33)	Cl <sub>2</sub> (80.9)	C <sub>2</sub> H <sub>6</sub> (12.9)	4 UVC 90s	0.477	2.72
2(5H)F						<b>2.94</b>
10	3M2(5H)F (5.66)	Cl <sub>2</sub> (66.4)	C <sub>2</sub> H <sub>6</sub> (8.56)	1 UVA 50s	2.64	15.0
11	3M2(5H)F (4.74)	Cl <sub>2</sub> (66.3)	C <sub>2</sub> H <sub>2</sub> (9.09)	1 UVA 50s	3.18	16.2
12a	3M2(5H)F (5.60)	Cl <sub>2</sub> (76.4)	C <sub>2</sub> H <sub>2</sub> (10.8)	4 UVC 140s	3.22	16.4
12b	3M2(5H)F (5.60)	Cl <sub>2</sub> (76.4)	C <sub>2</sub> H <sub>6</sub> (11.6)	4 UVC 140s	2.94	16.8
3M2(5H)F						<b>16.1</b>



The results from investigating the reaction GVL + Cl are shown in Figure 3.11.

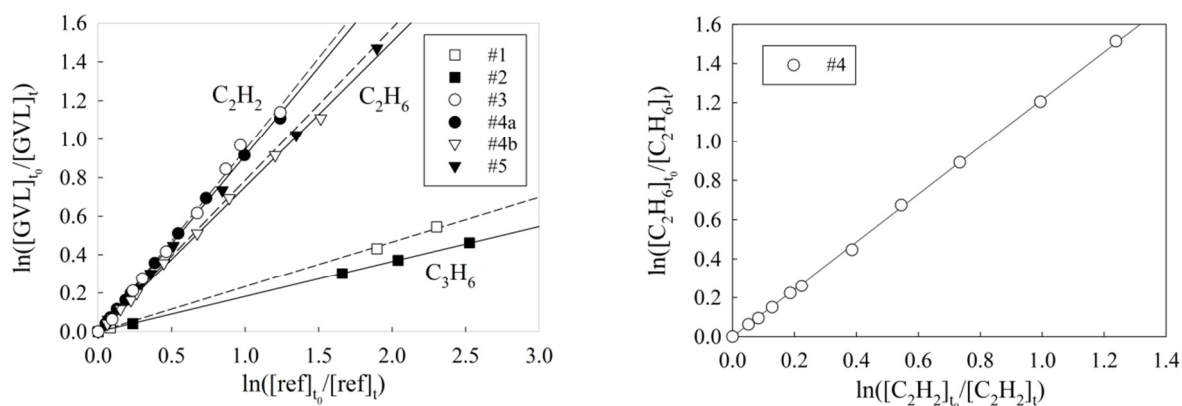


**Figure 3.11.** Left: Measured data and linear regressions from relative rate analyses of the reaction GVL + Cl, photolysis with UVA for 2-10 s per step. Right: Relative rate plot  $C_2H_6$  and  $C_2H_2$  used in parallel in one of the experiments.

The leftmost plot in Figure 3.11 shows the data from comparing the decrease in GVL with the decrease of the reference compounds. In one experiment, acetylene and ethane were used in parallel since no spectral features used in analysis were overlapping. From this experiment the rightmost plot in Figure 3.11 was obtained. This plot shows a relative rate comparison between the two references.

In Figure 3.11 it is seen that repeated measurements with acetylene and ethane respectively agree well.  $C_2H_6$  reacts slightly faster with Cl than  $C_2H_2$  (see Table 3.4) which is in agreement with a steeper gradient of the  $C_2H_2$  measurements in Figure 3.11.

For  $C_3H_6$  the slopes seen in Figure 3.11 vary more. It is also seen that the number of data points available is smaller for  $C_3H_6$  and the step between each point is larger, especially in the beginning. This is partly due to the fact that reaction between  $C_3H_6$  and Cl is relatively fast (see Table 3.4). When the reference reacts fast with Cl and the photolysis time is short it is difficult to obtain controlled and small decreases of the concentrations. During the experiments with  $C_3H_6$  there was also some trouble with the UVA lamps which did not respond perfectly to the computer program. Due to the lack of data in the low region in Figure 3.11, it is not possible to say whether the apparent linear trend is accurate or if there is a possible deviation not visible. For this reason the results from determining  $k_{GVL+Cl}$  using  $C_3H_6$  are not included in the average of the rate constant. The four experiments (#3-5) with higher quality give enough information.

The results from investigating the reaction  $2(5H)F + Cl$  are shown in Figure 3.12. This figure shows the data from comparing the decrease in  $2(5H)F$  with the decrease of the reference compounds. No experiment was performed with both references used in parallel since there was a spectral overlap with the products formed from the reactions.

Comparing Figure 3.12 with the result for GVL in Figure 3.11 it is seen that the linear behaviour is not present in the same way for  $2(5H)F$  as for GVL. The data tends to deviate towards a lower slope with increasing values, i.e. with increasing time. This indicates that there are some other losses present than the reaction with Cl.  $2(5H)F$  might react with the products or the wall adsorption and photolysis has become significantly large to affect the result, see Table 3.5. The deviation from linearity is hence due to loss mechanisms other than the studied reaction.

For this reason it was decided that the data points with  $\ln([2(5H)F]_{t0}/[2(5H)F]_t)$  larger than 0.3, i.e. on the vertical axis, should not be used for determining the rate constant, simply by cutting off the data which most clearly deviates from the initial trend line. There is an additional data point belonging to experiment number 7, located at around (3,3) which is not included for visual reasons. The linear regressions used for determining the rate constant are calculated only using the white and black symbols in Figure 3.12 and not the shaded grey.

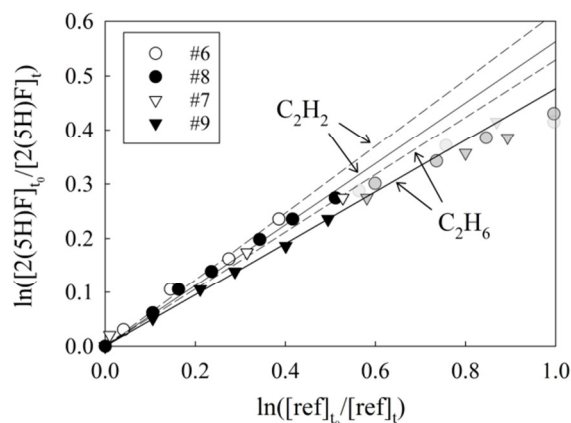


**Figure 3.12.** Measured data of the reaction  $2(5H)F + Cl$  and linear regressions. The data is cut off above  $\ln([2(5H)F]_{t0}/[3(5H)F]_t) = 0.3$  and the excluded points are shown as shaded symbols.

The results from investigating the reaction  $3M2(5H)F + Cl$  are shown in Figure 3.13.

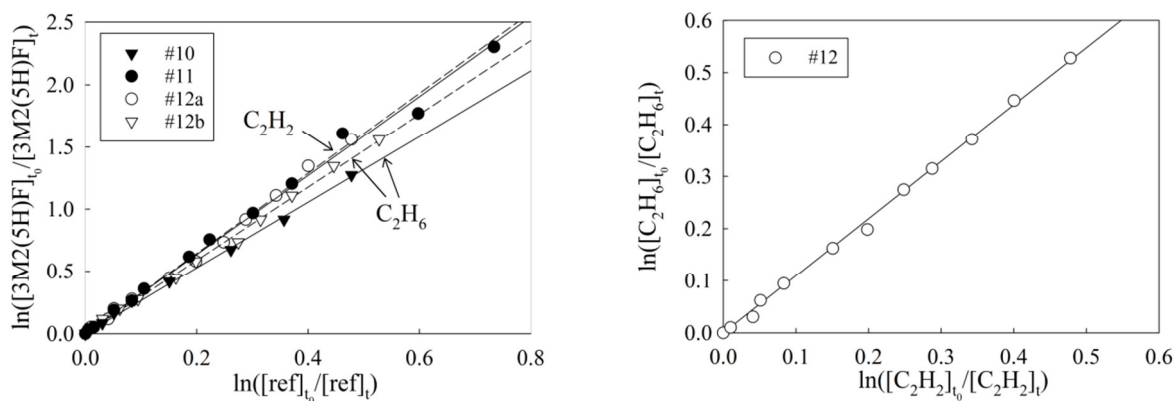


**Figure 3.13.** Left: Measured data and linear regressions from relative rate analyses of the reaction  $3M2(5H)F + Cl$ . Right: Relative rate plot of two references used in parallel in one of the experiments.

The leftmost plot in Figure 3.13 shows the data from comparing the decrease in  $3M2(5H)F$  with the decrease of the reference compounds. In one experiment,  $C_2H_2$  and  $C_2H_6$  were used in parallel since no spectral features overlapped. From this experiment the rightmost plot in Figure 3.13 was obtained which shows a relative rate comparison between the two references. In Figure 3.13 it is seen that repeated measurements reproduce the slope relatively well especially for the results using  $C_2H_2$ .

By evaluating how well the reference rate constants are reproduced in the experiments an indication of the uncertainty related to the results is obtained. From the results in Figure 3.11 (right) and 3.12 (right) the slope, which correspond to the rate constant ratio, is compared with the expected slope from literature values. In Table 3.7 all experiments using two references are listed. The Experiment Numbers correspond to the labelling in Table 3.6 and Table 3.9. The calculated errors from linear regressions are smaller than those given in the latest recommendation by Sander et al. [16] seen in Table 3.4, hence the contribution to the total uncertainty from the experimental performance is assumed to be small.

**Table 3.7.** Summary of relative rate comparisons of reference compounds. The reactions noted “1” has the rate constant is  $k_1$  and reactions noted “2” has  $k_2$ . Values of  $k_1$  and  $k_2$  are obtained from Table 3.4

Exp. no.	Reactions	$k_1$ / $10^{-13}$ $\text{cm}^3 \text{molecule}^{-1} \text{s}^{-1}$	$k_2$ / $10^{-13}$ $\text{cm}^3 \text{molecule}^{-1} \text{s}^{-1}$	Literature slope ( $k_2/k_1$ )	Experimental slope
#4	1: C <sub>2</sub> H <sub>2</sub> + Cl 2: C <sub>2</sub> H <sub>6</sub> + Cl	510	570 ± 40	1.12	1.22
#12	1: C <sub>2</sub> H <sub>2</sub> + Cl 2: C <sub>2</sub> H <sub>6</sub> + Cl	510	570 ± 40	1.12	1.10
#15	1: C <sub>2</sub> H <sub>2</sub> + OH 2: C <sub>2</sub> H <sub>4</sub> + OH	8.19 ± 0.82	75.4 ± 15.1	9.21	14.0
# 16	1: C <sub>2</sub> H <sub>2</sub> + OH 2: C <sub>2</sub> H <sub>6</sub> + OH	8.19 ± 0.82	2.5 ± 0.18	0.31	0.28
#17	1: C <sub>2</sub> H <sub>2</sub> + OH 2: C <sub>2</sub> H <sub>4</sub> + OH	8.19 ± 0.82	75.4 ± 15.1	9.21	13.0
#19	1: C <sub>2</sub> H <sub>2</sub> + OH 2: C <sub>2</sub> H <sub>4</sub> + OH	8.19 ± 0.82	75.4 ± 15.1	9.21	10.2
#20	1: C <sub>2</sub> H <sub>2</sub> + OH 2: C <sub>2</sub> H <sub>4</sub> + OH	8.19 ± 0.82	75.4 ± 15.1	9.21	15.35

In Table 3.7 the experiments 4, 12, 16 and 19 show a relatively good agreement between the experimental slope and the literature value. These include all experiments in which C<sub>2</sub>H<sub>6</sub> is compared against C<sub>2</sub>H<sub>2</sub>. Using C<sub>2</sub>H<sub>4</sub> and C<sub>2</sub>H<sub>2</sub> resulted in larger deviation and less success in reproducing values, except for experiment 19. There is over all an overestimate of the slope for experiment 15, 17 and 20 showing that the results show good reproducibility. Since the rate constant for the reaction C<sub>2</sub>H<sub>4</sub> + OH is the least accurately determined, seen in Table 3.7, it is not surprising with a larger uncertainty in the use of C<sub>2</sub>H<sub>4</sub> as a reference.

When looking at the contribution of C<sub>2</sub>H<sub>4</sub> to the measurements in Table 3.9 (see e.g. exp. #13 and #15a for GVL) it is seen that it gives a lower reaction rate constant of the lactone. This is true for GVL and 2(5H)F and to some extent for 3M2(5H)F. If it is true that the C<sub>2</sub>H<sub>4</sub> measurements are the least reliable and these measurements generally result in lower determination of the rate constants it is possible that the final values in Table 3.11 are underestimates.

#### 3.4.2.2 Product studies

The identified products from reactions between lactones and chlorine, in a background bath gas of pure N<sub>2</sub> or a mixture of N<sub>2</sub> and O<sub>2</sub> respectively, are listed in Table 3.8 for the individual reactions.

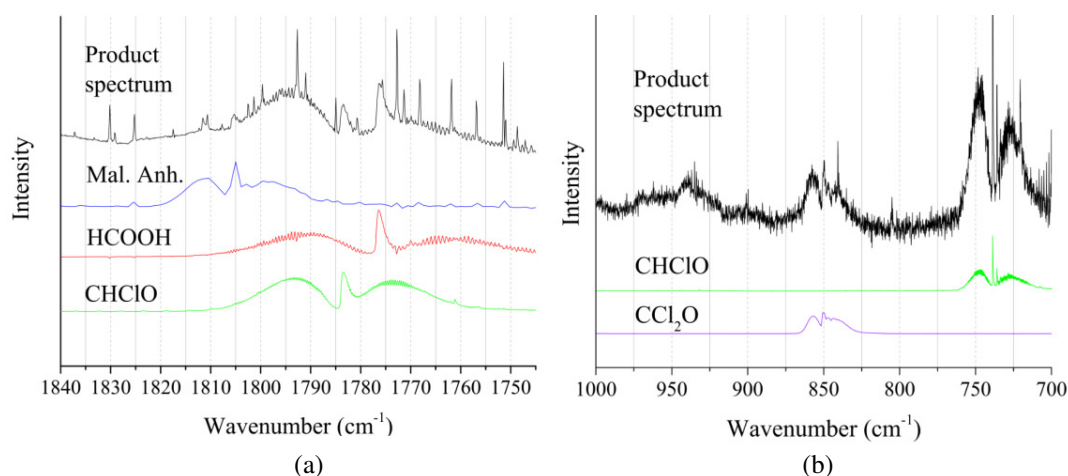
Many products are common for the three lactones but the relative amounts produced differ somewhat. By determining the concentrations of the products, using quantified reference spectra, and comparing these with the initial amount of a lactone a carbon balance can be set up to estimate how large fraction of the products that are quantified. As an example some percentage yields for products formed from the reaction 2(5H)F + Cl in N<sub>2</sub>/O<sub>2</sub> have been calculated and are 4% HCOOH, 10-15% CHClO and 3% maleic anhydride by the end of the experiment but > 40 % MA before it starts to undergo losses. Since all products are not identified a complete reaction scheme cannot be produced.

**Table 3.8.** Summary of identified products in lactone + Cl reactions.

Reaction	Bath gas	Identified products
GVL + Cl	N <sub>2</sub>	HCl, CO <sub>2</sub>
GVL + Cl (+ O <sub>2</sub> )	N <sub>2</sub> /O <sub>2</sub>	HCl, CO <sub>2</sub> , CO, HCOOH, CHClO, CCl <sub>2</sub> O
2(5H)-F + Cl	N <sub>2</sub>	HCl, CO <sub>2</sub> , CO
2(5H)-F + Cl (+ O <sub>2</sub> )	N <sub>2</sub> /O <sub>2</sub>	HCl, CO <sub>2</sub> , CO, HCOOH, CHClO, CCl <sub>2</sub> O, Maleic anhydride
3M-2(5H)-F + Cl	N <sub>2</sub>	HCl, CO <sub>2</sub> , CO
3M-2(5H)-F + Cl (+ O <sub>2</sub> )	N <sub>2</sub> /O <sub>2</sub>	HCl, CO <sub>2</sub> , CO, HCOOH, CHClO, CCl <sub>2</sub> O

The reaction 2(5H)F + Cl in an environment with oxygen is the one where most products have been identified and some of these are shown in Figure 3.14. The two spectral regions (a) 1840-1759 cm<sup>-1</sup> and (b) 1000-700 cm<sup>-1</sup> are shown separately in which the products formic acid (HCOOH), formyl chloride (CHClO), maleic anhydride, MA, (C<sub>2</sub>H<sub>2</sub>(CO)<sub>2</sub>O) and phosgene (CCl<sub>2</sub>O) are present. HCl, CO and CO<sub>2</sub> are always formed in large amounts and these are not of significant interest for the moment since these are difficult to quantify and do not contribute with much information about reaction pathways.

In general the product concentrations increase linearly with reaction time, but an exception is observed for maleic anhydride. Maleic anhydride is built up during the first minute of photolysis but then exhibits losses and decreases in concentration towards the end of an experiment. This indicates that MA is reactive towards some other molecule in the chamber. No Cl-initiated breakdown mechanism of GVL, 2(5H)F or 3M2(5H)F is given here since further investigations are necessary.

**Figure 3.14.** The spectrum from a photolysed sample of 2(5H)F, Cl<sub>2</sub> and N<sub>2</sub>/O<sub>2</sub>.

The 2(5H)F is reduced to two percent of its initial value after approximately 2 min of UVA photolysis and the final spectrum is the uppermost, in black. Intensities are arbitrary.

For all lactones not all product species have been possible to identify and there are clearly other products present. There is a consistent difference in the studies performed with O<sub>2</sub> present and absent as can be seen in Table 3.13. The reasons for this are not fully understood but some observations and suggestions are presented below.

In the experiments with O<sub>2</sub> absent there is in general no big difference between the initial spectrum with the lactone and the product spectrum. A shift in wavenumber and change in shape of the spectral features are seen and also a buildup of HCl. No new distinct features appear and there is little formation of CO and CO<sub>2</sub>. For GVL and 3M2(5H)F the product present around 1800-1780 cm<sup>-1</sup> could indicate an acid anhydride, by comparing with Table 3.3 in Section 3.2.1. Several spectra of anhydrides were compared to the product spectrum and similarities but no convincing agreement was found. Most suitable was acetic formic anhydride but the reference spectrum had a coarse resolution compared to the product spectrum, but it is possible that some chlorinated anhydride is formed. A substitution of a hydrogen atom with a chlorine atom in a molecule can yield a similar spectrum but with a shift due to the change in mass balance of the molecule. Many chlorinated compounds, especially ring-structured species, do not have available reference spectra and might be non-commercial. The results could be further investigated to account for such products e.g. with theoretical spectra.

In the experiments with O<sub>2</sub> present there is a different trend. There is no peak similar to the initial lactone and the products does almost completely consist of the small molecules listed in Table 3.13. There are some other features but all with a weak intensity. Since wall adsorption was observed for 2(5H)F this can account for some of the loss. There might also be formation of solid aerosols in the chamber which is not visible for the FTIR spectrometer. A suggestion of such a product is succinic anhydride which has a structure very similar to 2(5H)F with only the addition of one oxygen atom.

### 3.4.3 OH kinetics

As mentioned in Section 3.3.4.5 the radical used to determine the reaction rate constants with OH are OD. Since the effect on the reaction rate constant is insignificant within experimental uncertainties the results and discussions will be treated as results of OH reactions. All the experiments in this section were carried out at room temperature at a total pressure of 700 Torr with a mixture of 150 Torr O<sub>2</sub> and 550 Torr N<sub>2</sub> as bath gas if nothing else is stated. CD<sub>3</sub>ONO was synthesized by Martyn Jevric and Mogens Brønsted Nielsen from Organic Synthesis at the Department of Chemistry at Copenhagen University.

The references were acetylene (C<sub>2</sub>H<sub>2</sub>) and ethylene (C<sub>2</sub>H<sub>4</sub>) for all lactones and in addition ethane (C<sub>2</sub>H<sub>6</sub>) was used for 2(5H)F. Two separate experiments were performed for each reference compound as described in section 3.3.4.5 “OD experiments” and in some cases the references were used in parallel. The result was plotted according to Equation (3.18).

As discussed in Section 3.4.2 regarding non-linearity of measurements using the relative rate method, some data points are excluded. This is mentioned in connection with Figure 3.17 where such a result was obtained.

#### 3.4.3.1 Relative rate studies

The details of the relative rate experiments with OH are shown in Table 3.9. The slopes of linear regressions as well as the calculated rate constants are given in this table. The “Experiment Number” is used as a reference and is correlated with the numbers referred to in figure legends.

**Table 3.9** Details of OH kinetics experiments. Each row contains a labelling of the experiment, the participating compounds and their concentration, the total photolysis and the slope obtained from linear regression in SigmaPlot. The lactone rate constant obtained for each experiment is given together with the average value (**bold**).

Exp. No.	Compound (ppm)	Radical precursor (ppm)	Reference (ppm)	Photolysis lamp and time	Slope	$k_{\text{compound}} / 10^{-12}$ ( $\text{cm}^3 \text{molec}^{-1} \text{s}^{-1}$ )
13	GVL (6.10)	CD <sub>3</sub> ONO (140)	C <sub>2</sub> H <sub>4</sub> (15.6)	4 UVC 165s	0.358	2.70
14	GVL (5.94)	CD <sub>3</sub> ONO (136)	C <sub>2</sub> H <sub>2</sub> (15.4)	4 UVC 215s	3.90	3.19
15a	GVL (5.89)	CD <sub>3</sub> ONO (140)	C <sub>2</sub> H <sub>4</sub> (19.1)	4 UVC 460s	0.305	2.30
15b	GVL (5.89)	CD <sub>3</sub> ONO (140)	C <sub>2</sub> H <sub>2</sub> (15.1)	4 UVC 460s	4.26	3.49
GVL						<b>2.92</b>
16a	2(5H)F (1.94)	CD <sub>3</sub> ONO (144)	C <sub>2</sub> H <sub>2</sub> (16.3)	4 UVC 110s	5.14	4.21
16b	2(5H)F (1.94)	CD <sub>3</sub> ONO (144)	C <sub>2</sub> H <sub>6</sub> (11.2)	4 UVC 110s	18.3	4.58
17a	2(5H)F (2.03)	CD <sub>3</sub> ONO (163)	C <sub>2</sub> H <sub>2</sub> (13.8)	4 UVC 80s	5.76	4.72
17b	2(5H)F (2.03)	CD <sub>3</sub> ONO (163)	C <sub>2</sub> H <sub>4</sub> (9.93)	4 UVC 80s	0.442	3.33
18	2(5H)F (1.70)	CD <sub>3</sub> ONO (139)	C <sub>2</sub> H <sub>4</sub> (11.8)	4 UVC 145s	0.459	3.46
2(5H)F						<b>4.06</b>
19a	3M2(5H)F (2.69)	CD <sub>3</sub> ONO (157)	C <sub>2</sub> H <sub>2</sub> (12.4)	4 UVC 55s	12.7	10.4
19b	3M2(5H)F (2.69)	CD <sub>3</sub> ONO (157)	C <sub>2</sub> H <sub>4</sub> (24.0)	4 UVC 55s	1.35	10.2
20a	3M2(5H)F (2.56)	CD <sub>3</sub> ONO (140)	C <sub>2</sub> H <sub>2</sub> (~7)	4 UVC 105s	21.7	17.7
20b	3M2(5H)F (2.56)	CD <sub>3</sub> ONO (140)	C <sub>2</sub> H <sub>4</sub> (~13)	4 UVC 105s	1.60	12.0
3M2(5H)F						<b>12.6</b>

The results from investigating the reaction GVL + OD are shown in Figure 3.15.

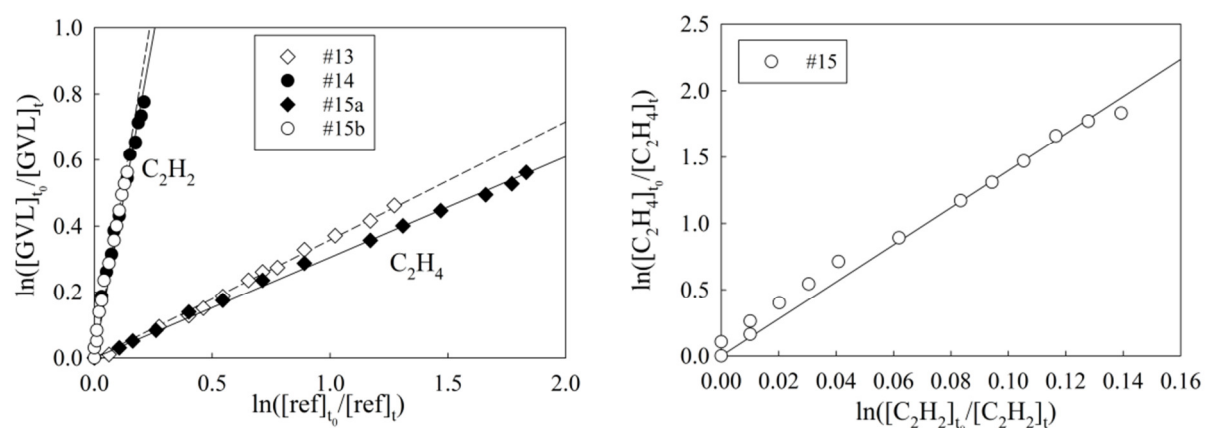


**Figure 3.15.** Left: Measured data and linear regressions from relative rate analyses of the reaction GVL + OD, photolysed with UVC. Right: Relative rate plot C<sub>2</sub>H<sub>4</sub> and C<sub>2</sub>H<sub>2</sub> used in parallel in one of the experiments.

In Figure 3.15 the result is well reproduced and the linearity in the data is clear. Comparing with the Experiment numbers (13-15) with the data in Table 3.9 it is seen that using  $C_2H_2$  yields a higher rate constant and  $C_2H_4$  yields a lower.

The results from investigating the reaction  $2(5H)F + OD$  are shown in Figure 3.16.

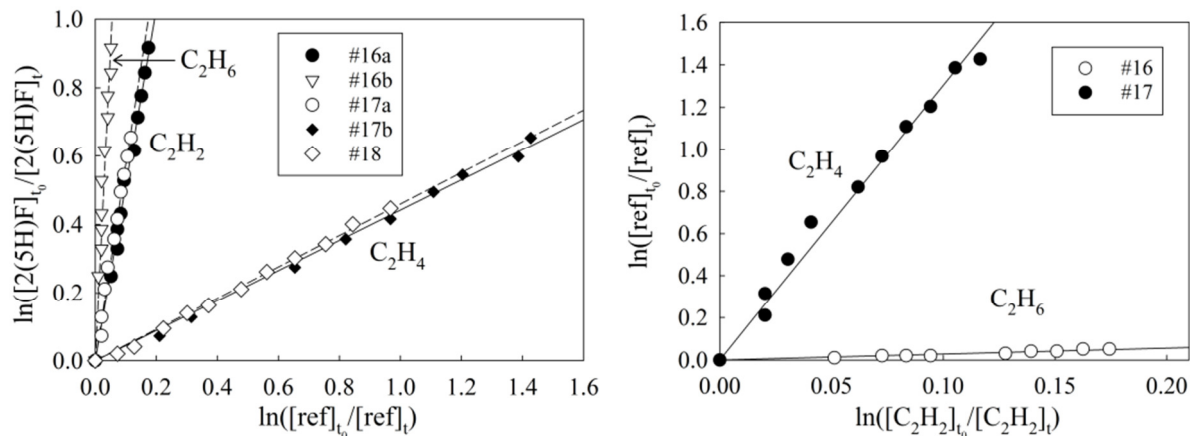


**Figure 3.16.** Left: Measured data and linear regressions from relative rate analyses of the reaction  $2(5H)F + OD$ , photolysed with UVC. Right: Relative rate plot for references used in parallel in two of the experiments.

For this reaction the additional reference  $C_2H_6$  was used as a reference once but it was not reproduced due to the large difference in reaction rate constant between  $C_2H_6$  and  $2(5H)F$  making it more difficult to analyse the data.

The results from investigating the reaction  $3M2(5H)F + OH$  are shown in Figure 3.17.

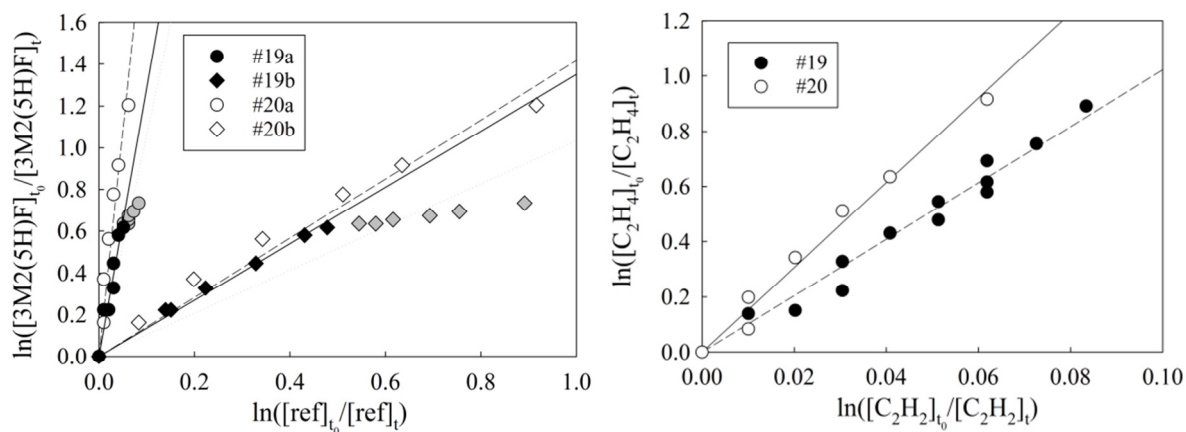


**Figure 3.17.** Left: Measured data and linear regressions from relative rate analyses of the reaction  $3M-2(5H)F + OD$ , photolysed with UVC. Right: Relative rate plot  $C_2H_4$  and  $C_2H_2$  used in parallel in both of the experiments.

When comparing Figure 3.15-16 it can be seen that the linearity of the relative rate method seem to be valid for  $GVL + OH$  and  $2(5H)F + OH$  were linear trends are observed while for  $3M-2(5H)F$  there is a clear shift in slope in one of the experiments. One reason for the results from  $3M-2(5H)F + OH$  measurements, not being as straightforward as for  $GVL$  and  $2(5H)F$  is that some of the most characteristic spectral features were not possible to use in analysis due to spectral overlap and due to low concentrations. Since there is only one experiment exhibiting this behaviour (compare with Figure 3.12, all results are similar) this result is concluded to be a result of analysis issues and not unwanted loss mechanisms. Lower concentrations were used in some experiments due to lack of more samples and evaporated

amounts were limited to the low vapour pressure of the chemical. Hence the analysed results include a larger error towards the end of the measurement, and especially for experiment number 19 and this data is not useful and is marked in grey.

The relative rate evaluations of the rightmost plots in Figure 3.15-16 is previously shown and discussed in Section 3.4.2.1 and Table 3.7.

### 3.4.4 O<sub>3</sub> kinetics

The details of the O<sub>3</sub> kinetics experiments where the reaction rate constants of the lactones were determined absolutely and relatively are shown in Table 3.10. Experiment number 21 and 22 are of relative rate type while the rest use the absolute rate method. For all experiments about 150 ppm of C<sub>6</sub>H<sub>12</sub> was added to remove OH. The concentrations listed in Table 3.10 are not exact since all the space in the manifold was used to insert the lactones to get sufficient amounts.

**Table 3.10** Details of O<sub>3</sub> kinetics experiments. Each row contains a labelling of the experiment, the participating compounds and their concentration and the slope obtained from linear regression in SigmaPlot. The lactone rate constant obtained for each experiment is given

Exp. No.	Lactone (ppm)	[O <sub>3</sub> ] / ppm	Reference (ppm)	Slope	$k_{\text{compound}} / 10^{-20}$ (cm <sup>3</sup> molec <sup>-1</sup> s <sup>-1</sup> )
21	2(5H)F (2.89)	ca 1000	C <sub>2</sub> H <sub>2</sub>	7.438	7.44
22	3M2(5H)F (ca 5)	Ca 1500	C <sub>2</sub> H <sub>4</sub>	-	-
23(a-e)	GVL (ca 5)	1500-3000	-	-	-
22(a-d)	2(5H)F (ca 5)	500-1500	-	-	6.01
23(a-e)	3M2(5H)F (varying)	500-2000	-	-	54.2

#### 3.4.2.1 Absolute rate studies

The data from the absolute rate measurements of the GVL + O<sub>3</sub> reaction together with the pseudo-first-order plot are shown in Figure 3.18. The experiments with GVL + O<sub>3</sub> induced some difficulties. As can be seen in the embedded plot in Figure 3.18 the measurements do not show a linear behaviour. In most of the data sets there is a change in gradient indicating that there are at least two different processes with two different reaction rates involved in producing this result. This could for example be competition between reactions with O<sub>3</sub> and OH respectively. Different molecules were used in attempts to remove OH-radicals but no suitable scavenger was found. It is deduced from this result that the rate constant for

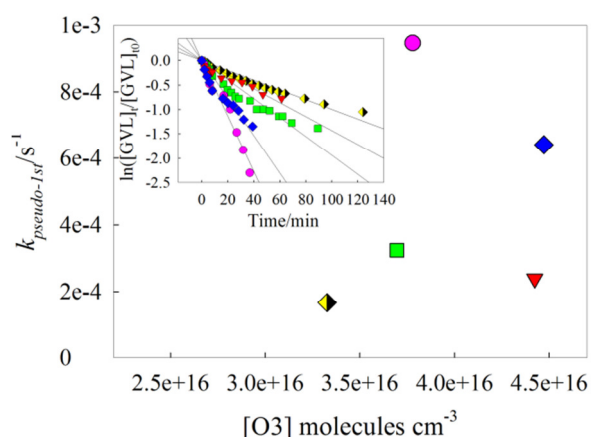


**Figure 3.17.** Pseudo-first order loss of GVL vs. O<sub>3</sub> concentration. The inserts show the decay of GVL in 1470 ppm (yellow/black diamonds), 1950 ppm (red triangles), 1630 ppm (green squares), 1470 ppm (blue diamonds) and 1470 ppm (pink circles) of O<sub>3</sub>, respectively



this reaction is too small to be detected using this method.

For 2(5H)F the absolute rate measurements with O<sub>3</sub> gave reasonable results when using cyclohexane as an OH-scavenger. The experiment was repeated four times with different O<sub>3</sub> concentrations and the results are shown in Figure 3.19.

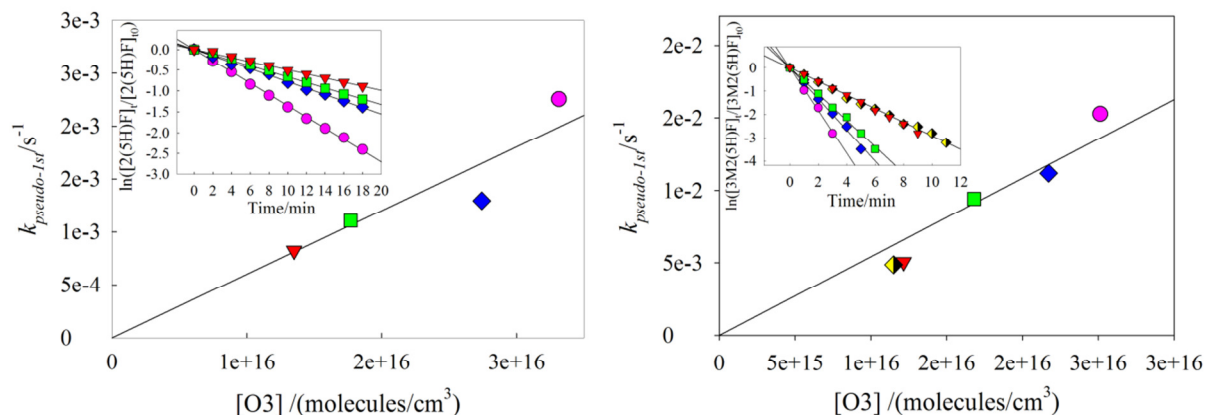


**Figure 3.19** Pseudo-first order loss of 2(5H)F (left) and 3M2(5H)F (right) vs. O<sub>3</sub> concentration. The inserts show the decay of 2(5H)F in 780 ppm (red triangles), 595 ppm (green squares), 1461 ppm (blue diamonds) and 1209 ppm (pink circles) of O<sub>3</sub>, respectively and the decay of 3M2(5H)F in 536 ppm (yellow/black diamonds), 741 ppm (red triangles), 985 ppm (green squares), 1108 ppm (blue diamonds) and 1891 ppm (pink circles) of O<sub>3</sub>, respectively.

In Figure 3.19 it is seen that there is a linear trend in the pseudo-first order plot but also that more data would be preferable in order to get a more even spread in the slopes in the embedded plots in Figure 3.19. It was difficult to control the O<sub>3</sub> concentration from experiment to experiment. The predicted concentration of O<sub>3</sub> after injection sometimes turned out to be higher than the result from analysing spectra with MALT. This is probably due to O<sub>2</sub> being present in the ozone trap. The accuracy of the predicted O<sub>3</sub> concentration varied from the first experiment to the last, one batch of O<sub>3</sub> lasting for three to four experiments, with more O<sub>2</sub> in the beginning. It is the MALT output concentration that is used in Figure 3.18-3.18.

### 3.4.2.1 Relative rate studies

Relative rate experiment were also performed for 2(5H)F and 3M2(5H)F and the resulting plots are shown in Figure 3.21.

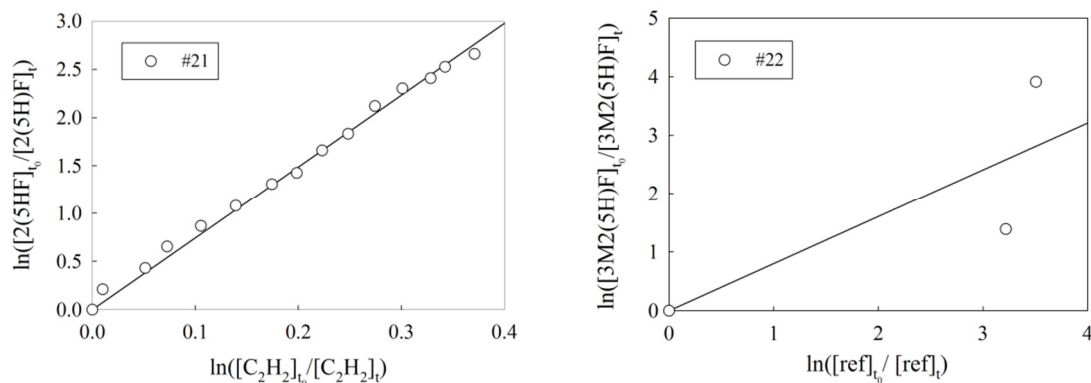


**Figure 3.20.** Measured data points together with linear regressions from relative rate analysis of the reaction (left) 2(5H)F + O<sub>3</sub> in N<sub>2</sub> and cyclohexane (right) 3M2(5H)F + O<sub>3</sub> in N<sub>2</sub> and cyclohexane.

There is clearly a difference in the quality of experiment number 21 and 22. This is, as can be seen in Table 3.10, due to the faster rate constant of 3M2(5H)F which is roughly one order of magnitude larger than the rate constant of 2(5H)F. Most of the 3M2(5H)F had simply reacted before enough data was collected.

The agreement of the rate constants of 2(5H)F between the absolute and the relative rate measurements is relatively good, enhancing the validity of the result since two methods were used.

### 3.5 Conclusions and atmospheric implications

The values from Table 3.6 have been averaged for each compound and the resulting rate constants are shown in Table 3.11.

**Table 3.11.** Final results, average of data from Table 3.6 and uncertainties.

Reaction	$k_f / \text{cm}^3 \text{molecule}^{-1} \text{s}^{-1}$
GVL + Cl	$(4.6 \pm 0.5) \cdot 10^{-11}$
2(5H)F + Cl	$(2.9 \pm 0.4) \cdot 10^{-11}$
3M-2(5H)F + Cl	$(16 \pm 2) \cdot 10^{-11}$
GVL + OH	$(2.9 \pm 0.6) \cdot 10^{-12}$
2(5H)F + OH	$(4.1 \pm 0.7) \cdot 10^{-12}$
3M-2(5H)F + OH	$(13 \pm 5) \cdot 10^{-12}$
GVL + O <sub>3</sub>	-
2(5H)F + O <sub>3</sub>	$(6.7 \pm 0.7) \cdot 10^{-20}$
3M-2(5H)F + O <sub>3</sub>	$(5.4 \pm 1.2) \cdot 10^{-19}$

The uncertainties for the Cl reaction rate constants are calculated using Equation (3.25)-(3.26). For the OH reactions the measured rate constants differed more than the calculated uncertainty and the error is hence given as the discrepancy between the average rate constant and the extremes of the measurements. Comparing the properties of the lactones using the information in Table 3.11 shows that 3M2(5H)F has the fastest reaction rate constant towards Cl, OH and O<sub>3</sub>. The reaction rate constants of GVL and 2(5H)F towards Cl and OH are in the same order of magnitude.

Comparing the measured rate constants in Table 3.11 with the literature values in Table 3.2 gives information on reproducibility of results and highlights differences or similarities between different furan derivatives. The rate constant for “GVL + OH → products” is in agreement with the literature value by Barnes et al. [34]  $((2.81 \pm 0.34) \cdot 10^{-12})$  who used relative rate kinetic experiments with similar conditions as in this work as well as theoretical calculations in the determination of the rate constant. The rate constant for “2(5H)F + O<sub>3</sub> → products” is not in absolute agreement with the previously determined value by Grosjean and Grosjean [35]  $((22 \pm 5) \cdot 10^{-20})$ , who also used pseudo-first order methods but used different ratios of lactone/ozone and also cyclohexane/ozone compared to this work. In the previous

study ozone losses in an excess of 2(5H)F were monitored, instead of the opposite way which was the method used in this work. Another difference is that they performed experiments in humid air and also made corrections for the wall-losses of 2(5H)F. These experimental differences might explain the different rate constants measured, which are still in reasonable agreement when including uncertainties and the fact that few experiments have been performed in total to determine this value.

The rate constants for reactions of the studied lactones with Cl and OH are lower, with about an order of magnitude, compared to the different furan derivatives presented in Table 3.2 The isomers of 2(5H)F and 3M2(5H)F that have double bonds and substituent on different positions, i.e. 2(3H)F and 5M23HF, have rate constants for reactions with OH that are faster than that what is observed for the furanones in the present work.

From trends in current data and the data presented in Table 3.2 it is apparent that the lactone double bonded oxygen has a retarding effect on the reactivity, since it gives in general lower rate constants. Another trend is that position of the double bond seem to affect the rate, and apparent from comparison of 25HF and 3M25HF with their isomers 23HF and 5M23H.

The atmospheric lifetimes of the lactones towards OH, Cl, and O<sub>3</sub> were calculated using Equation (3.13), the rate constants in Table 3.11 and the average global concentration of OH (1·10<sup>6</sup> molecules/cm<sup>3</sup>), the low and high limit observed concentrations of Cl (1·10<sup>2</sup> and 1·10<sup>5</sup> molecules/cm<sup>3</sup>) and different concentrations of O<sub>3</sub> which illustrates different levels of pollution in cities, with 100 ppb being hazardous. The lifetimes for these scenarios are presented in Table 3.12.

**Table 3.12.** Lifetime of GVL, 2(5H)F and 3m2(5H)F for reactions with OH, Cl and O<sub>3</sub> respectively. Different concentrations are representative for local variations.

Compound	OH (4.07·10 <sup>-2</sup> ppt)	Cl (4.07·10 <sup>-6</sup> ppt)	Cl (4.07·10 <sup>-3</sup> ppt)	O <sub>3</sub> (1ppb)	O <sub>3</sub> (10 ppb)	O <sub>3</sub> (100 ppb)
GVL	40 days	70 years	25 days	-	-	-
2(5H)F	29 days	110 years	39 days	190 years	19 years	1.9 years
3M-2(5H)	9 days	20 years	7 days	24 years	2.4 years	0.24 years

Total lifetimes are not calculated since they will depend on local conditions in Cl and O<sub>3</sub> concentrations as well as photolysis which have not been measured in this work. Of the chemical reactions the removal will however be dominated by OH and in extreme cases Cl can become equally important. O<sub>3</sub> will not be dominant in removal of the lactones. A lifetime against OH in the order of tens of days corresponding to transport times within the troposphere on the same hemisphere as the source. Implications can hence be both local and cover larger regions but are limited to the troposphere.

Regarding the identified products from reactions of lactones with Cl, most have low toxicity at low concentrations or are unstable and will decompose rapidly in the atmosphere. Phosgene however is very toxic and has e.g. previously been used in chemical warfare. Phosgene is present in all studies with O<sub>2</sub> present and the produced amount varies between lactones. It will be important to accurately quantify the yield of phosgene and also identify more products.

# **PART IV - Bromine Chemistry modeling**

## **4.1 Bromine in the troposphere**

Below the different compounds referred to in this project as well as their sources, sinks and general tropospheric importance are presented. The model output is later, in Section 4.3, compared against atmospheric measurements from a recent campaign and some details on the collection of this data are given here.

### **4.1.1 Inorganic bromine ( $\text{Br}_y$ )**

$\text{Br}_y$  is the notation for inorganic bromine i.e. compounds containing bromine atoms but no carbon atoms.  $\text{Br}_y$  cycles between the radicals  $\text{BrO}_x$  and other non-radical compounds such as  $\text{Br}_2$ ,  $\text{HBr}$ ,  $\text{HOBr}$  and  $\text{BrONO}_2$ .  $\text{Br}_y$  in the troposphere is a result of debromination of sea salt aerosols, photolysis and oxidation of organic brominated compounds (bromocarbons) and transport from the stratosphere. Closest to the Earth's surface, in the marine boundary layer (MBL), sea salt constitutes the largest  $\text{Br}_y$  source (ca 70%) and the second largest source (ca 20%) is bromocarbons. However, in the free troposphere above the MBL, bromocarbons contribute to the production of approximately 50% of the total  $\text{Br}_y$  since  $\text{Br}_y$  from sea salt is rapidly deposited at the surface while bromocarbons to a larger extent are transported to the free troposphere [14]. The bromine is finally lost from the atmosphere by deposition, e.g. through precipitation or sedimentation.

$\text{Br}_y$  cannot be measured directly and its concentration is interpreted by measurements of  $[\text{BrO}]$  which in principle is the only compound convenient to observe which is also closely related to  $[\text{Br}_y]$  [66]. When implementing changes in the bromine chemistry it is hence useful to look at the effects on  $\text{BrO}$ , and consequently  $\text{Br}_y$ .

### **4.1.2 Bromoform ( $\text{CHBr}_3$ )**

Tribromomethane, or bromoform ( $\text{CHBr}_3$ ), is a naturally occurring compound, mainly emitted from algae and plankton in oceans and along coasts [67]. According to the United States Environmental Protection Agency, bromoform is hazardous to humans and an intake of large amounts of the compound can result in damages on liver and kidneys. Exposure to damaging levels can occur via drinking-water or swimming pool water which has been disinfected with chlorine in the presence of bromine, however the natural occurring levels of bromoform are not dangerous [68].

$\text{CHBr}_3$  is a very short-lived tropospheric compound with an atmospheric lifetime in the order of tens of days [67]. A short lifetime makes local conditions such as temperature, air convection and solar radiation important for the effect of bromoform on the troposphere.

Bromoform is the single largest bromocarbon source of Br<sub>y</sub> in the troposphere through photolysis and oxidation. New and more accurate measurements suggest changes relative to the latest recommended values of the temperature dependent absorption cross section [67] as well as the rate constant for the reaction with OH [71] which affects the two single most important destruction pathways of CHBr<sub>3</sub>.

#### 4.1.3 Bromine nitrate (BrONO<sub>2</sub>)

Bromine nitrate (BrONO<sub>2</sub>) is an important Br<sub>y</sub> reservoir in the bromine chemistry included in the GEOS-Chem model. The daytime BrO/Br<sub>y</sub> ratio does mainly depend on the following reactions



where reaction (4B) and (4C) have different quantum yield, with (4B) accounting for 15% and (4C) for 85% of the photolysis mechanism. The production of BrONO<sub>2</sub> (loss of BrO) depends on the rate constant  $k_{\text{BrO}+\text{NO}_2}$  and the loss of BrONO<sub>2</sub> (production of BrO) depends on the photolysis rate  $J_{\text{BrONO}_2}$ . Hence the total amount of the available BrO depends on both these rate constants and this will be treated as a ratio  $J_{\text{BrONO}_2} / k_{\text{BrO}+\text{NO}_2}$ .

A study by Kreytcy et al. (2013) [66] finds that the currently accepted BrONO<sub>2</sub> production and loss kinetics differ from new measurements and that this affects simulations of Br<sub>y</sub> concentrations in the stratosphere. They suggest an increase of the ratio  $J_{\text{BrONO}_2} / k_{\text{BrO}+\text{NO}_2}$  of 70%. In this work the suggested change in  $J_{\text{BrONO}_2} / k_{\text{BrO}+\text{NO}_2}$  will be implemented in the GEOS-Chem bromine chemistry to examine the impact on Br<sub>y</sub> in the troposphere.

#### 4.1.4 HIPPO-campaign summary

In this project the output from a chemical transport model is going to be compared with actual atmospheric concentrations to test the accuracy of the model. The observational data used was collected during an aircraft campaign funded by the National Science Foundation (NSF) and the National Oceanic and Atmospheric Administration (NOAA) [69].

The campaign, hereafter referred to as HIPPO (HIAPER Pole-to-Pole Observations, where HIAPER stands for High-performance Instrumented Airborne Platform for Environmental Research), provides the first extensive and systematic measurements of over 90 species of greenhouse gases and aerosols. The species are both of natural and anthropogenic origin and the data is supposed to be used for climate research.

The data consists of in situ measurements as well as analysis of air samples at well-defined locations in the atmosphere. Since the concentrations are not averaged and the aircraft varied its altitude the measurements provide high resolution information in three dimensions. Five separate flights were performed during different seasons (January 2009, October-November 2009, March-April 2010, June-July 2011 and August-September 2011) and together they cover nearly all latitudes from the North to the South Pole, mainly over the Pacific Ocean and Northern America [17], [69].

## 4.2 Method

### 4.2.1 GEOS-Chem model and settings

The model used in this work is called GEOS-Chem and it is managed and developed by Harvard University, Dalhousie University and NASA [70]. In the model the transport is driven by meteorological fields from the Goddard Earth Observing System (GEOS) of the NASA global modeling and assimilation office. By including extensive information on emissions, chemistry and deposition an adjustable three-dimensional CTM for tropospheric studies has been made available by the user community.

The spatial and temporal resolutions are the same through all simulations performed in this work. A two-dimensional resolution of  $4^\circ$  latitude times  $5^\circ$  longitude is used and vertically the atmosphere is divided into 47 pressure dependent layers (totally around 80 km). The temporal resolution is 30 minutes for a simulation in the range of a few years.

The bromine chemistry scheme used includes the same compounds as described by Parella et al. (2012) [14] with the addition of BrCl giving a total of 11 brominated compounds (three organic and eight inorganic). The  $\text{Br}_y$  output from the model is the sum of the bromine atoms of all the 8 inorganic compounds, i.e.  $\text{Br}_2$  contributes twice as much as HOBr and so on. The chemical properties to be read by the model were adjusted according to the values presented in the Sections 4.2 and 4.3 below and otherwise kept at the default values.

For each simulation a spin-up part extending for one year is performed in order to let the model adjust to any changes made, this data is not used as a result. The simulation does thereafter continue and this reference or *benchmark data* is used for comparing different model outputs. When a simulation is going to be compared with observed data, the model simulation is set to cover the entire sampling period. For the  $\text{CHBr}_3$  simulation the model is run from 2006-01-01 to 2012-01-01 with the year 2006 being the spin-up, 2007 being the benchmark and 2008-2011 overlaps with the HIPPO campaign. Files with data in sets of 6 months are created and put into the model one by one. For the  $\text{BrONO}_2$  simulation the model is set to cover years 2006-2007, i.e. a spin-up and a benchmark period. No comparison with observed data is done for  $\text{BrONO}_2$ . Due to a more extensive chemistry scheme, i.e. a need of more computation, files with data in sets of 3 months are created and put into the model one by one. Two simulations are run in parallel, one with the updated chemistry and one where no changes are made.

### 4.2.2 Updated rate constants

For the oxidation of  $\text{CHBr}_3$  by OH the total reaction is assumed to be



The rate constant for this reaction has been measured recently by Orkin et al. [71] and the values for  $A$ ,  $B$  and  $E_a/R$  in the Arrhenius equation used in GEOS-Chem,

$$k = A(300/T)^B e^{-E_a/RT}, \quad (4.1)$$

are shown in Table 4.1 together with the recommended values from the latest JPL evaluation by Sander et al. (2011) [72].

The updated rate constants are roughly 1.5-2 times larger than the recommended value in the temperature range 230-370 K, which is the range measured by Orkin et al. [71].

The rate constant for reaction (4A) was not given a specific value by Kreycy et al. but instead the total change in  $J_{\text{BrONO}_2} / k_{\text{BrO}+\text{NO}_2}$  should be 1.7. By considering the data presented, the median value of the change was chosen for  $J_{\text{BrONO}_2}$  and  $k_{\text{BrO}+\text{NO}_2}$  respectively. The revised reaction rate constant is hence decreased by 25% and the corresponding change of the Arrhenius constants is presented in Table 4.1. Reaction (4A) is pressure dependent and  $A_0$  is valid for the low pressure limit while  $A_\infty$  is used for the high pressure limit. Only  $A_0$  and  $A_\infty$  are changed since the suggested change in  $J_{\text{BrONO}_2} / k_{\text{BrO}+\text{NO}_2}$  is not shown to be temperature dependent.

**Table 4.1.** Kinetic data for the reaction  $\text{CHBr}_3 + \text{OH} \rightarrow 3\text{Br} + \text{products}$  (4D) and  $\text{BrO} + \text{NO}_2 + \text{M} \rightarrow \text{BrONO}_2 + \text{M}$  (4A) as suggested by different studies.

	$A_0 / (\text{cm}^3 \text{molecule}^{-1} \text{s}^{-1})$	$A_\infty / (\text{cm}^3 \text{molecule}^{-1} \text{s}^{-1})$	$B$	$(-E_a/R)/\text{K}$
<i>React. (4D)</i> <b>JPL Eval. No. 17</b>	-	$1.35 \cdot 10^{-12}$	0	600
<i>React. (4D)</i> <b>Orkin et al.</b>	-	$(9.94 \pm 0.76) \cdot 10^{-13}$	0	$387 \pm 22$
<i>React. (4A)</i> <b>JPL Eval. No. 17</b>	$5.2 \cdot 10^{-31}$	$6.9 \cdot 10^{-12}$	3.2	0
<i>React. (4A)</i> <b>0.75·JPL, Kreycy et al.</b>	$3.90 \cdot 10^{-31}$	$5.18 \cdot 10^{-12}$	2.9	0

### 4.2.3 Updated absorption cross sections

The photolysis mechanism for bromoform is simplified as



and for bromine nitrate photolysis reaction (4B) and (4C) are considered. The reaction actually occurs in several steps but for the present work only the net reaction is of interest. In GEOS-Chem the variable governing photolysis is the absorption cross section,  $\sigma$ , which is defined for seven wavelength intervals, covering the range 289-850 nm. The definition of the intervals can be seen in Table 4.2.

The  $\text{CHBr}_3$  cross section has most recently been measured by Papanastasiou et al. (2014) at the wavelengths 300-345 nm in steps of 5 nm at temperatures between 260 and 330K [67]. The results show a lower  $\sigma$  than what has previously been measured. The precision of the new measurements is claimed to be high but with larger uncertainty for larger wavelengths (>320 nm) due to the very low  $\sigma$  in this region, see Figure 4.1.

Since the recent measurements do not cover all the wavelengths where  $\text{CHBr}_3$  is absorbing it is necessary to extend the data with values from another measurement. After studying different sets of data as well as parameterizations it was decided that the data by Moortgat et al. (1993) [73], recommended by Sander et al. (2001) [72] should be used in the regions 286-299 nm and 346-362 (both with steps of 2 nm).

In GEOS-Chem the absorption cross section is not included as a function but rather the values for specific wavelengths intervals are used. The wavelength spectrum is divided into seven parts, called *bins*, and in order to assign a cross section,  $\sigma$ , to each wavelength bin an average value of  $\sigma$  must be calculated. To get the value most representative for the entire bin, which covers several nanometres, both the cross section and the actinic flux,  $I$ , in the region are considered. If the cross section or actinic flux is non-uniform around the centre of the bin, but e.g. as for  $\sigma$  which decreases over the whole range of the first bin (from 289 to 298.25 nm) it would be a misrepresentation to use the centre value. By calculating a weighted average of  $\sigma$ , the best reproduction of the values used in GEOS-Chem by Parella et al. was obtained. The bromoform  $\sigma$  and  $I$  as a function of wavelength can be seen respectively in Figure 4.1 and the binned values of the previous and the updated cross sections at different temperatures is presented in Table 4.2.

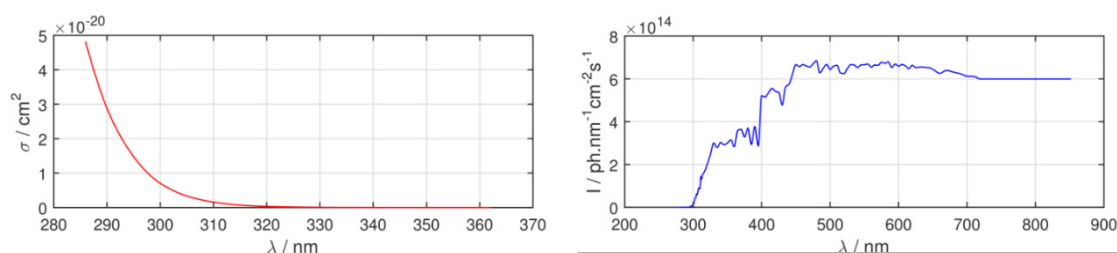


**Figure 4.1.** Absorption cross section of  $\text{CHBr}_3$  at 296 K with data from Papanastasiou et al. extended with data from Moortgat et al. (left) and actinic flux in the wavelength range 200-900 nm (right).

The total photolysis rate constant depends on the product of the wavelength dependent  $\sigma$  and  $I$ . The photolysis is hence dampened by the actinic flux around 300 nm.

The low temperature (230 K) cross section values were calculated using the ratio between the high and low temperature values from the parameterization by Papanastasiou et al. [67] multiplied with the measured values at 296 K. It was highlighted that extrapolation of  $\sigma$  to lower temperatures than 260 K is less reliable since no measurements are available for comparison. For  $\text{CHBr}_3$  the bin contributing most to the total  $J$ -value is bin number two. The regions where the non-updated  $\sigma$  is used i.e.  $\lambda < 300$  nm and  $\lambda > 345$  nm contributes with  $< 1\%$  and approximately 6 % of the total photolysis and hence the use of this extensional data is concluded to not affect the results significantly. By implementing the changes described above the total  $J$ -value decreases with 10%.

As mentioned in Section 4.2 recent studies suggest an increase of the ratio  $J_{\text{BrONO}_2} / k_{\text{BrO}+\text{NO}_2}$  of 70% and the choice to decrease  $k_{\text{BrO}+\text{NO}_2}$  by 25% consequently imply an increase of  $J_{\text{BrONO}_2}$  by 30%. The update of the photolysis mechanism was simply implemented by increasing each binned  $\sigma$  with 30% since no wavelength dependence was reported. For  $\text{BrONO}_2$  the sixth bin contributes the most to the total  $J$ . The  $\text{BrONO}_2$  cross section used in the model by Parella et al. [14] was not temperature dependent. Some measurements at 298 K have been reported but since the cross section show little temperature dependence the assumption is kept in the update. The previously used  $\text{BrONO}_2$  cross sections as well as the updated values are presented in Table 4.2.

**Table 4.2.** Binned cross sections for the photolysis of  $\text{CHBr}_3$  (Reaction (4E)) and  $\text{BrONO}_2$  (Reaction (4B)+(4C)) as used in the standard GEOS-Chem (“gc”) model as well as updated values from this work (“up”).



	T (K)	Bin #1	#2	#3	#4	#5	#6	#7
$\lambda$ -range (nm)	-	289.0- 298.25	298.25- 307.45	307.45- 312.45	312.45- 320.30	320.30 -345.0	345.0- 412.45	412.45- 850
$\sigma_{\text{CHBr}_3}(\text{gc})$ $/ 10^{-22} \text{ cm}^2$	210	73.71	18.84	5.808	2.106	0.2441	$2.035 \cdot 10^{-3}$	0
	296	162.8	48.70	17.07	7.074	0.9311	$9.691 \cdot 10^{-3}$	0
$\sigma_{\text{CHBr}_3}(\text{up})$ $/ 10^{-22} \text{ cm}^2$	210	56.54	15.13	5.123	1.622	0.1456	$5.180 \cdot 10^{-4}$	0
	296	125.8	39.58	15.70	5.883	0.7671	$1.011 \cdot 10^{-2}$	0
$\sigma_{\text{BrONO}_2}(\text{gc})$ $/ 10^{-19} \text{ cm}^2$	230	2.069	1.739	1.487	1.264	0.8798	0.3698	0.01433
$\sigma_{\text{BrONO}_2}(\text{up})$ $/ 10^{-19} \text{ cm}^2$	230	2.690	2.261	1.933	1.643	1.144	4.807	1.863

## 4.3 Results and discussion

### 4.3.1 CHBr<sub>3</sub>

#### 4.3.1.1 Benchmark (data obtained for the year 2007)

As mentioned previously, a comparison will be made between the non-updated (hereafter referred to as *reference*) and the *updated* model output. The results of interest are the concentrations of CHBr<sub>3</sub>, Br<sub>y</sub> and BrO in three dimensions as well as the loss rate of CHBr<sub>3</sub> due to photolysis and oxidation respectively. The location of the tropopause is given in the model output and is marked with a dashed green line in the plots and the result of interest is below this line, in the troposphere.

The figures below show the concentrations averaged over longitude and the ratio between the updated and the non-updated model, all averaged over the year 2007. Figure 4.2 shows plots of [CHBr<sub>3</sub>] in the latitude-altitude plane in the unit ppt from the reference and the updated model respectively. The ratio between the outputs is also shown in Figure 4.2.

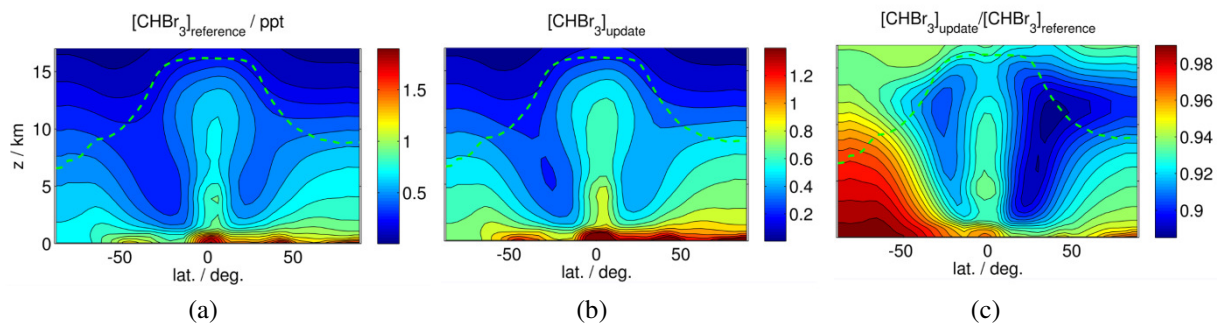


**Figure 4.2.** Annual mean concentration of CHBr<sub>3</sub> from standard reference model (left), the updated version (middle) and ratio between the update and the reference (right). Dashed green line indicates tropopause level.

In Figure 4.2 it can be seen that the highest concentration of CHBr<sub>3</sub> is found near the surface, which is in good agreement with oceanic emissions. The convection in the tropics is contributing to the upward transportation of CHBr<sub>3</sub> to the free troposphere in the tropics. There is a decrease of 2-10% in [CHBr<sub>3</sub>] with the largest difference found in the upper

troposphere and in the region where the downward transport from the stratosphere is found, at  $\pm 30^\circ$  latitude.

There is no directly visible difference between the reference and updated model output, as can be seen when comparing Figure 4.2a and 4.2b, and the same is true for the result of  $\text{Br}_y$  and  $\text{BrO}$  too. Therefore only one of these (the updated) is shown throughout the rest of this report. The corresponding results in the latitude-altitude plane for  $\text{Br}_y$  and  $\text{BrO}$  are presented in Figure 4.3.

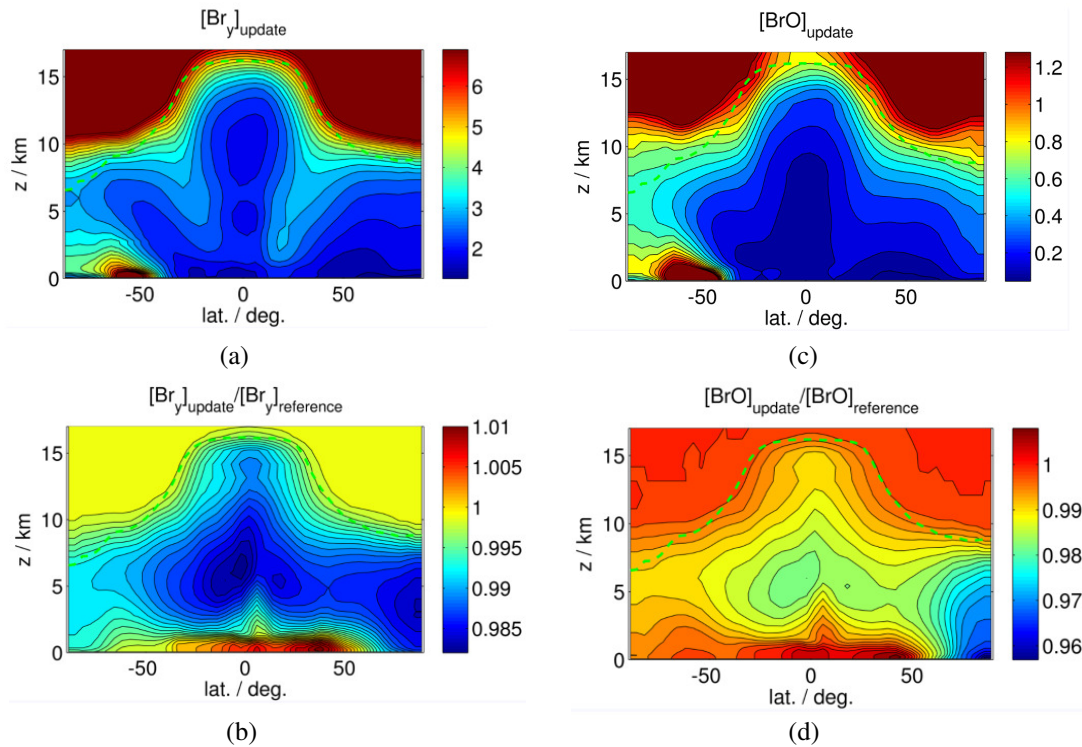


**Figure 4.3.** Annual mean concentration from the updated version of  $\text{Br}_y$  (a) and  $\text{BrO}$  (c). The ratio between the update and the reference model is shown for  $\text{Br}_y$  (b) and  $\text{BrO}$  (d). Dashed green line indicates tropopause level.

In Figure 4.3 it can be seen that the largest concentrations of  $[\text{Br}_y]$  and  $[\text{BrO}]$  are found in the MBL in the southern hemisphere due to large sea salt emissions. In the free troposphere ( $>2\text{km}$ ) the distribution of  $\text{BrO}$  is relatively uniform, decreasing somewhat with altitude and towards the poles. Minimum concentrations are found in the tropical upper troposphere due to scavenging in the updraft. The change in mean concentration shows the same behaviour for both  $\text{Br}_y$  and  $\text{BrO}$  which can be seen in Figure 4.3 as a small increase closest to the surface and a decrease of a few percent in the free troposphere, mostly in the tropics.

The results from the same simulations as above are also shown in Figure 4.4 a-f, plotted in a latitudinal-longitudinal plane. The data is averaged over the full height of the troposphere.

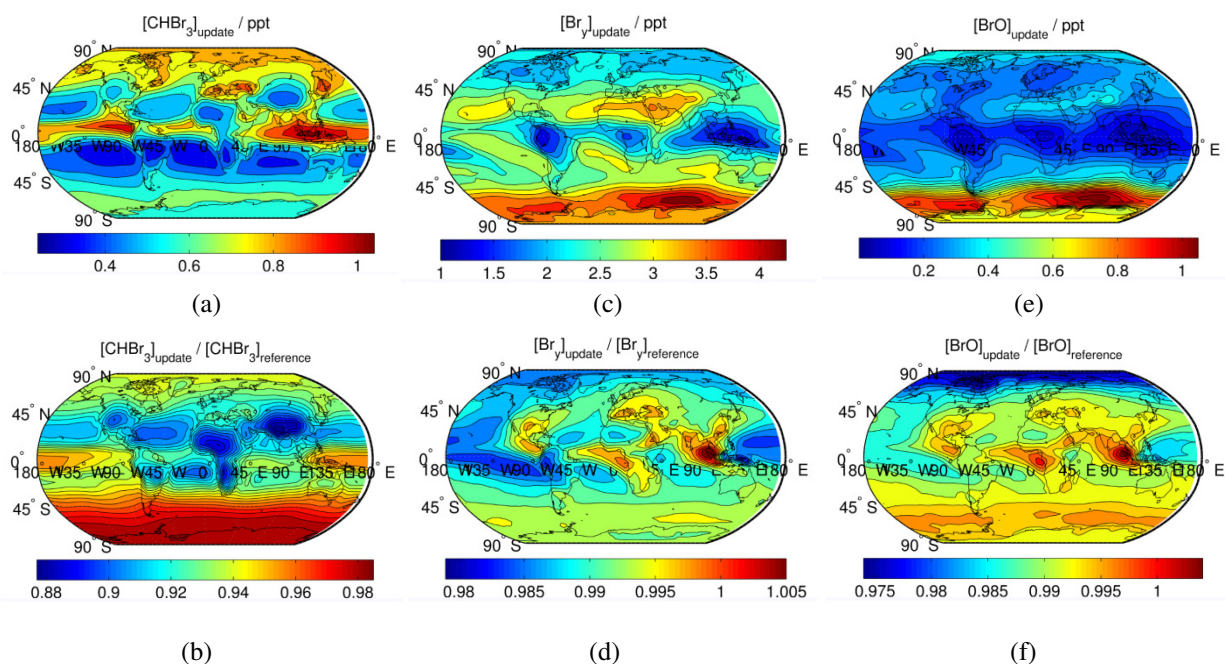


**Figure 4.4.** Annual mean concentration of  $\text{CHBr}_3$  (a,b),  $\text{Br}_\gamma$  (c,d) and  $\text{BrO}$  (e,f) from the updated model in the unit ppt (upper row) and the ratio between the updated and the reference version (lower row).

In Figure 4.4 a-b it can be seen that the concentration of  $\text{CHBr}_3$  is lowered over the entire globe with the updated kinetics, with a relative change of approximately 2-10%. The largest difference is located over the large land masses. This is a result of keeping the sources which are of oceanic and coastal origin unchanged while increasing the sinks. Combined with a short lifetime the updates result in less transport to remote land areas. With this in mind it is interesting that a decrease in  $\text{CHBr}_3$  is observed over the oceans at mid-latitudes. It was mentioned before that there is a larger downdraft in this region and hence transport of stratospheric species will be of larger importance. In Figure 4.5 the global ozone concentration from the same simulation is shown.

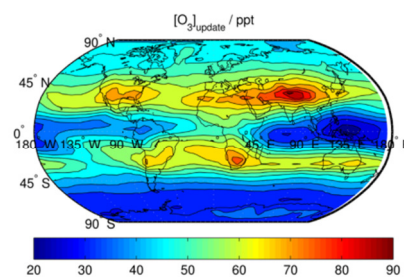


**Figure 4.5.** Annual mean concentration of ozone, output from the updated model.

Comparing Figure 4.4 and 4.5 a similar pattern can be seen, where higher ozone concentrations overlap with lower  $\text{CHBr}_3$  concentrations. It is hence believable that the transport of ozone from the stratosphere at  $\pm 30^\circ$  latitude results in a lower  $\text{CHBr}_3$  concentration in the air column.

The result is similar for  $\text{Br}_\gamma$  and  $\text{BrO}$  with a general decrease of a few percent across the globe except for the Southeast Asia which exhibits a small increase. This can be explained by ocean sources together with convection, which both are large in this area. Since the lifetime of these compounds is longer in the free troposphere than in the boundary layer, a faster uplift to higher altitudes results in a larger accumulation. The changes due to the updated kinetics are hence not significant for the global  $\text{Br}_\gamma$  and  $\text{BrO}$  distribution within the uncertainties.

The lifetime of a compound against photolysis depends on the photolysis rate constant which among other things depends on temperature and wavelength. The photolysis rate constant of  $\text{CHBr}_3$  in the latitude-altitude plane is shown in Figure 4.6 together with the ratio between the updated  $J$  and the reference  $J$ .

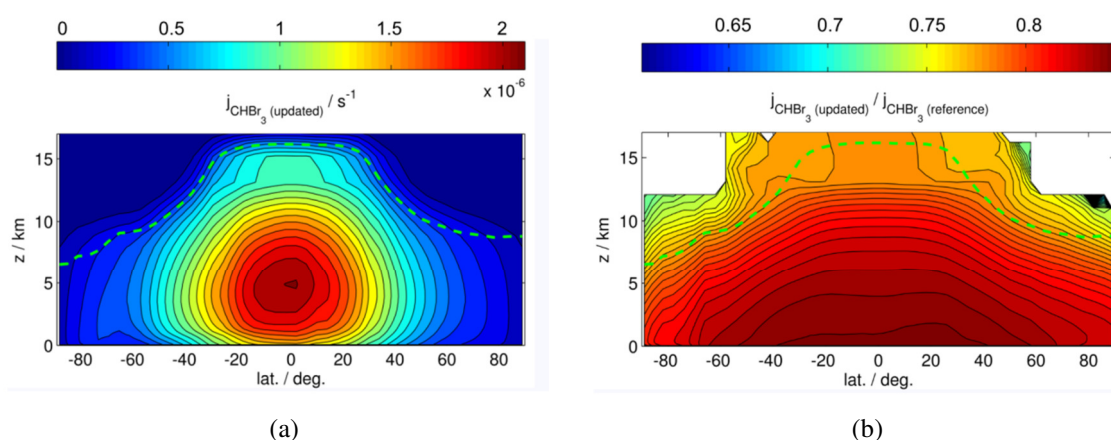


**Figure 4.6.** Annual mean value of the bromoform photolysis rate constant,  $J$ , from the updated model (left) and the ratio of  $J$  between the update and the reference (right).

It can be seen in Figure 4.6 that the temperature dependence is important for photolysis at different altitudes. The leftmost plot in Figure 4.6 shows that  $J_{\text{CHBr}_3}$  reaches its largest value at about 5 km altitude over the equator and decreases towards the poles as well as towards the Earth's surface and the tropopause. The changes are relatively large with roughly a factor 2 difference between the maximum  $J$  and the tropopause. There is hence a competition between actinic flux and temperature, yielding the Gaussian like profile of  $J$ . Papanastasiou et al. mention the temperature dependence of the photolysis rate constant to be important but also highlight the lack of measurements at low temperatures due to vapour pressure of  $\text{CHBr}_3$ .

The rightmost plot in Figure 4.6 shows the ratio between the photolysis rate from the updated and the reference simulation. The cut-off in the stratosphere is due to removal of data above a certain pressure level. The values are about 15-20 % lower in the updated model, with largest changes at higher altitude i.e. lower temperature. This can be compared with the cross section data in Table 4.2.

#### 4.3.1.2 HIPPO-campaign comparisons (2009-2011)

Two simulations, one reference and one with updated kinetics, using the same settings as above were run for the period 2009-2011 covering the HIPPO-campaign flight times. The model output corresponding to the HIPPO flight tracks are selected and compared to observations. The vertical profile averaged in bins of 10 km is presented in Figure with observations in black, reference GEOS-Chem simulation in blue and updated GEOS-Chem simulation in red.

Some general features found from observing the data in Figure 4.7 is that the updated  $\text{CHBr}_3$  loss mechanism does not significantly change the model output and the model does generally reproduce the observations well. The updated model does show a small negative bias compared to observations in the zonal band  $30^\circ\text{--}60^\circ\text{N}$  and also in the polar regions while a large bias is seen in the northern tropics,  $0^\circ\text{--}30^\circ\text{N}$ .

The different campaigns were also studied individually showing seasonal differences in observations. The model was less successful at reproducing observations during some periods, especially the flight from August. There is a seasonal scaling factor for the emissions in the model [14] and when comparing the flight paths it was found that the largest bias was corresponding to flights with more measurements over land areas. This raised the question of emission from land versus water since the model in general catches the  $\text{CHBr}_3$ ,  $\text{Br}_y$  and  $\text{BrO}$  concentrations well in the upper troposphere indicating good assumptions of transport and kinetics. The emissions from land areas are currently zero in the model. Figure 4.8 shows vertical profiles from the northern mid-latitudes where the data has been separated into different longitudinal ranges, one covering the Pacific Ocean and one covering North America.

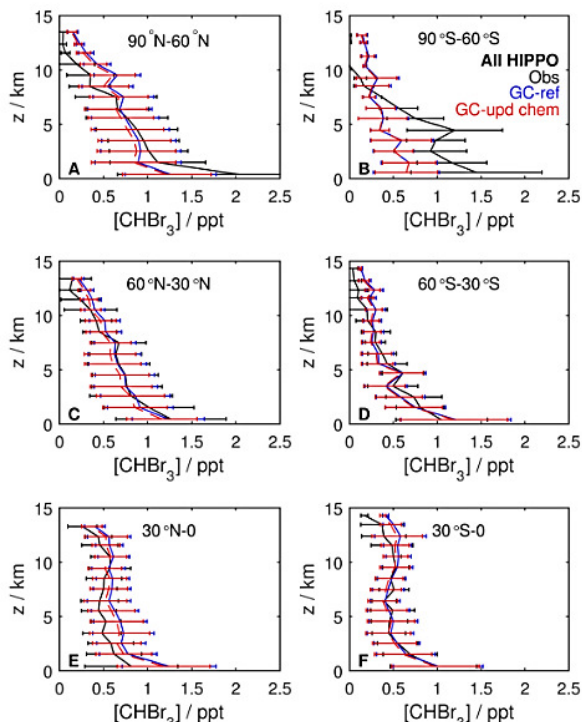


**Figure 4.7.** Vertical concentration profile for six zonal bands. Data from all HIPPO campaigns included.

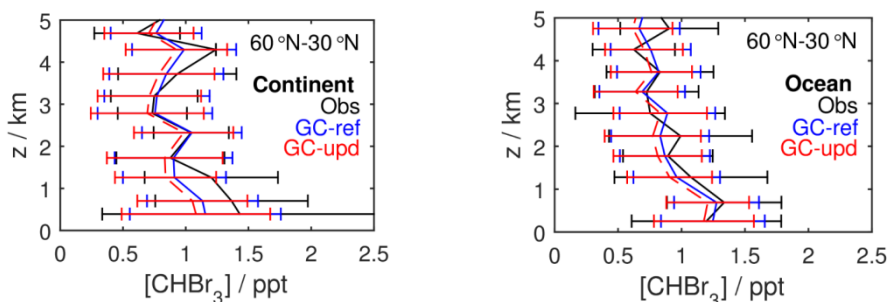


**Figure 4.8.** Vertical profile for northern mid-latitude land data,  $80\text{--}120^\circ\text{W}$  (left) and ocean and coast data,  $120\text{--}180^\circ\text{W}$  (right).

It can be seen in Figure 4.8 that in the lowest kilometre where the local emissions are of greater importance there is a bias on the continent but not over the ocean. In order to estimate the magnitude of possible emissions the simulated data was plotted as a function of the observed data. A linear regression yields the correlation between the simulation and observations. A comparison between oceanic and continental data in the lower and upper troposphere respectively can be seen in Figure 4.9.

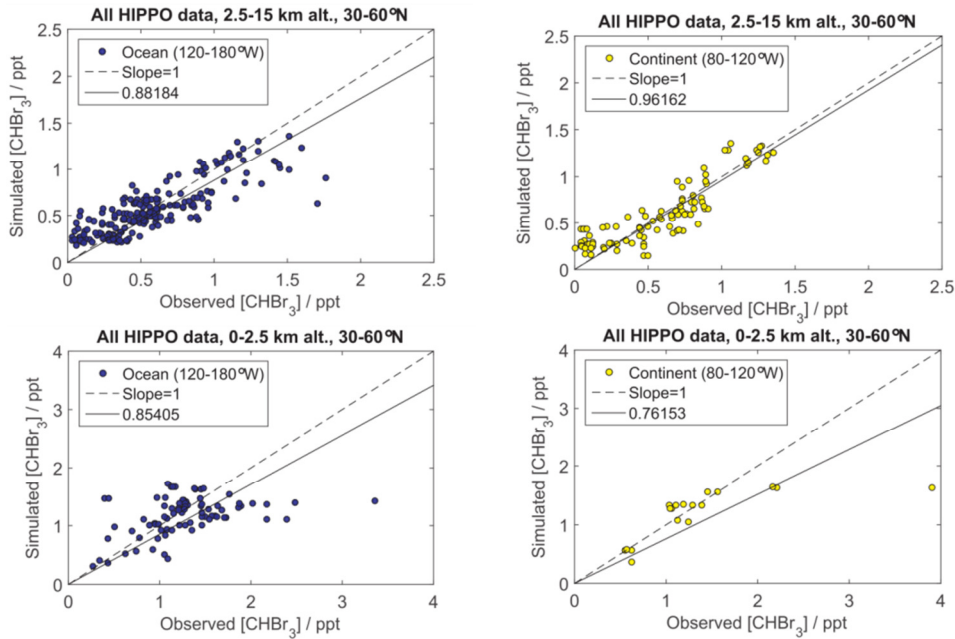


**Figure 4.9.** Scatter plots of simulated concentrations of  $\text{CHBr}_3$  versus observations and linear regressions (solid lines). The dashed lines indicate a slope of 1.

It can be seen in Figure 4.9 that there is in general a linear trend in the data with a slope less than 1 indicating that the model predicts to low concentrations. The coarse resolution of the model cannot catch the extremes in the observations which are found in the PBL and the amount of low level observations over the continent is not very large. According to Figure 4.9 there is a larger bias in the continental PBL which could indicate a lack of existing emissions.

A simulation was performed with increased emissions in the polar regions, including the coastline of Antarctica, a decrease of emissions in northern mid-latitude oceanic regions since a large bias was observed in 0-30°N. The result was varying with improvements in some regions and a larger bias in some. Hence no conclusions are drawn about the emission fields in this work and there are also different suggestions on bromoform emissions within the scientific community with total annual emissions varying between 300 and 500 Gg.

### 4.3.2 BrONO<sub>2</sub>

The results from simulating a reference model with chemistry and transport, utilizing the most recent recommended values and the updated version described earlier is evaluated in Figure 4.10. Figure 4.10 shows the change in global distribution of BrONO<sub>2</sub>, Br<sub>y</sub> and BrO.

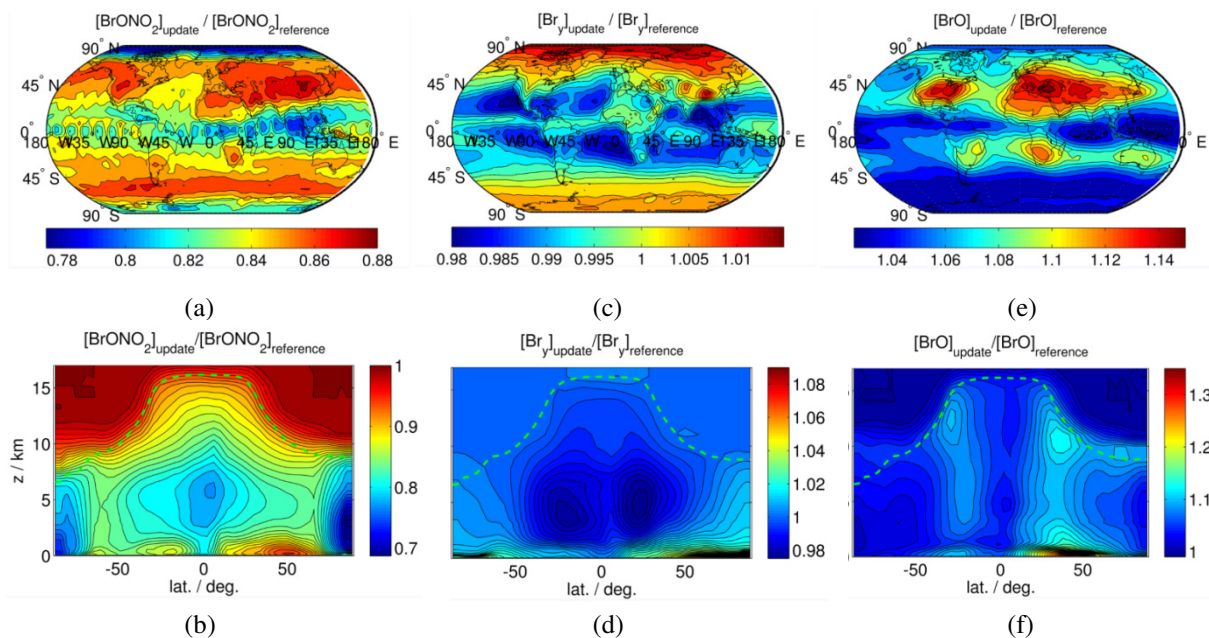


**Figure 4.10.** Ratio of the reference and updated model output of the annual mean concentration of BrONO<sub>2</sub> (a,b), [Br<sub>y</sub>] (c,d) and [BrO] (e,f). Result shown in the latitudinal-longitudinal plane (upper row) in the latitudinal-altitudinal plane (lower row).

From Figure 4.10 it can be seen that the changes in the source and loss mechanisms of BrONO<sub>2</sub> affects the global BrO concentration which is increased by 5-15% and the total Br<sub>y</sub> is altered with  $\pm 2\%$  due to the updated kinetics. This is not extreme but could be significant for evaluations using BrO as tropospheric ozone destruction pathway. The reason for the small change in Br<sub>y</sub> compared to BrO is that the compounds within the group Br<sub>y</sub> have changed in concentration with more BrO and less of other compounds as a result but the total Br<sub>y</sub> is roughly constant.

Parella et al. obtained a global decrease in [O<sub>3</sub>] by 6.5% and in [OH] by 4% by using the same values for the bromine kinetics as in the reference simulation in this work. A change in [BrO] of approximately 10%, being the result of this work, could hence alter these global changes in [O<sub>3</sub>] and in [OH] by about 1%.

## 4.4 Conclusions and atmospheric implications

The lifetime of  $\text{CHBr}_3$  against OH reaction and photolysis respectively is calculated using Equation (3.11) and the rate constants presented earlier. The updated lifetime can be compared against the recommended value from the most recent evaluation for two different temperatures, the result is presented in Table 4.3.

**Table 4.3.** Lifetime of  $\text{CHBr}_3$  for reactions with OH and photolysis respectively.

<b>Temp. dependent mechanism</b>	<b>OH</b> ( $4.07 \cdot 10^{-2}$ ppt)	<b>Photolysis</b>
Updated (296 K)	1.18 years	1.51 days
Reference (296 K)	1.78 years	1.35 days
Updated (230 K)	1.71 years	5.08 days
Reference (230 K)	3.19 years	3.99 days

In Table 4.3 it is seen that the largest changes in both OH and photolysis lifetime is observed at lower temperatures, i.e. higher altitudes. The updated kinetics result in a decreases lifetime against OH and the opposite for photolysis. However the dominating sink of  $\text{CHBr}_3$  is photolysis throughout the atmosphere.

It is difficult to evaluate the effects on ozone due to the above implications since there are so many sources and sinks of ozone besides what has been described here. Using a factor which is not well reproduced by models as a diagnostics tool is not suitable since a good agreement could be a result of several poor assumptions cancelling each other.

Assuming that the most recent measurements are the most accurate, it is a recommendation to include the updated rate constants in the GEOS-Chem model for a better general representation of the Br chemistry in the troposphere.



## **PART V - Summary and outlook**

In this project the rate coefficients of the reactions (I)-(IX) on page 10 have been measured. The result was used to calculate atmospheric lifetimes which indicate that the lactones will be removed from the troposphere and not be transported to the stratosphere to any significant extent. The lifetime will depend on the local Cl atom concentration and can then have a larger local effect by less transport of the lactones and their products. For the reaction rate constant of O<sub>3</sub> reactions, more experimental data is needed to get a better absolute measurement and the relative rate measurement should be reproduced to confirm the result.

Another sink of the lactones except for chemical reactions is photolysis, which was found to be small but not insignificant in this work. To be able to calculate accurate total lifetimes and eventually the climate effects of the lactones, the photolysis rate constant should also be measured.

It would be interesting to do further studies on compounds similar to the lactones studied in this work, for example with the double bond in another position or additional methyl groups at different positions.

A toxic product, phosgene, was found to be formed under atmospheric conditions as a result of the reaction lactone + Cl. Further investigations regarding this are necessary before any large scale use of the lactones is undertaken. The other products are not harmful but there are still unidentified, possibly chlorine containing, products and further studies should be performed. Since the largest reaction sink will be through OH it is also of interest to study the products from these reactions.

This work has also showed that the updated rate constant of the CHBr<sub>3</sub> photolysis and reaction with OH has negligible effect on the inorganic bromine budget in the troposphere. The updated kinetics of the BrONO<sub>2</sub> sources and sinks has a relevant effect on the inorganic bromine. Further investigations of the CHBr<sub>3</sub> emission field could be performed, especially for determining whether emissions from land are true or not.

## References

- [1] Stocker, T.F., D. Qin, G.-K. Plattner, M. Tignor, S. K. Allen, J. Boschung, A. Nauels, Y. Xia, V. Bex and P.M. Midgley (eds.): *Summary for Policymakers. In: Climate Change 2013: The Physical Science Basis. Contribution of Working Group I to the Fifth Assessment Report of the Intergovernmental Panel on Climate Change*, **IPCC**, 2013 Cambridge University Press, Cambridge, United Kingdom and New York, NY, USA.
- [2] Field, C.B., V.R. Barros, D.J. Dokken, K.J. Mach, M.D. Mastrandrea, T.E. Bilir, M. Chatterjee, K.L. Ebi, Y.O. Estrada, R.C. Genova, B. Girma, E.S. Kissel, A.N. Levy, S. MacCracken, P.R. Mastrandrea, and L.L.White (eds.): *Summary for policymakers. In: Climate Change 2014: Impacts, Adaptation, and Vulnerability. Part A: Global and Sectoral Aspects. Contribution of Working Group II to the Fifth Assessment Report of the Intergovernmental Panel on Climate Change*, **IPCC**, 2014 Cambridge University Press, Cambridge, United Kingdom and New York, NY, USA, pp. 1-32.
- [3] Jacob, D. J.: *Introduction to Atmospheric Chemistry*, Princeton University Press, 1999.
- [4] Seinfeld, J. H., Pandis, S. N.: *Atmospheric chemistry and Physics –from air pollution to climate change*, 2<sup>nd</sup> edition, John Wiley & Sons Inc., Hoboken, New Jersey, 2006.
- [5] UN General Assembly, *United Nations Framework Convention on Climate Change : resolution / adopted by the General Assembly*, 20 January 1994, A/RES/48/189, available at: [http://unfccc.int/key\\_documents/the\\_convention/items/2853.php](http://unfccc.int/key_documents/the_convention/items/2853.php) [accessed 27 April 2015]
- [6] Fenger, J., Tjell, J. C.: *Air Pollution – from a local to a global perspective*, 1<sup>st</sup> edition, Polyteknisk Forlag, Denmark, 2009.
- [7] Edenhofer, O., R. Pichs-Madruga, Y. Sokona, E. Farahani, S. Kadner, K. Seyboth, A. Adler, I. Baum, S. Brunner, P. Eickemeier, B. Kriemann, J. Savolainen, S. Schlömer, C. von Stechow, T. Zwickel and J.C. Minx (eds.): *Climate Change 2014: Mitigation of Climate Change. Contribution of Working Group III to the Fifth Assessment Report of the Intergovernmental Panel on Climate Change*, **IPCC**, 2014, Cambridge University Press, Cambridge, United Kingdom and New York, NY, USA.
- [8] Ragauskas, A. J., Williams, C. K., Davison, B. H., Britovsek, G., Cairney, J., Eckert, C. A., Frederick Jr., W. J., Hallett, J. P., Leak, D. J., Liotta, C. L., Mielenz, J. R., Murphy, R., Templer, R., Tschaplinski, T.; *The Path Forward for Biofuels and Biomaterials*, **Science**, Vol. 311 (5760), 484-489, 2006.
- [9] Young, C. J., Washenfelder, R. A., Edwards, P. M., Parrish, D. D., Gilman, J. B., Kuster, W. C., Mielke, L. H., Osthoff, H. D., Tsai, C., Pikelnaya, O., Stutz, J., Veres, P. R., Roberts, J. M., Griffith, S., Dusanter, S., Stevens, P. S., Flynn, J., Grossberg, N., Lefer, B., Holloway, J. S., Peischl, J., Ryerson, T. B., Atlas, E. L., Blake, D. R., and Brown, S. S.: *Chlorine as a primary radical: evaluation of methods to understand its role in initiation of oxidative cycles*, **Atmos. Chem. Phys.**, 14, 3427-3440, doi:10.5194/acp-14-3427-2014, 2014.

- [10] Andersen, V. F.: *PhD Thesis: Physical Properties and Atmospheric Chemistry of Biofuels*, Department of Chemistry, University of Copenhagen, 2012.
- [11] Mielke, L. H., Stutz, J., Tsai, C., Hurlock, S., Roberts, J. M., Veres, P. R., Froyd, K., Hayes, P., Cubison, M., Jimenez, J. L., Washenfelder, R. A., Young, C. J., Gilman, J. B., de Gouw, J., Flynn, J., Grossberg, N., Lefer, B., Liu, J., Weber, R., and Osthoff, H. D.: *Heterogeneous formation of nitryl chloride and its role as a nocturnal NO<sub>x</sub> reservoir species during CalNex-LA 2010*, **J. Geophys. Res.**, 118, 10638–10652, doi:10.1002/jgrd.50783, 2013.
- [12] Sitch, S., Cox, P. M., Collins, W. J., Huntingford, C.; *Indirect radiative forcing of climate change through ozone effects on the land-carbon sink*, **Nature**, Vol. 488, 791-794, 2007.
- [13] Lippmann, M.: *Health effects of tropospheric ozone*, **Environ. Sci. Technol.**, Vol. 25, No. (12), 1954-1962, 1991.
- [14] Parrella, J. P., Jacob, D. J., Liang, Q., Zhang, Y., Mickley, L. J., Evans, M. J., Yang, X., Pyle, J. A., Theys, N., Van Roozendaal, M., *Tropospheric bromine chemistry: implications for present and pre-industrial ozone and mercury*, **Atmos. Chem. Phys.**, 12, p. 6723-6740, 2012.
- [15] Parrish, D. D., Lamarque, J.-F., Naik, V., Horowitz, L., Shindell, D. T., Staehelin, J., Derwent, R., Cooper O. R., Tanimoto, H., Volz-Thomas, A., Gilge, S., Scheel, H.-E., Steinbacher, M., Fröhlich, M., *Long-term changes in lower tropospheric baseline ozone concentrations: Comparing chemistry-climate models and observations at northern midlatitudes*, **Journ. Geophys. Res. Atmos.**, 119(9), 5719-5736, 2014.
- [16] Sander, S. P., Abbatt, J., Barker, J. R., Burkholder, J. B., Friedl, R. R., Golden, D. M., Huie, R. E., Kolb, C. E., Kurylo, M. J., Moortgat, G. K., Orkin, V. L., Wine, P. H., *Chemical Kinetics and Photochemical Data for Use in Atmospheric Studies, Evaluation No. 17*, **JPL Publication 10-6**, Jet Propulsion Laboratory, Pasadena, 2011.
- [17] Wofsy, S. C., *HIAPER Pole-to-Pole Observations (HIPPO): fine grained, global-scale measurements of climatically important atmospheric gases and aerosols*, **Phil. Trans. R. Soc. A**, 369, 2073-2086, 2011.
- [18] Westbrook, C. K.: *Biofuels combustion*, **Annu. Rev. Phys. Chem.**, 64, 201-219, 2013.
- [19] Galletti, A. M. R., Antonetti, C., Ribechini, E., Colombini, M., P., Di Nasso, N., N., Bonari, E.: *From giant reed to levulinic acid and gamma-valerolactone: A high yield catalytic route to valeric biofuels*, **Applied Energy**, Vol. 102, 157-162, 2012.
- [20] Savage, N.: *Fuel options: The ideal biofuel*, **Nature**, 474, 9-11, 2011.
- [21] Molina, M. J., Rowland, F. S., *Stratospheric sink for chlorofluoromethanes: chlorine atom-catalysed destruction of ozone*, **Nature**, 249, 810-812, 1974.

- [22] Andersen, C., *Master's thesis: Atmospheric Chemistry of THFs and Lactones – Potential New Biofuels*, Faculty of Science, Copenhagen University, 2015.
- [23] Matrix Scientific, *Catalog Number 070417 2(5H)-Furanone, 96%*, <http://www.matrixscientific.com/>. (Accessed: 2015-05-13.)
- [24] Biosynth Chemistry & Biology, *Products, W-200229 – 3-Methyl-2(5H)-furanone*, <https://www.biosynth.com/>. (Accessed: 2015-05-13.)
- [25] Horváth, I. T., Mehdi, H., Fábos, V., Boda, L., Mika, L.,  *$\gamma$ -Valerolactone – a sustainable liquid for energy and carbon-based chemicals*, **Green Chem.**, 10, 238-242, 2008.
- [26] Alonso, D. M., Wettstein, S. G., Dumesic, J. A., *Gamma-valerolactone, a sustainable platform molecule derived from lignocellulosic biomass*, **Green Chem.**, 15, 584-595, 2013.
- [27] Lange, J. P., Prince, R., Ayoub, P., Louis, J., Petrus, Leo., Clarke, L., Gosselink, H., *Valeric Biofuels: A Platform of Cellulosic Transportation Fuels*, **Angewandte Chemie Int. Ed.**, 49(26), 4479-4483, 2010.
- [28] Bereczky, Á., Lukács, K., Farkas, M., Dóbbé, S., *Effect of  $\gamma$ -Valerolactone Blending on Engine Performance, Combustion Characteristics and Exhaust Emissions in a Diesel Engine*, **Natural Resources**, 5, 117-191, 2014.
- [29] Wettstein, S. G., Alonso, D. M., Gürbüz, E. I., Dumesic, J. A.: *A roadmap for conversion of lignocellulosic biomass to chemicals and fuels*, **Current Opinion in Chem. Engin.**, Vol. 1, Issue 3, 218-224, 2012.
- [30] Román-Leshkov, Y., Barrett, C. J., Liu, Z. Y., Dumesic, J. A.: *Production of dimethylfuran for liquid fuels from biomass-derived carbohydrates*, **Nature**, 447, 982-985, 2007.
- [31] Zhang, L., Yu, H., Wang, P., Li, Y.: *Production of furfural from xylose, xylan and corncob in gamma-valerolactone using  $FeCl_3 \cdot 6H_2O$  as catalyst*, **Bioresource Tech.**, Vol. 151, 355-360, 2014.
- [32] Sigma-Aldrich – Safety data sheets, *Ethanol,  $\gamma$ -Valerolactone, 2(5H)-Furanone and 3-Methyl-2(5H)-furanone*, sigma-aldrich.com. (Accessed: 2015-05-13 (ethanol) and 2014-08-27 (lactones)).
- [33] Wu, R., Pan, S., Li, Y., Wang, L., *Atmospheric Oxidation Mechanism of Toluene*, **J. Phys. Chem. A**, 118 (25), 4533-4547, 2014.
- [34] Barnes, I., Kirschbaum, S., Simmie, J. M.: *Combined Experimental and Theoretical Study of the Reactivity of  $\gamma$ -Butyro- and Related Lactones, with the OH radical at Room Temperature*, **J. Phys. Chem. A**, 118 (27), 5013-5019, 2014.
- [35] Grosjean, E., Grosjean D.: *Rate constants for the gas-phase reaction of ozone with unsaturated oxygenates*, **Int. J. of Chem. Kinet.**, Vol. 30, Issue 1, 21-29, 1998.

- [36] Bierbach, A., Barnes, I., Becker, K. H., Wiesen, E.: *Atmospheric Chemistry of Unsaturated Carbonyls: Butenedial, 4-Oxo-2-pentenal, 3-Hexene-2,5-dione, Maleic Anhydride, 3H-Furan-2-one, and 5-Methyl-3H-furan-2-one*, **Environ. Sci. Technol.**, 28 (4), 715–729, 1994.
- [37] Alwe, H. D., Walawalkar, M., Sharma, A., Pushpa, K. K., Dhanya, S., Naik, P.D.: *Rate Coefficients for the Gas-Phase Reactions of Chlorine Atoms With Cyclic Ethers at 298 K*, **Int. J. of Chem. Kinet.**, Vol. 45, Issue 5, 295-305, 2013.
- [38] Giri, B. R., Roscoe, J. M.: *Kinetics of the reactions of Cl Atoms with Several Ethers*, **J. Phys. Chem. A**, 114 (32), 8369-8375, 2010.
- [39] Winer, A. M., Lloyd, A. C., Darnall, K. R., Atkinson, R., Pitts Jr, J. N.: *Rate constants for the reaction of OH radicals with n-propyl acetate, sec-butyl acetate, tetrahydrofuran and peroxyacetyl nitrate*, **Chem. Phys. Lett.**, Vol. 51 (2), 221-226. 1977.
- [40] Moriarty, J., Sidebottom, H., Wenger, J., Mellouki, A., Le Bras, G.: *Kinetic Studies on the Reactions of Hydroxyl Radicals with Cyclic Ethers and Aliphatic Diethers*, **J. Phys. Chem. A**, 107, 1499-1505, 2003.
- [41] Wallington, T. J., Liu, R., Dagaut, P., Kurylo, M. J.: *The Gas Phase Reactions of Hydroxyl Radicals with a Series of Aliaphatic Ethers over the Temperature Range 240-440 K*, **Int. J. of Chem. Kinet.**, Vol. 20, Issue 1, 41-49, 1988.
- [42] Ravishankara, A. R., Davis, D. D.: *Kinetic Rate Constants for the Reaction of OH with Mehtanol, Ethanol, and Tetrahydrofuran at 298 K*, **J. Phys. Chem.**, 82 (26), 2852-2853, 1978.
- [43] Wallington, T. J., Siegl, W. O., Liu, R., Zhang, Z., Huie, R. E., Kurylo, M. J.: *The Atmospheric Reactivity of  $\alpha$ -Methyltetrahydrofuran*, **Environ. Sci. Technol.**, 24 (10), 1596-1599, 1990.
- [44] Cabañas, B., Villanueva, F., Martín, P., Baeza, M. T., Salgado, S., Jiménez, E.: *Study of reaction processes of furan and some furan derivatives initiated by Cl atoms*, **Atmos. Environ.**, Vol. 39 (10), 1935-1944, 2005.
- [45] Atkinson, R., Aschmann, S. M., Carter W. P. L.: *Kinetics of the reactions of O<sub>3</sub> and OH radicals with furan and thiopene at 298 ± 2 K*, **Int. J. of Chem. Kinet.**, Vol. 15, Issue 1, 51-61, 1983.
- [46] Bierbach, A., Barnes, I., Becker, K. H.: *Rate coefficients for the gas-phase reactions of hydroxyl radicals with furan, 2-methylfuran, 2-ethylfuran and 2,5-dimethylfuran at 300 ± 2 K*, **Atm. Environ. Part A General Topics**, 26 (5), 813-817, 1992.
- [47] Alwe, H. D., Walavalkar, M. P., Sharma, A., Dhanya, S., Naik, P. D.: *Tropospheric oxidation of cyclic unsaturated ethers in the day-time: Comparison of the reactions with Cl, OH and O<sub>3</sub> based on the determination of their rate coefficients at 298K*, **Atmos. Environ.**, Vol. 82, 113-120, 2014.

- [48] [Aschmann, S. M., Nishino, N., Arey, J., Atkinson, R.: *Kinetics of the Reactions of OH radicals with 2- and 3-Methylfuran, 2,3- and 2,5- Dimethylfuran, and E- and Z-3-Hexene-2,5 dione, and Products of OH + 2,5-Dimethylfuran*, **Environ. Sci. Technol.**, 45 (5), 1859–1865, 2011.
- [49] Liljegren, J. A., Stevens, P. S.: *Measurements of the Kinetics of the Reaction of OH Radicals with 3-Methylfuran at Low Pressure*, **Int. J. of Chem. Kinet.**, Vol. 45, Issue 12, 784-794, 2013.
- [50] Tapia, A., Villanueva, F., Salgado, M. S., Cabañas, B., Martinez, E., Martín, P.: *Atmospheric degradation of 3-methylfuran: kinetic and products study*, **Atmos. Chem. Phys.**, 11, 3227-3241, 2011.
- [51] Matsumoto, J.: *Kinetics of the Reaction of Ozone with 2,5-Dimethylfuran and Its Atmospheric Implications*, **Chem. Lett.**, Vol. 40, No. 6, 582-583, 2011.
- [52] Williams, D. H., Fleming, I.: *Spectroscopic methods in organic chemistry*, 5<sup>th</sup> edition, McGraw-Hill Publishing Company, Bell & Bain Ltd., Glasgow, 1995.
- [53] Svanberg, S.: *Atomic and Molecular Spectroscopy, Basic Aspects and Practical Applications*, 4<sup>th</sup> edition, Springer-Verlag Barlin Heidelberg Germany, 2004.
- [54] Thorne, A., Litzén, U., Johansson, S.: *Spectrophysics – Principles and Applications*, MediaTryck, Lund, 2007.
- [55] Nilsson, E. J. K., Eskebjerg, C., and Johnson, M. S.: *A photochemical reactor for studies of atmospheric chemistry*, **Atmos. Environ.**, 43(18), 3029-3033, 2009.
- [56] Andersen, V. F., Nilsson, E. J. K., Jørgensen, S., Nielsen, O. J., Johnson, M. S., *Methyl acetate reaction with OH and Cl: Reaction rates and products for a biodiesel analogue*, **Chem. Phys. Lett.**, 472, 23-29, 2009.
- [57] Sulbaek Andersen, M. P., Nilsson, E. J. K., Nielsen, O. J., Johnson, M. S., Hurley, M. D., Wallington, T. J., *Atmospheric chemistry of trans-CF<sub>3</sub>CH=CHCl: Kinetics of the gas-phase reactions with Cl atoms, OH radicals and O<sub>3</sub>*, **Journ. Photochem. and Photobiol. A: Chem.**, 199, 92-97, 2008.
- [58] Griffith, D. W. T.: *Synthetic calibration and quantitative analysis of gas-phase FT-IR spectra*, **Appl. Spectrosc.**, 50, 59-70, 1996.
- [59] Nielsen, O. J., Javadi, M. S., Sulbaek Andersen, M. P., Hurley, M. D., Wallington, T. J., Singh, R.: *Atmospheric chemistry of CF<sub>3</sub>CF=CH<sub>2</sub>: Kinetics and mechanisms of gas-phase reactions with Cl atoms, OH radicals and O<sub>3</sub>*, **Chem. Phys. Lett.**, Vol. 439, Issues 1-3, 18-22, 2007.
- [60] Atkins, P., de Paula, J.: *Atkins' Physical Chemistry*, 8<sup>th</sup> edition, W. H. Freeman and Company, 2006.
- [61] Atkinson R., Carter, W. P. L.: *Kinetics and Mechanisms of the Gas-Phase reactions of Ozone with Organic Compounds under Atmospheric Conditions*, **Chemical Reviews**,

Vol. 84, No. 5, 437-470, 1984.

- [62] Atkinson, R., Carter, W. P. L., Winer, A. M. and Pitts Jr., J. N. *An Experimental Protocol for the Determination of OH Radical Rate Constants with Organics Using Methyl Nitrite Photolysis as an OH Radical Source*, **Journal of the Air Pollution Control Association**, 1981, 31:10, 1090-1092, DOI: 10.1080/00022470.1981.10465331.
- [63] Raff, J. D., Finlayson-Pitts, B. J., *Hydroxyl Radical Quantum Yields from Isopropyl Nitrite Photolysis in Air*, **Environ. Sci. Technol.**, 44(21), 8150-8155, 2010.
- [64] Greiner, N. R., Hydroxyl radical kinetic by kinetic spectroscopy. IV. Some deuterium isotope effects., **J. of Chem. Phys.**, 48 (3), 1413, 1968.
- [65] From Østerstrøm, F., Nielsen, O. J., Sulbaek Andersen, M., Wallington T. J., *Atmospheric chemistry of CF<sub>3</sub>CH<sub>2</sub>OCH<sub>3</sub>: Reaction with chlorine atoms and OH radicals, kinetics, degradation mechanism and global warming potential*, **Chem. Phys. Lett.**, 524, 32-37. 2012.
- [66] Kreycy, S., Camy-Peyret, C., Chipperfield, M. P., Dorf, M., Feng, W., Hossaini, R., Kritten, L., Werner, B., Pfeilsticker, K., *Atmospheric test of the  $J(\text{BrONO}_2)/k_{\text{BrO}+\text{NO}_2}$  ratio: implications for total stratospheric Br<sub>y</sub> and bromine-mediated ozone loss*, **Atmos. Chem. Phys.**, 13, 6263-6274, 2013.
- [67] Papanastasiou, D. K., McKeen, S. A. and Burkholder, J. B., *The very short-lived ozone depleting substance CHBr<sub>3</sub> (Bromoform): revised UV absorption spectrum, atmospheric lifetime and ozone depletion potential*, **Atmos. Chem. Phys.**, 14, p. 3017-3025, 2014.
- [68] EPA, United States Environmental Protection Agency, Air Toxics Web Site, *Bromoform*, <http://www.epa.gov/ttnatw01/hlthef/bromofor.html>, updated 2013-10-18. (Accessed: 15-04-02)
- [69] *HIAPER Pole-to-Pole Observation*, <http://hippo.ucar.edu/>. (Accessed 2015-05-04)
- [70] *GEOS-Chem model*, <http://www.geos-chem.org/>, updated 2015-05-05. (Accessed 2015-05-11)
- [71] Orkin, V. L., Khamaganov, V. G., Kozlov, S. N., Kurylo, M. J., *Measurements of Rate Constants for the OH Reaction with Bromoform (CHBr<sub>3</sub>), CHBr<sub>2</sub>Cl, CHBrCl<sub>2</sub>, and Epichlorohydrin (C<sub>3</sub>H<sub>5</sub>ClO)*, **J. Phys. Chem. A**, 117, p. 3809-3818, 2013.
- [72] Iwasaki, E., Chiba, H., Nakayama, T., Matsumi, Y., Wallington, T. J., *PLP-LIF study of the reactions of chlorine atoms with C<sub>2</sub>H<sub>2</sub>, C<sub>2</sub>H<sub>4</sub>, and C<sub>3</sub>H<sub>6</sub> in 2-100 Torr of N<sub>2</sub> diluent at 295 K*. **Chem. Phys. Lett.**, 494 (4-6), 174-178, 2010.
- [73] Moortgat, G. K., Meller, R., Schneider, W., *Temperature dependence (256-296 K) of the Absorption Cross-Sections of Bromoform in the Wavelength Range 285-360 nm*, in: *The Tropospheric Chemistry of Ozone in the Polar Regions*, edited by H. Niki and K.H. Becker, Springer-Verlag, Berlin, p. 359-369, 1993.

## Appendix A

Measured and calibrated reference spectra of 2(5H)F (3.01 ppm) and 3M2(5H)F (3.24 ppm) in N<sub>2</sub> diluent, at (298±2) K and a total pressure of 700 Torr.

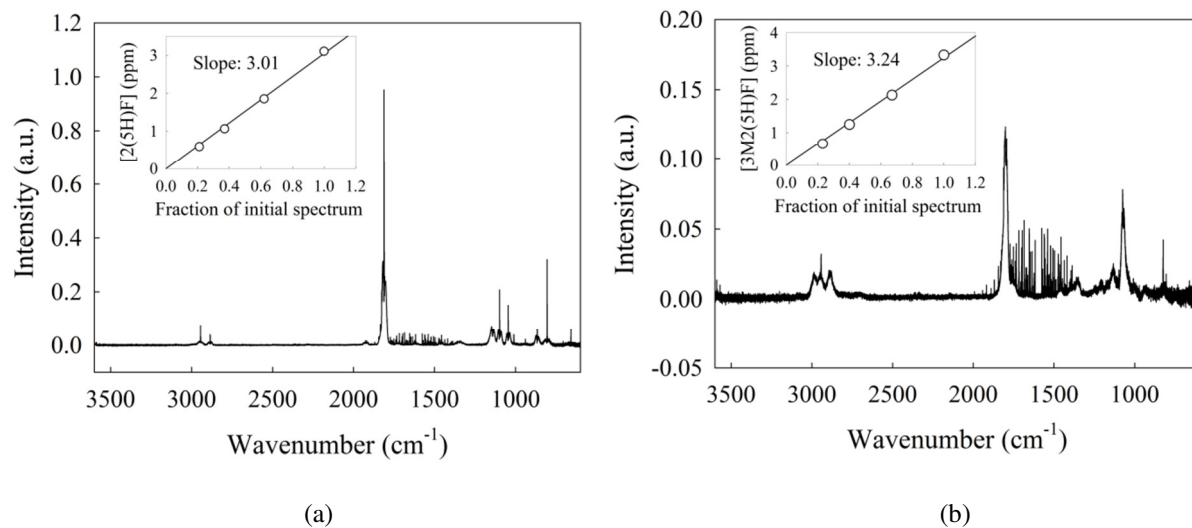


Figure A1. (a) Calibrated reference spectrum of 2(5H)F yielding a concentration of 3.01 ppm and (b) calibrated spectrum of 3M2(5H)F yielding a concentration of 3.24 ppm.